DISSERTATION

DIFFERENTIAL EQUATION MODELS OF WILDFIRE SUPPRESSION ALLOCATION

Submitted by

Alex Taylor Masarie

Department of Forest and Rangeland Stewardship

In partial fulfillment of the requirements

For the Degree of Doctor of Philosophy

Colorado State University

Fort Collins, Colorado

Spring 2018

Doctoral Committee:

Advisor: Yu Wei

Iuliana Oprea
Matt Thompson
Erin Belval

ABSTRACT

DIFFERENTIAL EQUATION MODELS OF

WILDFIRE SUPPRESSION ALLOCATION

(CHAPTER 1) Current policy calls for efficient and effective wildfire response, which requires an understanding of the system's complexity. Data visualization often provides key insight to initiate any normative modeling effort to reveal best practices when implementing the policy. This chapter outlines a procedure to make MATLAB structures from a resource tracking database. We prepared a wildfire suppression allocation database, built an animation and graphical user interface, and initiated our investigation of differential equations using GIS maps and phase plane as descriptive aides.

(CHAPTER 2) Efficient and effective wildland fire response requires interregional coordination of suppression resources. We developed a mathematical model to examine how scarce resources are shared. This chapter outlines how we collected and processed the data, set up the model, and applied both to identify best-fit parameters. We interpret model outputs on interregional test cases that reflect the difficult tradeoffs in this resource allocation problem. By regressing a linear system of ordinary differential equations with GIS-data for demand predictors like suppression resource use, ongoing fire activity, fire weather metrics, accessibility, and population density onto pre-smoothed Resource Ordering Status System (ROSS) wildfire personnel and equipment requests, we fit a national scale regression. We interpret these parameters, report additional statistical properties, and indicate how these findings might be interpreted for personnel and equipment sharing by examining test cases for national,

central/southern Rockies, and California interregional sharing. Abrupt switching behavior across medium and high alert levels was found in test cases for national, central/southern Rockies, and California interregional sharing. Workloads are expected to increase over time as well.

(CHAPTER 3) Accumulation of burnable forest fuels is changing natural wildfire regimes. Recent megafires are an unintended consequence. Our capability to suppress unwanted fires stems from a complex national sharing process in which specialized firefighting resources mobilize around the United States. This work elaborated a coupled system of PDE equations and tested them on an archive of risk and allocation data from 2011-2016. This chapter poses a consistent math model for wildfire suppression management that explains how spatiotemporal variation in fire risk impacts allocation. Analogies between the seasonal flow of fire suppression demand potential and dynamics of physical flows are outlined for advection, diffusion, reaction, rotation, and feedback. To orient these mathematical methods in the context of resource allocation, we present multi-fire management examples varying in scope from local demand interactions on the Holloway/Barry Point/Rush Fires in 2012 to large perturbations in national allocation. We prototype objective functions.

PREFACE

The year 2012 was a particularly busy fire season in the United States with engine mobilization 55% and 36% above previous 5- and 10-year averages [NICC.gov/]. The Rush fire in northern California and the Holloway Complex fire straddling northern Nevada and Oregon were the first and third largest fires of 2012 With final contained sizes of 480,850 and 315,577 acres burned respectively, they were managed simultaneously during the month of August. These fires burned in close proximity to one another, straddled state lines, and exhibited periods of extreme fire behavior. An even larger mobilization on the Barry Point fire near the town of Lakeview, Oregon (pop. 2,294) also reached its peak levels on August 21, 2012 with 1,398 total personnel noted in the 2012 Situation Reports [NIFC.gov/]

Assignment data for these fires provides an opportunity to study such large perturbations to the national wildfire suppression system. Moreover, building a model that will respond to incidents and generate data about a suite of actions can help clarify what to do in real life.

This dissertation aims to explore the national level process of wildland fire resource allocation. What is macro- and micromanagement look like in the fire business? Numerical analysis staples help analyze our data in new ways; it is macro- and microscopic fire management. We worked with both ordinary differential equation (ODE) and partial differential equation (PDE) systems models. We solve inverse problems for an ODE system and a parabolic heat-type PDE. This led us to a full calibration and forward prediction problem. We prepared GIS databases amalgamating fire behavior and risk metrics; data citation is made in text.

Residuals and data in our models were analyzed for accuracy, stability, precision, and smoothness. Existence is another, even more important tenant for these dynamical models, but theorems in ODE and PDE theory guarantee it.

Four motivations provided the impetus for this project. First, model realism matters; realistic wildland fire management models are complex. Thus, we used data on resource allocation that is drawn from a national database of resource requests and assignments. In addition, we drew upon historical archives of geospatial time series for fire starts, large fire activity, large fire potential, fire weather, and human infrastructure. Second, visualization helps bridge the gap between PDE math methods and end user. We draw upon accepted practices such as state space reduction, interpolation, and data visualizations that allow us to explore both the raw data and model output. Third, developing a framework that allows for a normative objective function of a data-driven model is crucial to developing a system for examining fire management decisions. Fourth, the model(s) developed must be stable, accurate, and precise. PDEs capitalize on numerical finite difference and finite element schemes that are well-known for the class of parabolic, heat-type equations we find useful.

Given the extent of the data and large scope of the problem, we made headway in small forays in theory and practice. Selection of test cases was incredibly difficult in this dissertation because our data extent $2011 - 2016$ covers many fascinating fire seasons. Within those seasons, there have been costly fires, simultaneous large fires, and countless hours spent on initial attack. We settled on three, local to the United States:

- August 2012 western United States: Holloway, Barry Point, and Rush fires (see above),
- Risk sensitivity in fire demand data for collaborating fire management zones,

- A final scenario is an "all-hands" model for the continental U.S., Alaska, and Hawaii. We used this mode to test data and algorithm limitations at several key junctures throughout the development.

This dissertation provides qualitative information about continuous math models and quantitative information about the data. All data and code are available.

For wildfire management support systems to function, explicit policies must dictate how nationally-shared resources be allocated to meet demand. National resources provide highly qualified fire suppression resources to fires; these resources are often in high demand. For example, members of 112 national Interagency Hotshot fire crews have extensive training and experience responding to incidents around the country, year in and year out. When a Hotshot crew is assigned to a fire, there is an opportunity cost in their absence. As national resources become scarcer, each additional fire resource mobilizes to an incident and becomes unavailable for other work decreases the availability of resources for responding to new incidents. Scarcity increases the chance that a request will go unfilled. As a fire season worsens, the risk of the system being overtaxed compounds. When many incidents are drawing resources, a manager is potentially without critical personnel. To avoid this interagency sharing policy dictates drawdown levels as well as a national ready reserve to balance the workloads.

Dissertation format note: All chapters have been prepared as manuscripts; all references, figures, and tables for a chapter are found at the end of the chapter's main text. Appendices are numbered in sequence with the chapters. This is a multi-part dissertation.

TABLE OF CONTENTS

ABSTRACT……ii
PREFACE……...iv
LIST OF TABLES……..ix
LIST OF FIGURES…….x
LIST OF SYMBOLS…….....…xi
LIST OF ACRONYMS……...…xiii
1. CHAPTER 1 – DYNAMIC SUPPLY AND DEMAND VISUALS……..1 – 29
1.1 Background and motivation……..1
1.2 Data processing…….3
1.2.1 Resource requests and data for risk layers…….4
1.2.2 Visualization of ROSS data……...7
1.2.3 Smoothing procedures……...9
1.2.4 GUI display……..…12
1.3 Long-range allocation…….13
1.4 Regional boundaries……....14
1.5 Risk-contouring versus risk-seeking allocation……..14
1.6 System level objectives……...15
2. CHAPTER 2 – VALUATING FIRE SUPPRESSION RISK DATA……...30 – 66
2.1 Introduction…….30
2.2 Solving an inverse problem for ODE model……...34
2.3 Test cases, U.S. data – 2011 through 2016…….40
2.4 Interregional resource assignment and factor data analysis……43
2.5 Conclusion and discussion……..50
3. CHAPTER 3 – PDE-CONSTRAINED ALLOCATION……...…….67 - 103
3.1 Why PDEs? What is being constrained? Fire management background.....67
3.2 Literature Review……....68
3.3 PDE Model Specification……...73
3.4 Optimization Framework……....76

3.4.1 Continuous Objective Functions……..78
3.4.2 Grid Transformation Procedure……...79
3.4.3 Adjoint Version of PDE and Finite Difference Methods…….80
3.4.4 Inverse Problem for Nodal PDEs…….82
3.4.5 Calibration and Forecast Theory…….….84
3.5 Results of the Adjoint PDE constrained and $\dim = 2$ Optimization Model……..….85
3.6 Conclusion and Discussion...……..90
3.7 Future work……..……...92
4. APPENDICES…….……...……..104 – 121
4.1 RELEVANT FIRE RISK INFORMATION DATA DOCUMENTATION……....104
4.2 WILDFIRE SUPER-COMPLEXES…….106
4.3 BLOCK ASSEMBLY OF REGRESSION MATRICES/VECTORIZATION……108
4.4 LATEX CODEX FOR ALL RISK LAYERS……..……109
4.5 RESULTS OF ODE TEST CASE, AN ALL-GACCS INVERSION PROBLEM..110
4.6 RUN TIME AND DATA SIZE ANALYSIS……...……....113
4.7 RISK STENCILS……..114
4.8 LINEAR PROGRAM RELAXATION…...…….116
4.9 LONG RANGE RESPONSE IN ALASKA ……...…….118
4.10 MODIS EDGE FEATURES……..…….119
4.11 POTENTIAL MODELS IN MOUNTAINEERING…..……120

LIST OF TABLES

TABLE 2.1 – FIRE SUPPRESSION RESOURCES…….53
TABLE 2.2 – U.S. GEOGRAPHIC AREA COORDINATION CENTERS (GACCS)……...53
TABLE 2.3 – PREPAREDNESS LEVEL ARCHIVE PARTITION……53
TABLE 2.4 – ODE EQUATION COUPLING (R,G) = (3,2) ; (3,3) ; (4,3)……..54
TABLE 2.5 – SIGNIFICANT RISK INFORMATION LAYERS ALL-GACC MODEL……...54

TABLE 3.1 – NONLINEAR PROCESS DETAIL……93
TABLE 3.2 – PDE CONSTRAINT MECHANISMS……...94
TABLE 3.3 – REALLOCATION METRIC PENALTIES BY HAND……95
TABLE 3.4 – TEST CASE FAST FACTS……95

LIST OF FIGURES

FIGURE 1.1a – CONCEPTUAL MODEL OF DEMAND PROCESS…….16
FIGURE 1.1b – CONCEPTUAL MODEL OF SUPPLY PROCESS……...16
FIGURE 1.2 – PHASE PLANES…...……..…….17
FIGURE 1.3 – SUPERPOSITION OF DEMAND……18
FIGURE 1.4 – SNAPSHOTS OF SMOOTHED DEMAND, 2012 FIRE SEASON……19
FIGURE 1.5 – SCREENSHOTS OF ALLOCATION DYNAMICS ANIMATION……20
FIGURE 1.6 – DEMAND_RISK_GUI.m CONSOLE……..21
FIGURE 1.7 – GIS DATA ANALYSIS, USE CASE OF DEMAND_RISK_GUI.m……..22
FIGURE 1.8 – RISK-SEEKING VERSUS RISK-CONTOURING MODIS MOCK-UP……23
FIGURE 1.9 – EXAMPLES OF STRESS TO ALLOCATION SYSTEM……...24
FIGURE 1.10 – ROSS REQUEST DATA DETAIL 2011-2016……..25

FIGURE 2.1a – ODE METHOD INPUT DATA……..56
FIGURE 2.1b – LAG STRUCTURE IN THEORY AND PRACTICE……57
FIGURE 2.2 – CENTRAL/SOUTHERN ROCKIES, TYPE 1 FIRE FIGHTERS/ENGINES….58
FIGURE 2.3 – ENGINE ODE COEFFICIENT VARIABILITY……..60
FIGURE 2.4 – TYPE 1 FIRE FIGHTER ODE COEFFICIENT VARIABILITY……62
FIGURE 2.5 – COOPERATIVE DEMAND IMPACT PANEL……...63
FIGURE 2.6 – NORTHERN/SOUTHERN CALIFORNIA, INTERCOMPARISON……..64

FIGURE 3.1 – ADVECTIVE, DIFFUSIVE, REACTIVE (ADR) LITERATURE REVIEW…..96
FIGURE 3.2 – ESTIMATES FOR DIFFUSION AND ADVECTION PARAMETERS…….97
FIGURE 3.3 – ESTIMATED VECTORS AUGUST 15, 2012……...……..…98
FIGURE 3.4 – DEMOBILIZATION SCENARIO……....99
FIGURE 3.5 – PREDICTING $n+1, n+3, n+6$ FOR TYPE 1 FIREFIGHTERS…….100
FIGURE 3.6 – LARGE PERTURBATION DETECTION, COLORED BY DAY 2015……...101

LIST OF SYMBOLS

k vector index
$\kappa > 0$ smoothing parameter
$SLIM$ smoothing in code, $SLIM = 1/\kappa$
Np number of points, referring to problem difficulty

Σ summation
$\forall$ for all

$r,\ R = 1,\ 2, \dots ,\ \#R$ resource type index
$g,\ G = 1,\ 2, \dots ,\#G$ subdomain index
s lag index
$Lag(R,G)$ set of lag intervals
$FACTORS$ set of risk information layers
$\hat{a}_{i,R,G,g}(t-s)$ lagged risk coefficient
$\hat{y}_{R,r,G}(t-s)$ "reinforce/release" coefficient
$\hat{z}_{R,G,g}(t-s)$ cooperative sharing coefficient
$U_{R,G}(t)$ exogenous resource demand
$D_G(t)$ risk data
$D_i(t-s, lx, ly)$ GIS risk information layer
$\overline{\overline{D^s_{i,g}}}(t)$ quadrature average (same for U)
$\overline{D^s_{i,g}}(t)$ non-dimensionalized (also U)
$\overrightarrow{\partial_t U_{R,G}}$ vectorized rate model
$\hat{x}_{R,G} \approx \boldsymbol{A}^{-1}_{R,G}\overrightarrow{\partial_t U_{R,G}}$ inverse problem
N sample size
E number of replicates
$\chi^2_{E-1,0.05}$ 95% confidence in coefficient

t time moment
t_n sample time
Δt time step
Φ potential
$\vec{\Phi}$ vector potential
Φ_D scalar demand potential
$\vec{\Phi}_S$ vector supply potential
U smoothed demand data

Ω spatial domain
$\partial\Omega$ domain boundary
Ω_g subdomain
$\partial\Omega_g$ subdomain boundary
$\hat{n}$ outward, ccw unit normal

dim spatial dimension of problem
$\mathbb{R}$ real line
$\mathbb{Z}$ integers
$\mathbb{Z}^+$ counting numbers
x spatial variate
y second spatial variate
lx degrees NAD83 longitude
ly degrees NAD83 latitude
$\mathcal{T}$ bijective grid transformation
$\begin{pmatrix} \boldsymbol{J}_{11} & \boldsymbol{J}_{12} \\ \boldsymbol{J}_{21} & \boldsymbol{J}_{22} \end{pmatrix}$ numerical grid Jacobian
$\begin{pmatrix} \boldsymbol{H}_{11} & \boldsymbol{H}_{12} \\ \boldsymbol{H}_{21} & \boldsymbol{H}_{22} \end{pmatrix}$ numerical grid Hessian
$\xi = 1, \dots ,\ X$ spatial index
$\eta = 1, \dots ,\ Y$ second spatial index
$\Delta\xi = \Delta\eta = 1$ unit spacing
$\vec{\nabla}$ gradient operator
$\mathcal{G}$ process model to identify
$\mathcal{G}^{-1}$ inverse problem
$\frac{d}{dt}$ ordinary time derivative
∂ partial derivative
$\partial_t, \frac{\partial}{\partial t}$ partial time derivative
∂_x, ∂_ξ partial spatial derivative

i risk index
α_i, β_i risk weights
$\mathcal{R}_i(t,x)$ continuous risk component
$\mathcal{R}^n_\xi$ discrete risk component
$\mathcal{R}$ linear risk mental model
$\vec{\mathcal{R}}$ vector risk
a adjoint coefficient function
$\langle a\xi, a\eta \rangle$ dim = 2 fit field
b diffusive parameter

$[T_0, T_F]$ time interval
$\mathbb{R}^{\dim}, \mathbb{Z}^{\dim}$ higher dimensional spaces

Υ objective function

$\|z\|_p$ norm
λ penalties
ψ dispatch network
L_2 square integrable functions
$\sqrt{RME}$ root mean square error
ϵ error or residual

$\left\|\mathcal{L}(\mathcal{R}, \vec{\mathcal{R}})\right\|_1$ total variation see (Aster, Borchers, and Thurber 2013)

$\Delta_{\text{disc.}}$ Discrete Laplacian see MATLAB

Np-hardness
Non-deterministic polynomial time
A simplex must visit each node

LIST OF ACRONYMS

ADR, advective diffusive reactive
BI, burning index
CGLS, conjugate gradient least squares
CONUS, Continental United States
Demob, demobilization
ERC, energy release component
ETD/ETA, estimate time of departure/arrival
FFT1, firefighter type 1
FFT2, firefighter type 2
FMZ, fire management zone
FOD, Fire Occurrence Database
FS, Forest Service
GACC, Geographic Area Coordination Center
GIS, Geospatial Information System
GUI, graphical user interface
HTML, Hypertext Markup Language
IMT, incident management team
LP, linear program
MATLAB, Matrix Laboratory
Mob, mobilization
MODIS, Moderate Resolution Imaging Spectroradiometer
MW, megawatts 10^6 watts
NAD83, North American Datum 83 projection
NMAC, National Multi-Agency Coordination Group
ODE, ordinary differential equation
OR, operations research
PDE, partial differential equation
PL, preparedness level
PSA, Predictive Service Area
ROSS, Resource Ordering Status System
SMKJ, smokejumper
sys, system
US, United States
USDA, United States Department of Agriculture
WFDSS, Wildland Fire Decision Support System
WindVel, wind velocity

CHAPTER 1 – DYNAMIC SUPPLY AND DEMAND VISUALS

1.1 Background and motivation

The cost of wildland fire suppression is an important problem currently facing the United States. Wildland firefighting currently uses more than 50% of the US Department of Agriculture (USDA) Forest Service (FS) budget, up from 16% in 1995, and firefighting is expected to consume 66% of the agency's budget by 2025 (USDA The Rising Cost of Fire Operations: Effects on the Forest Service's Non-Fire Work, 2015). The cost of wildland firefighting has been increasing for several reasons. First, the past century of fire management has exacerbated fuel loads, leading to larger and more severe wildland fires. (Calkin, Thompson, and Finney 2015) argue the great extent to which the human/fire system is currently out of natural equilibrium, concluding with a suggestion that getting back on track will require clear, yet complicated objectives. Second, wildland fire resource use may be changing, as more expensive resources are in higher demand (Stonesifer et al. 2016). Third, climate change has been lengthening fire seasons, increasing the period during which wildland fires are occurring and increasing the fire load that suppression resources must address (K. L. Riley and Loehman 2016; Westerling 2016). This is an era of tough management calls impacting multiple, competing objectives as we try to let fire burn naturally whenever and wherever possible, while still protecting important infrastructure and human lives.

In this study, resources are defined as the equipment and personnel working on wildland fires. On an individual incident level, the initial response to a fire detection is typically a small team of resources, for example, one to two engines with two to five personnel or a crew of three to twenty people. If a fire is not contained (or let burn with monitoring), the next period of response is referred to as extended attack. Fires under extended attack may require more

resources, for example, several engines and/or crews. If the fire experiences periods of significant growth and/or threatens infrastructure or other values, the fire is typically managed as a large fire, which requires an Incident Management Team (IMT) of fire managers to coordinate the high numbers of resources that work in tandem to contain the fire. During a fire season, many wildland fires may co-occur across the nation, each at varying stages of management. Thus, coordination between local, regional, and national agencies is necessary to manage the allocation of resources across large regions (states, geographic areas, and the country). Currently, during periods of high fire activity and low resource availability, national and regional resource allocation decisions are made by groups of experts convened in multiagency coordination groups. At these high alert levels, the mental models behind these resource assignments are based on years of learned experiences, consequences, and learning contingency pathways. Discussion amongst the coordination group should theoretically lead to a rigorous decision that is defendable to stakeholders. We assumed that numerical evidence exists in the resource allocation data available to show trends and patterns within the decisions made by the national wildland fire allocation experts. Furthermore, we assumed that we can model these trends using a nonlinear process.

Because of the complexity and importance of the resource allocation problem, many mathematical models have been built to examine allocation processes (Ntaimo et al. 2013; Chow and Regan 2011; Wei, Rideout, and Kirsch 2008; Ashe, McAneney, and Pitman 2009). As we reviewed these papers we found problems about allocation of fire suppression resources can be formulated with very different end users in mind. Some are operational and theoretically function in real time. Others are used for slower planning and budgeting tasks. They have end

users that work nearby the flaming fronts needing spatially explicit models. They also have end users far from the flaming front who might be sitting in a regional dispatch office, for instance.

(Martell 2015) reviews the role of operations research (OR) in wildland fire suppression and highlights key OR innovations that, via computer simulation and modeling, have led to better understanding of how multiple, complex objectives, as long as they are rigorously defined, can drive management of wildland fires. Regarding national level resource use in the US, previous works include explorations of trends in fire costs (Hand, Thompson, and Calkin 2016; Liang et al. 2008), an analysis of interregional engine assignments (Belval et al 2017), and an exploration of national airtanker usage (Calkin et al. 2014). Some work has been done to identify state-wide allocations patterns (Wei et al 2017, Lyons et al). Despite decades of past work, mathematical models still have not addressed all aspects of the fire management resource allocation system. (Pyne 2010; Calkin, Thompson, and Finney 2015; Martell 2015) all conclude with calls for additional complexity in math models of the system of wildland fire management. (FIGURE 1.1a) demonstrates a conceptual model of the demand process and (FIGURE 1.1b) does the same for the supply process.

This chapter documents the contents of each data source, presents some of our most interesting findings from our initial data exploration, and describes aspects of the standardization methods we used for GIS data. We will refer to a partial differential equation model as the PDE model as we identify some of its parts.

1.2 Data processing

There are several sources of archived data regarding fire resource use, fire activity and weather. We postulated that drivers of resource allocation, which we call “risk layers” would

include new fire starts, ongoing large fires, the potential for significant fire behavior, and the values that were at risk from fire. Each of these drivers required at least one geospatial database. Such Geospatial Information System (GIS) data are critical to fire decision support systems and research in use around the world and in the United States. For more examples see (Westerling 2016; K. L. Riley and Loehman 2016; K. Riley et al. 2015; Chow and Regan 2011; Duff, Chong, and Tolhurst 2015; Katuwal, Calkin, and Hand 2016). Because we chose to work with multiple geospatial time series data, significant data processing was required.

1.2.1 Resource requests and data for risk layers

If firefighting resources had tracking devices, then the patterns of allocation might be accessed by studying different snapshots of the fire season. However, such tracking data was not available, thus we use the "point presence data" from the Resource Ordering and Status System (ROSS). By point presence, we mean our data show when resources are assigned to a given incident. The ROSS is a database that includes orders for wildland fire resources. The resource orders are extensive, including requests for ground based resources that create fireline (e.g., crews, engines, and dozers), aerial resources that drop retardant or slurry on the fire (planes and helicopters), teams to manage fires (Type 1, 2, and 3 IMTs), and other necessary items such as supplies, camp crews, single firefighters, safety officers, etc. The data were cleaned and tabulated to record approximate locations of resources from 2011 through 2016. We limit our analyses to Type 1 firefighters, Type 2 firefighters, engines, dozers, helicopters, airtankers, Type 1 IMTs, Type 2 IMTs, and Type 3 IMTs. Each request in ROSS includes several key pieces of information: which resource was ordered, the time ordered, and the incident that needed the resource. If the order was filled, then we also have information about the time the resource left

for the fire (MobETD), the time the resource arrived at the fire (MobETA) and the time the resource left the fire (DemobETD).

To simulate tracking data, we used these ETD/ETA time stamps in ROSS. Upon initial assignment, resources travel from their home-bases or current assignments to a requesting incident and begin participating in fire suppression activities. To determine whether the resource went from the previous incident to the new assignment or from their home base to previous assignment we screened each resource's allocation sequence. This correctly flagged the last assignment in a series before heading home. As an example of incident to incident travel: when twelve Type 1 firefighters and ten Type 3 engines were reallocated from the Holloway Fire in Nevada on August 16, 2012 to the Rush Fire in Northern California they listed less than a day's travel. Their MobETD indicates they left the Holloway fire in the morning and the DemobETA shows they arrived at the Rush fire in the early evening. In addition to checking assignments for incident to incident travel, routes are additionally flagged and filtered based on a travel speed switch. Any travel deemed to require speeds faster than 120 mph is flagged as a flight. A filter was applied when speeds in excess of 600 mph were discovered. For routes when driving was the most probable mode of travel, Dijkstra's algorithm from [Kirk 2015, dijkstra.m] worked well to project the start/stop locations onto the Google Earth interstate highway layer (Brown 2006) to determine travel distance. The algorithm used provides "road arcs" that pivot into and out of routes along the highway system and the shortest route is calculated to some tolerance. Using this heuristic to simulate driving paths allowed us to provide our PDE model with locations of resources at any time rather than just at times when they were at incidents.

Fires in different stages of management require different packages of resources. We postulated that fire ignitions draw resources differently than large fire activity and that having

two distinct risk layers in our analysis to represent each individually would provide valuable information as to how resources are allocated. For the fire ignition data we used the Fire Occurrence Database (FOD; Short 2015). The FOD is a geospatial database with the time and location of most of the wildland fire ignitions in the US. While the FOD does include other information including containment date, we chose to only use the discovery date and location, which were used as a proxy for the initial attack fire load. For large fire activity we used the Moderate Resolution Imaging Spectroradiometer (MODIS) database. MODIS provides several layers of geospatial data sensed using a satellite. We filtered 1.01 square kilometer resolution MCD14ML 2011-2016 files for detection confidence > 80%. It is thought the fire's radiative power is about 14 $\pm$ 3% of its total power (Wooster M. J. et al. 2005). We used MATLAB's scatteredInterpolant class of splines to re-grid the data in two steps. We clustered adjacent pixels within ~30 km radius and finally took the maximum for the interpolant. Fire radiative power is measured in Megawatts (MW); typical large fires radiate on the order of one thousand MW per day with a typically large fire producing thousands of them. Further information about MODIS data and its use can be found in (Mangeon et al. 2016; Giglio, Schroeder, and Justice 2016).

Fire managers are often risk averse (Wibbenmeyer et al. 2013). This can result in decisions to hold onto resources in case of a future fire event or order resources in advance of fire growth, or managers may also order during periods of significant fire growth activity. To test the effect of the potential future fire load, current fire conditions, and fire weather on resource allocation, we included the energy release component (ERC), burning index (BI) and wind velocity as risk layers in our analyses. ERC is a measure of the estimated energy that may be released per unit area at the head of a fire. BI is a measure of fire intensity. The wind velocity data were processed to create both scalar and vector maps. Higher windspeed tends to

correlate with faster and more intense fire growth. ERC, BI, and wind velocity data were translated from 585×1386 grids, see (Abatzoglou 2013).

Past studies (Hand et al. 2014; Calkin et al. 2011; Donovan and Rideout 2003) have identified human population as key indicators that fires will cost more. We postulate that human population will also influence resource allocation to fires. Many geospatial databases include information about where humans and their infrastructure are located on the landscape. For example, fire behavior analysts have GIS infrastructure layer-by-layer available in the Wildland Fire Decision Support System (WFDSS) (Calkin et al. 2011) and maps of the varying densities of the wildland urban interface configuration in the area. To provide a single, consistent estimate of where the presence of human population is found, we chose to use the Landscan global population distribution model for the US (Landscan, https://web.ornl.gov/sci/landscan/landscan_documentation.shtml). While populations may have changed from 2011-2016, we used a static layer throughout. The layer is called LSNITE. Another static GIS layer described interstate highway transit time. We built this layer using Google Earth to trace over six hundred interstate highways, save HTML data from these files, and the extracted their longitudes and latitudes for processing in MATLAB. For one, we used the roads structure as a model of the sharing network. For two, we computed a unitless arrival time value between 0 and 2. A "0" means right on the highway and a "2" is far from the highway. This layer is called geDIST. For full data listing see APPENDIX 4.1.

1.2.2 Visualization of ROSS data

Our first analysis is an aspatial study of discrete allocation counts from ROSS. A "phase plane" analysis is often used to understand how dependent variables change over time in the model. (FIGURE 1.2) shows a two-dimensional phase plane comparing Type 1 firefighter and

Engine allocation levels at each day from May 8, 2012 through October 10, 2012. It demonstrates important temporal equilibrium points: start and stop of season and how peak workloads might lag peak fire detection with long memory. The next phase plane includes fire starts. Here we see the lag between peak fire detection and peak allocation is well over a month. Top counts of fire starts occur in early July, while the maximum allocation takes place between August 13 and 20.

Phase plane visualizations of resource counts highlight three aspects of fire management dynamics. One, cooperation is a critical component of fire management. Each fire requires a certain suite of resource types to manage it; these packages of resources may vary together. For example, in (FIGURE 1.2) we observe an approximately linear relationship between engines and Type 1 firefighters on assignment. However, this does vary throughout the season. A measurement unit of ± 350 Engines is shown on the phase plane. This can be used to compute various balances throughout the season. Early season, the phase plane shows relatively more Type 1 firefighters. In early June, Engine assignments catches up. After the peak allocation during August 13 – 20, there is a demobilization of more than a dozen full crews followed by a rapid release of Engines. Two, each fire season has an absorbing state of the lowest allocation levels at their start and end. That the sharing system will experience times of quiescence is an element of the data that cannot be ignored. There is day-to-day quiescence at night. Some longer periods of quiescence can last days or weeks. The end of the season is the longest period of down time, even though fire starts occur in winter months too. Down times represent an opportune chance for re-allocation that is known to be effective (Ager and Finney 2009) (Chow and Regan 2011). Three, cycling behavior in national and regional workloads observed in these plots is an important consideration. During specific points during the season, workloads appear to surge.

By first understanding when and why these occur, then staggering our response appropriately, the system can be as efficient as possible.

Another visualization that helped us examine allocation data was an animation of resources as they moved around the country. Using the estimated travel paths from the ETA/ETD times, incident/home base location, and Dijkstra's algorithm, we mapped the resource movements across fire seasons. These animations revealed some interesting patterns. First of all, the animation shows nightly quiescence. Few resources travel at night in our approximations. Second of all, preparedness level contrasts between the regions are apparent. During high alert, allocation is busy. In low alert, allocations are sparser. Third, to assess interregional sharing is difficult. We found it productive to think of a lung function model with one region "breathing" resources to another compartment. Four, approximate ranges of each type of resources are evident. Type 1 firefighters travel the furthest, followed by Engines, then Type 2 firefighters. Dozers move with short range allocations.

1.2.3 Smoothing procedures

The data used in these analyses was of differing continuity, some was point presence data (ROSS), some were gridded. Thus, an important step in data processing was the continuization of discrete data. This is typically called smoothing, interpolation, or kriging. We found it advantageous to work with smoothed data when drawing maps, testing our intuition about resource movement in the PDE model, and testing prototypes based on similar PDE models in other fields. One disadvantage of smoothing the data is continuized data represent more numbers to store and organize than a count-based archive. We smoothed across both time (t) and space (x, y) using contemporary matrix storage methods and column-based re-indexing for vector GIS data.

The following example demonstrates how we smoothed the ROSS data: Say resource R is a fire engine in Black Hills National Forest dispatch (see Fire Management Plan). The smoothing coefficient κ in our model can change the resolution of demand hotspots (Short et al. 2010). When there is a single fire demand for four engines, we might see the demand for R is about 4.28 when integrated over space x. Smoothing κ broadens the discrete estimate, but the original 4 is not irrecoverable. In contrast, when four fire engines are allocated to four fires, κ creates a smoothing bias in demand to be lower when these incidents are in close proximity and κ causes overlaps.

In (FIGURE 1.3) we observe "wildfire super-complexes": when multiple, nearby incidents of managed wildfire results in a single spike of resource demand. For example, large regional demand introduces greater bias in the smoothed demand average than smaller regional demand. Isolated incidents of fire can add into the single spike as well. Theoretically, this smoothing is an approximation to Dirac-δ bumps. Radially symmetric basis functions help share the information about super-complexes.

A summary of the smoothing routine we used follows:

Let $U(t_n, lx_0, ly_0)$ be the demand from ROSS at time t_n at location (lx_0, ly_0). Then:

<u>Smoothing based on full-width-half-max κ:</u>

For fixed time step t_n, suppose request coordinates at (lx_0, ly_0),

Smooth bump with $U(t_n, lx_0, ly_0) = 1$ and decay $U(t_n, lx, ly) = e^{-[(lx-lx_0)^2+(ly-ly_0)]^2/\kappa}$,

Suppose $k = 1, \ldots, K$ additional requests at (lx_k, ly_k)

$$U(t_n, lx, ly) = U(t_n, lx, ly) + \sum_k e^{-[(lx-lx_k)^2+(ly-ly_k)^2]^2/\kappa}$$

This procedure can be implemented in any coding language, see APPDENIX 4.2 for a prototype.

Note that as $\kappa \to 0$ ($SLIM = 1/\kappa \to \infty$ in code), there is a Dirac-δ spike at each (lx_k, ly_k) for $k = 0,\ 1,\ \ldots,\ K$. As $\kappa \to \infty$ the model is oversmoothed and we lose the request locations. We set κ to be slightly smoothing ($SLIM \in [2.25, 9.998]$ in code) so that spikes are distinguishable, but clusters of requests can aggregate as a model for urgency in super-complexes.

For our smoothed animations, we displayed sequential pictures of allocation configurations in $\dim = 2$, using a smoothing parameter $\kappa = 5.54$ in most of our trials. Thus, the smoothed count density location data was attained from radial basis function smoothing (Evans 2010). Two instances of abstract math theory apply here: Monge-Kantorovich equations help explain energetics in the system and how the PDE will be related to some allocation equilibrium, if it exists. Economics models also feature PDEs (see Black-Scholes type model), but assign their variables specific meanings that are not being defined or explored here.

Even with a small set of GIS information layers, a purely discrete network approach to solve allocation would be Np-hard. That is, an optimal allocation would only be discoverable in non-deterministic polynomial time. Since the network solution would ultimately rely on assessing both risks and allocation levels at each node, the numerical solver would need to visit each node of search tree to determine the optimal. A more rigorous proof of this assertion might use combinatorial counting of index-spaces as Abelian groups, see (Galois 1959; Stewart 1998) for more information about these spaces. As a consequence, the large state spaces are tough to analyze and require modifications to solve.

Smoothing forces an intentional biasing of count-based ROSS data so that maps accentuate regional demand hotspots. Smoothing also to produces nice visuals. In order to identify the PDE system model for the problematically large and complex state space of the fire

management problem, visualization of smooth models was important. They helped us define the optimal state for this non-physical potential problem and deal with the lack of any continuous statistical mechanical limit. We later demonstrate how realistic visualization helps users to compare many normative options. (FIGURE 1.4) demonstrates an example of smoothed demand, which can be compared with (FIGURE 1.5) to show how the count data was smoothed to create a continuous surface. Like the animation of resources moving to and from fires, an animation of smoothed demand can provide several insights into ROSS data.

The smoothed demand revealed several components of ROSS that count data might mask. First, many allocations appear on or near the boundaries of management regions. ROSS is required for use when requesting resources across regional boundaries, but not required for use when resources are sent either to their own locality or a jurisdiction with which their home unit has a "neighborhood agreement." Thus, ROSS data may be biased toward resource use at boundaries of management regions. Second, the animation of smoothed demand does well to capture the seasonality present in almost all of our fire data; we observe large spikes and areas of large demand moving across the country to match regional. Third, since the basis functions used to smooth the data are fit one-per-incident, superposition of demand potential on nearby incidents create realistic large perturbations in ROSS.

1.2.4 GUI display

The graphical user interface (GUI) tool to interact with fire data layers is shown in (FIGURE 1.6). It has the following features:

- Side-by-side demand and risk axes with scaled colorbar,
    - Filled contourf.m or custom scatter3.m filled rectangle render modes

- Sample day menu, forwards and backwards step buttons,
    - Works with sequential or non-sequential days
- Resource type menu to select between firefighters, engines, dozers, aerial, and IMT
    - Shows thumbnail image of current settings
- Geographic Area Coordination Center (GACC) map menu
- Risk layers to specify GIS information to plot
    - Both GACCs and risks can be empty, in which case an empty grid is rendered

The GUI was an invaluable asset in model development. It was quick to load GIS data to check smoothing and troubleshoot storage problems.

1.3 Long-range allocation

Our initial analyses included Alaska; Alaska has its own wildfire management resources and it connects to and influences the interregional sharing network. For example, in April 2015, Alaska experienced some uncharacteristically early fire demand. As a result, they ran out of Type 2 firefighters and requested an additional 400. However, firefighting is seasonal work with many jobs coming online for full-time work in April; many of the available Type 2 firefighters did head to Alaska, but these 400 orders could not be filled. As this example demonstrates, Alaska can affect the pool of interregional resources. However, the Alaskan season is earlier than that of most of the CONUS, and typically the effect of fire activity in Alaska on national allocation is fairly minimal. Even in April 2015, the use of firefighters in Alaska did not seem to cause undue scarcity in the rest of the country. Unfortunately, several of our risk layers are missing data in Alaska, thus, we sometimes excluded it from our statistical analyses.

The extreme case of Alaskan interregional allocation led us to consider an important flaw of the physics-based model without a coupled network. PDE dynamics rely on continuous transfer of information. Demand interactions need to benefit from an action-at-a-distance principle. This is usually not included in a standard PDE system. Fortunately, a PDE also has an associated energy optimization problem, which we will leverage to incorporate a sharing network. Unless some penalty for long-range allocation is assessed in the optimization will be over-sensitive to long range demand.

1.4 Regional boundaries

(FIGURE 1.7) shows a historical super complex scenario. The map panel shows complete information about fire heat and growth. The four panels of GIS risk data bring this regional boundary area into detail. There are three fires. The Holloway fire is a complex of several smaller fires. Conditions are hot and dry. The GIS risk data maps give further detail about changes in the burning index of fuels. It shows southern Nevada is +38.9 BI than the previous day. By convolving geDIST with the MODIS layer we get a sense of how far these large fires are from the interstate. Finally, regional wind patterns are paramount risk information for fire managers. High winds can fan the flames and changes in the wind (as shown) can channel the flames in new directions. Both circumstances make the fire difficult to suppress.

1.5 Risk-contouring versus risk-seeking allocation

(FIGURE 1.8) shows how geometry of GIS data surfaces might interpreted in the PDE. It is a false elevation plot of MODIS fire radiative power as an interpolated surface. These data are for August 15, 2012. A cluster max fire detection on the Rush fire reaches 900 MW. A known reallocation took-place from the cooler Holloway fire to the Rush incident in California.

The surface is a false elevation because it is smoothed across space. Only dots have real heat, the interpolated surface shows differences between nearby fires.

1.6 System level objectives

We explored non-cost objective functions. Wildfire suppression allocation seeks a steady state in which resources rotate and shuffle efficiently. During busy times there is stress to the national system. Lastly, we performed a data exploration of system level objectives.

(FIGURE 1.9) shows count-based time series metrics. In (FIGURE 1.9a) we study unable to fills in 2010. At this time, the Great Basin (now managed jointly) was subdivided into two GACCs. There was the Eastern Great Basin Coordination Center (EGBCC) and Western (WGBCC). In August there are a number of requests. Our research treats this as a true scarcity event. (FIGURE 1.9b) shows the three fire super-complex resulting in substantial Cancelled Unable To Fill Requests for Type 1 firefighters. It was a large perturbation and impacted the rest of the system. A similar event is occurred in the Northwestern Coordination Center and is well documented in (Lyon et al. 2017).

(FIGURE 1.10) shows ROSS counts. Notice in 2011 early season there was a prominent switching behavior mid-season in the Southwestern Coordination Center. SWCC managers are subject to a dual, monsoonal-based fire season so their work arrives in two batches.

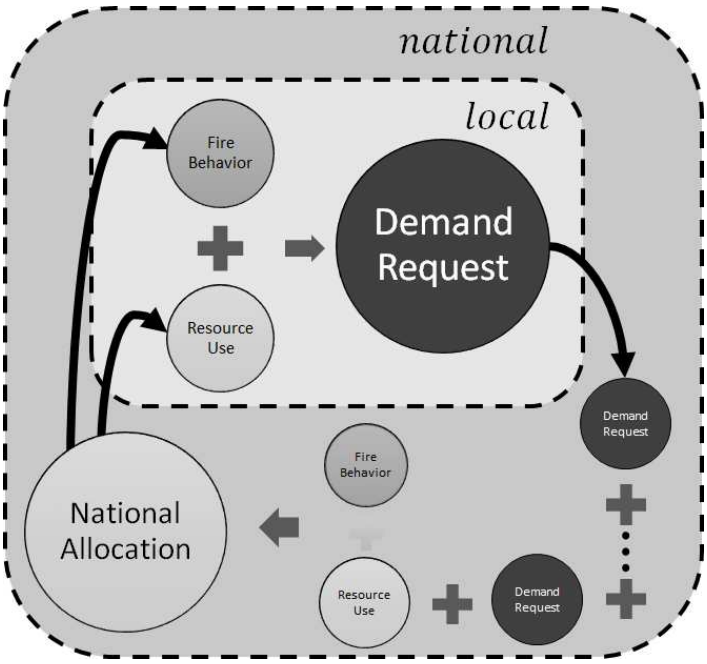

FIGURE 1.1a - Conceptual model of demand process

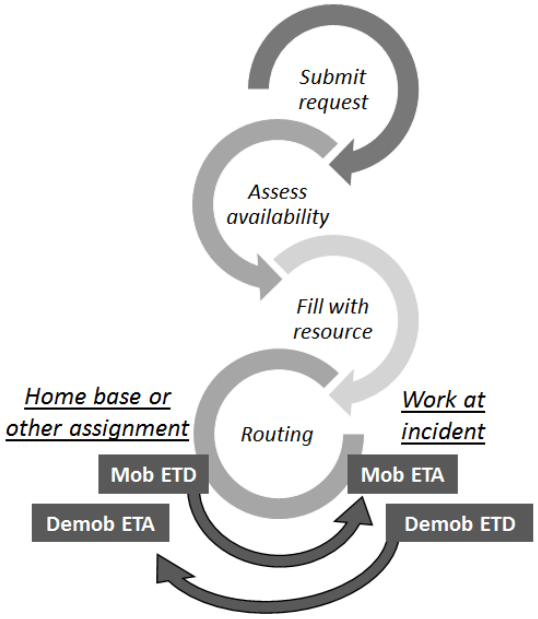

FIGURE 1.1b - Conceptual model of supply process

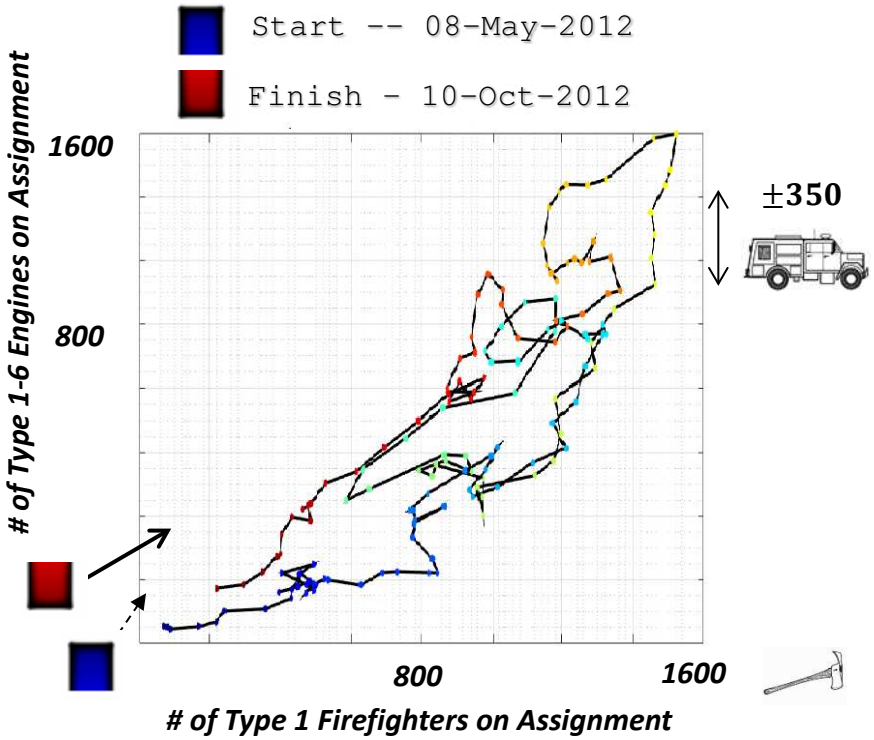

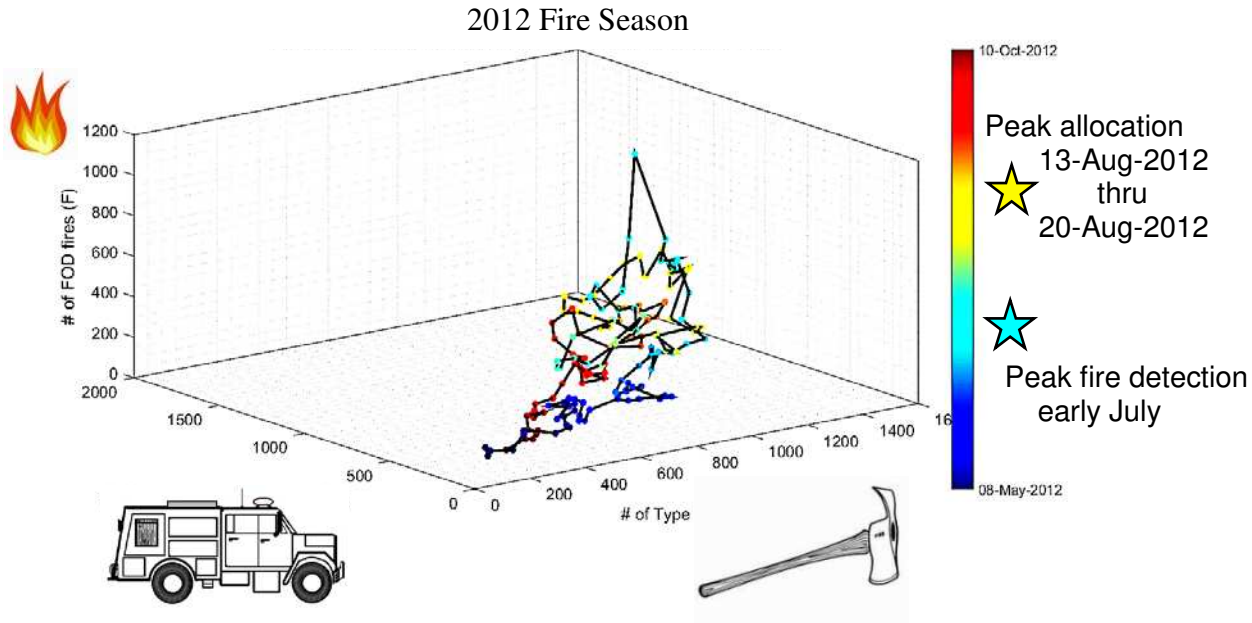

FIGURE 1.2 Phase planes - Type 1 firefighter and engine allocation during 2012 fire season

Caption: Ordinary differential equation analysis often begins with the phase plane.

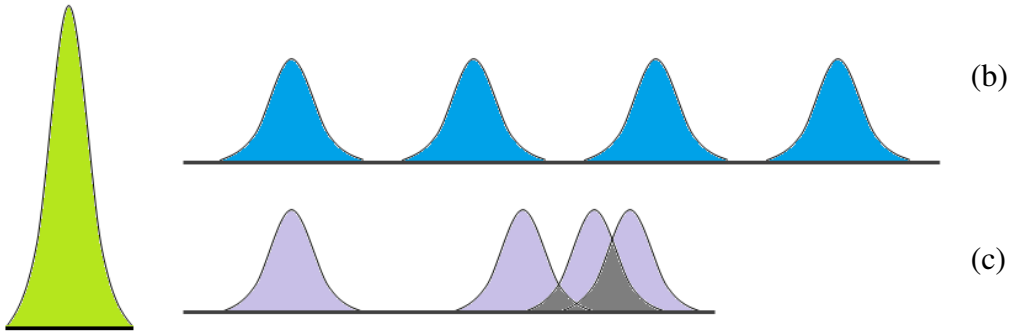

(a)

(b)

(c)

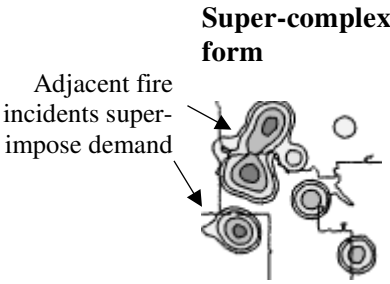

(d)

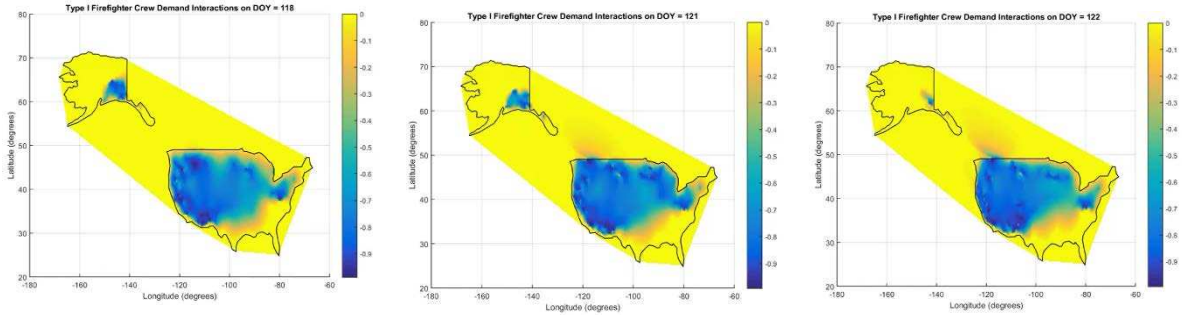

(e)

FIGURE 1.3 - Superposition of demand in $\dim = 1$, $\dim = 2$, and $\dim = 2 + 1$ for time

Caption:

Shows how fixed smoothing $\kappa > 0$ generates demand hotspots. In $\dim = 1$ (a) Spike in demand for many resources gives a slightly different estimate than (b) disparate demand. In turn, (c) shows a double-count bias for adjacent fires. (d) $\dim = 2$ Adjacent fire incidents super-impose demand. (e) $\dim 2 + 1$ for time. Overall, this shows the value of a quadrature-based approach smoothed averaging.

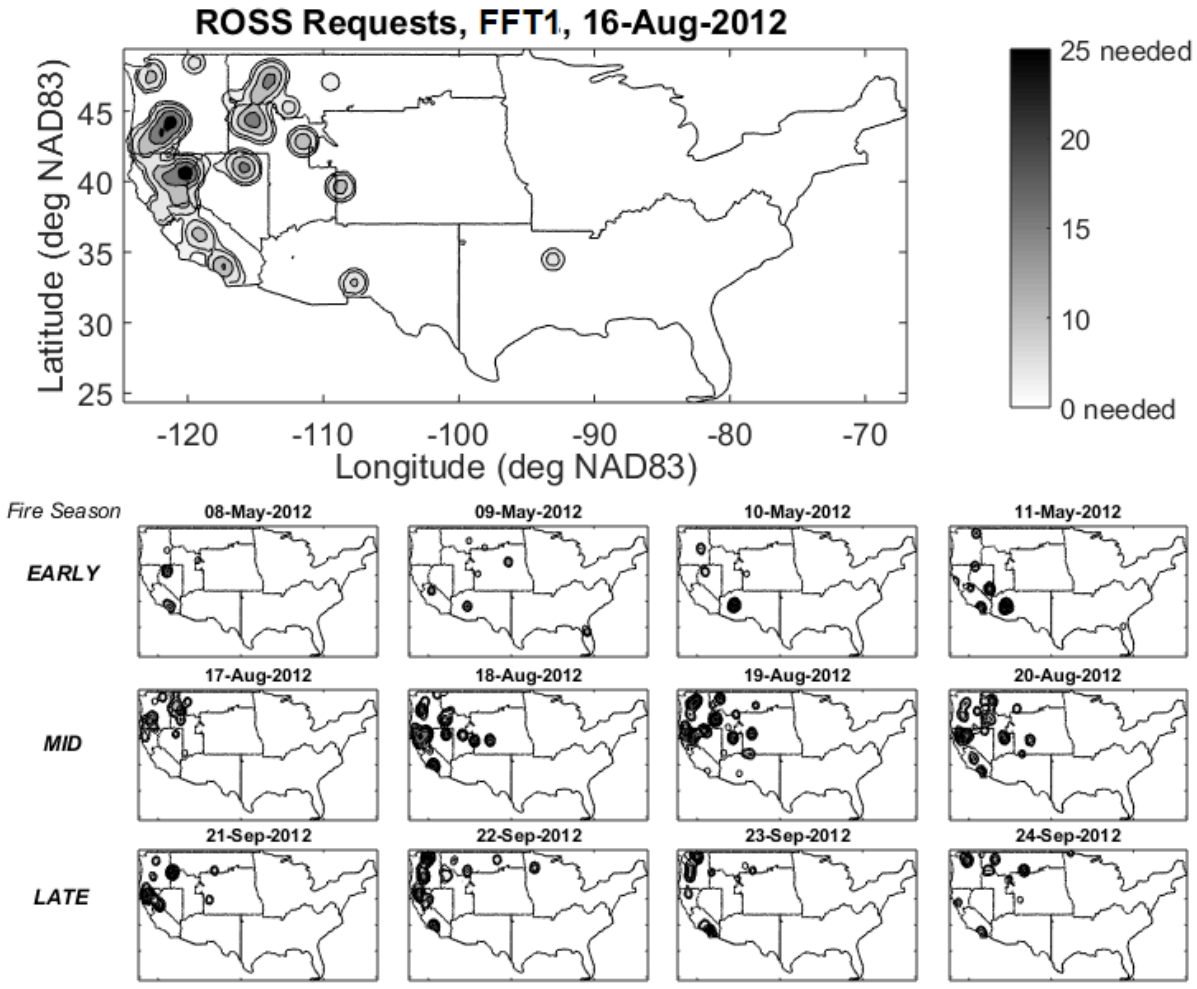

FIGURE 1.4 - Snapshots of smoothed demand, 2012 fire season

Caption:

Wildfire super-complexes also interact. August 16th, 2012 was a very tricky national allocation day in the archive. We chose this as a characteristic scenario for national PL 5 days in particular. Any day of the season is available for analysis.

Type 1 Firefighters, FFT1 ● & Type 2 Firefighters, FFT2 ■ & Engines ★ & Dozers ◆

Movement across regional Preparedness Levels 1 2 3 4 5

Sequence: August 15, 2012 16 17 18 19 20

AM

1200

PM

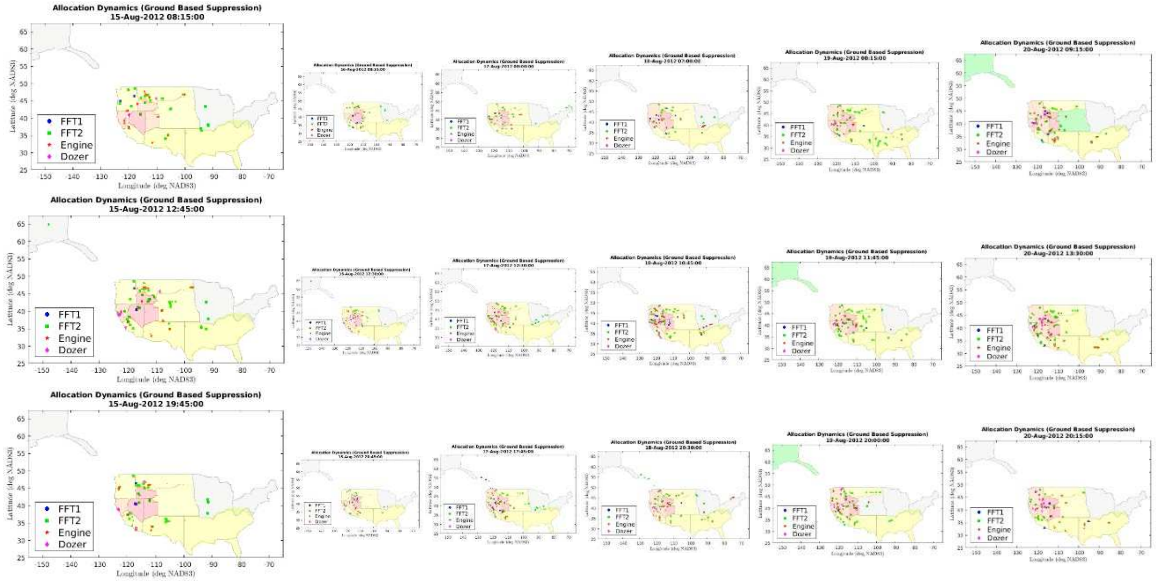

FIGURE 1.5 - Screenshots of allocation dynamics animation

Caption:

Single sample of days, see also (VIZ). Since the animation can be played forward and backward, time is an important independent variable to fully explore. (single frame) Snapshot of en-route assignments of four resource types in different colors.

(rows) From morning sample times in first row, near midday in second row, and between 7:45 pm and 11:45 pm. Along rows observe most travel is taking place in the morning, although resources in motion were observed at all hours of the day.

(columns) Sequence days August 15, 16, 17, 18, 19, and 20 of 2012. Calibrating $[PDEsys - LP]$ would help predict beyond August 21, 2012.

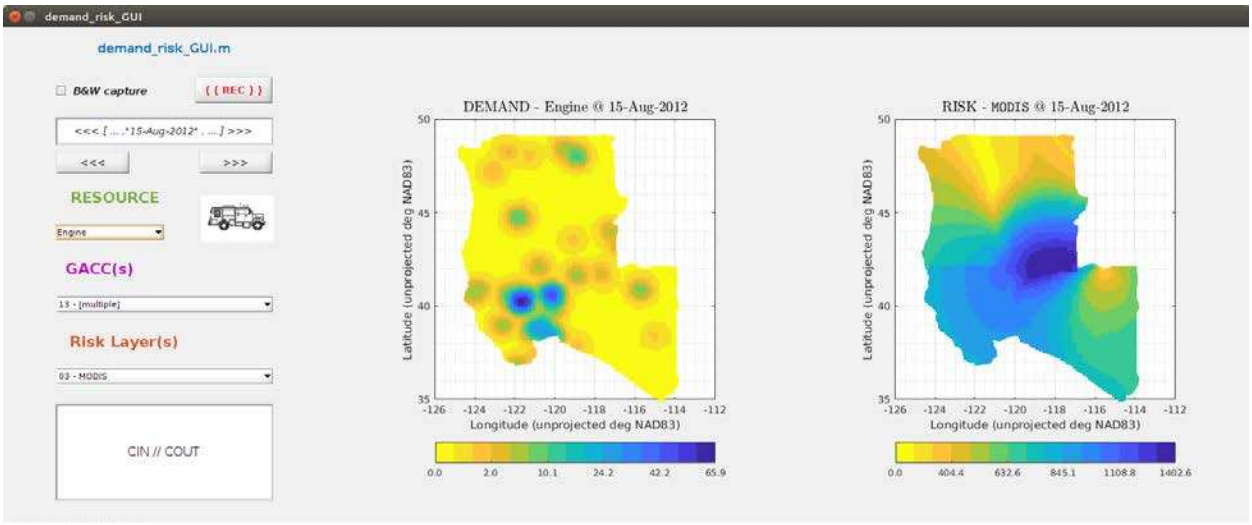

FIGURE 1.6 -demand_risk_GUI.m console

Caption:

This graphical user interface (GUI) was an important analysis tool for smoothed GIS data. (left panel) Demand hotspots and (right panel) interpolated MODIS fire radiative power, large fire risk. On August 15, 2012, the Rush Fire is requesting dozens of Engines even though the Holloway complex is still burning hot.

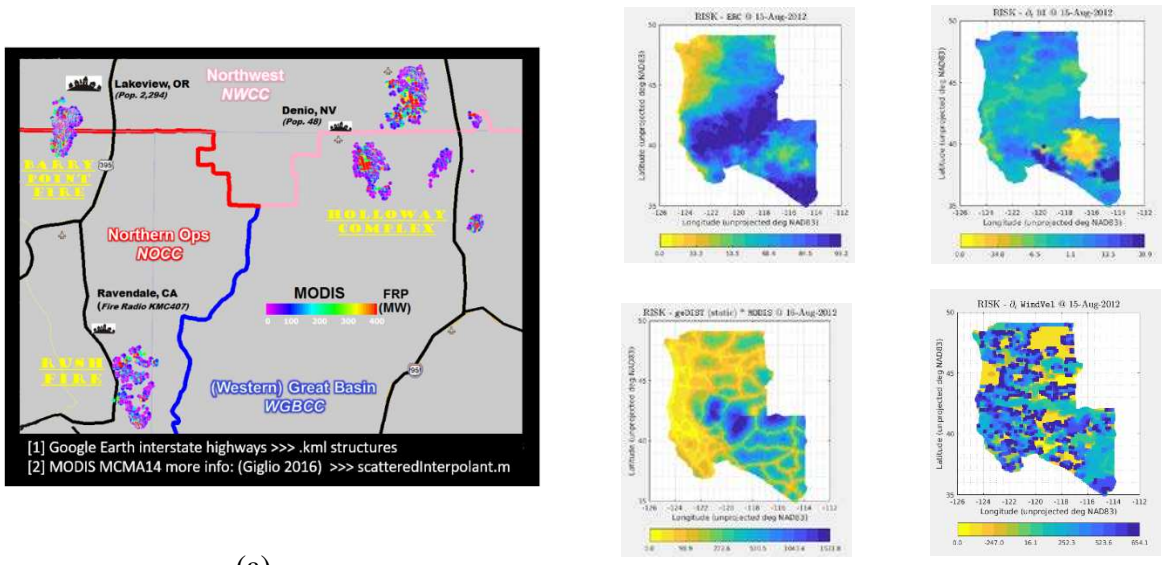

(a)

(b) (c)
(d) (e)

FIGURE 1.7 - GIS data analysis, use case of demand_risk_GUI.m

Caption:

National management of a historical scenario. (a) Three large fires and interstate highway access in August 2012. Dot color on map corresponds to fire radiative power FRP in megawatts, 10^6 $watts$ in SI standard units. These fires are nearing their containment and have exhibited extreme fire behavior to grow so large. Ongoing management by the three Geographic Area Coordination Centers highlighted would have to demobilize resources based on RISK assessment, modeled here with map-based information:

(b) the Energy Release Component (ERC) of fuels (Abatzoglou 2013) [darker] showing index levels near 90 for hot dry area overall

(c) change ∂_t since yesterday in Burning Index, wetness event showing in [yellow], but southern Nevada large change in expected fire behavior $+38.9$ points within a single day.

(d) "How hard are these fires to get to/from?"

(e) Frontal weather patterns producing marked changes in wind velocity [darker] versus areas of steady winds over eastern Washington in the Spokane area (also fire prone)

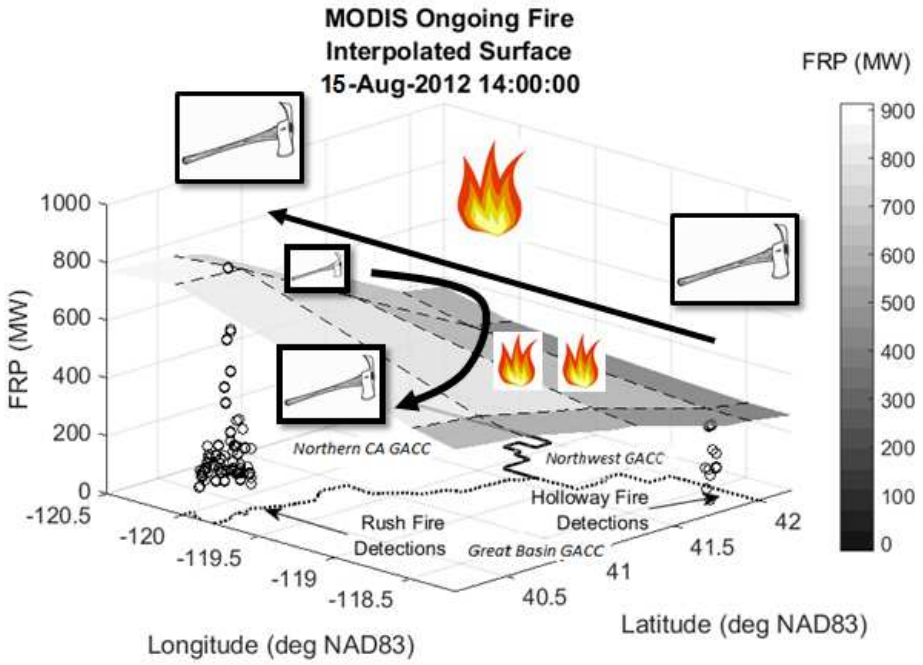

FIGURE 1.8 - Risk-seeking versus risk-contouring MODIS mock-up

Caption:

A false elevation plot of MODIS fire radiative power interpolated surface. As the surface patch color get lighter, cluster max fire detection on the Rush fire reaches 900 MW. These data are for August 15, 2012. A known reallocation took-place from the cooler Holloway fire to the Rush incident in California. The surface is a false elevation because it is smoothed across space. Only dots have real heat, our surface shows differences between nearby fires.

Firefighters are trained risk-seekers, but also know the value of keeping one's distance from a particularly hot fire. National allocation scales. Sometimes, the best option will be to seek the heat. Other times, a pre-positioning to confront future risk might be better.

This prototypes how supply and demand couple in a PDE version of this problem. Unfortunately, the eventual PDE will be more cumbersome for it, but the mechanism is clear.

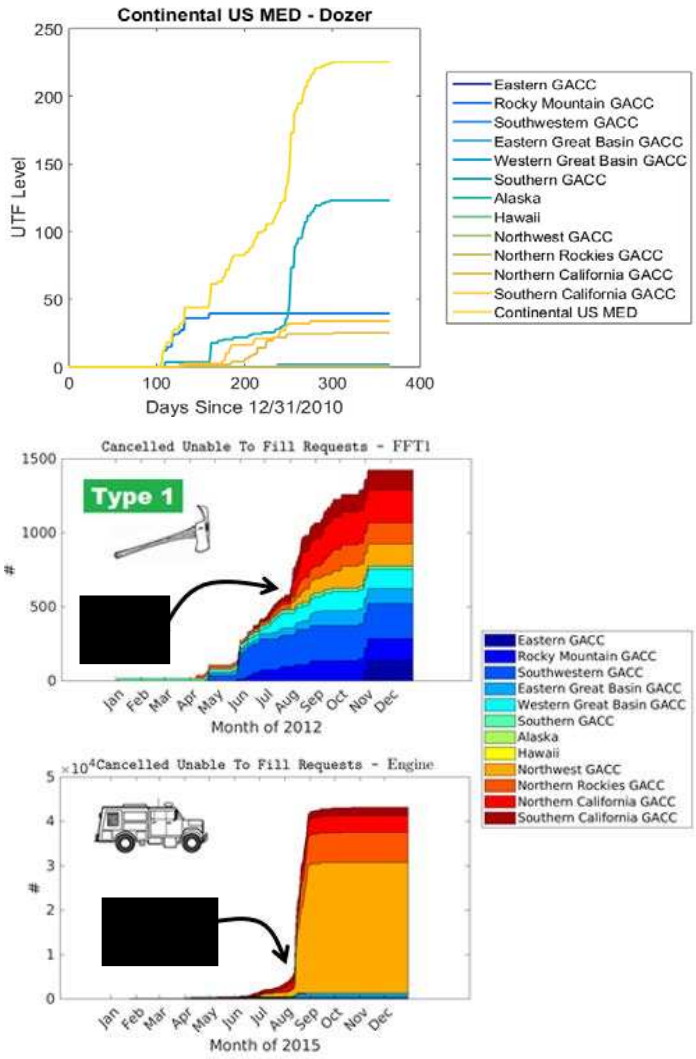

FIGURE 1.9 - Examples of stress to allocation system

Caption:

a. Nearly 50 unable to fill (UTF) Dozer requests in early season Eastern Great Basin GACC. Around 100 in late season Western Great Basin GACC. As true unable to fills further analysis would be warranted into this behavior.

b. Large perturbations in ROSS, marked $(*)$ and $(**)$

$(*)$ 2012, Arrow points to knee where Holloway, Barry Point, and Rush fires contributed or caused substantial unable to fills in August

$(**)$ 2015, the Northern Rockies and Northwest saw such heightened demand for Engines that the normal $fill : unfilled$ ratio of $23:1$ changed rapidly to $2:3$. This corresponds with large fire activity in late August and September (Lyon et al. 2017)

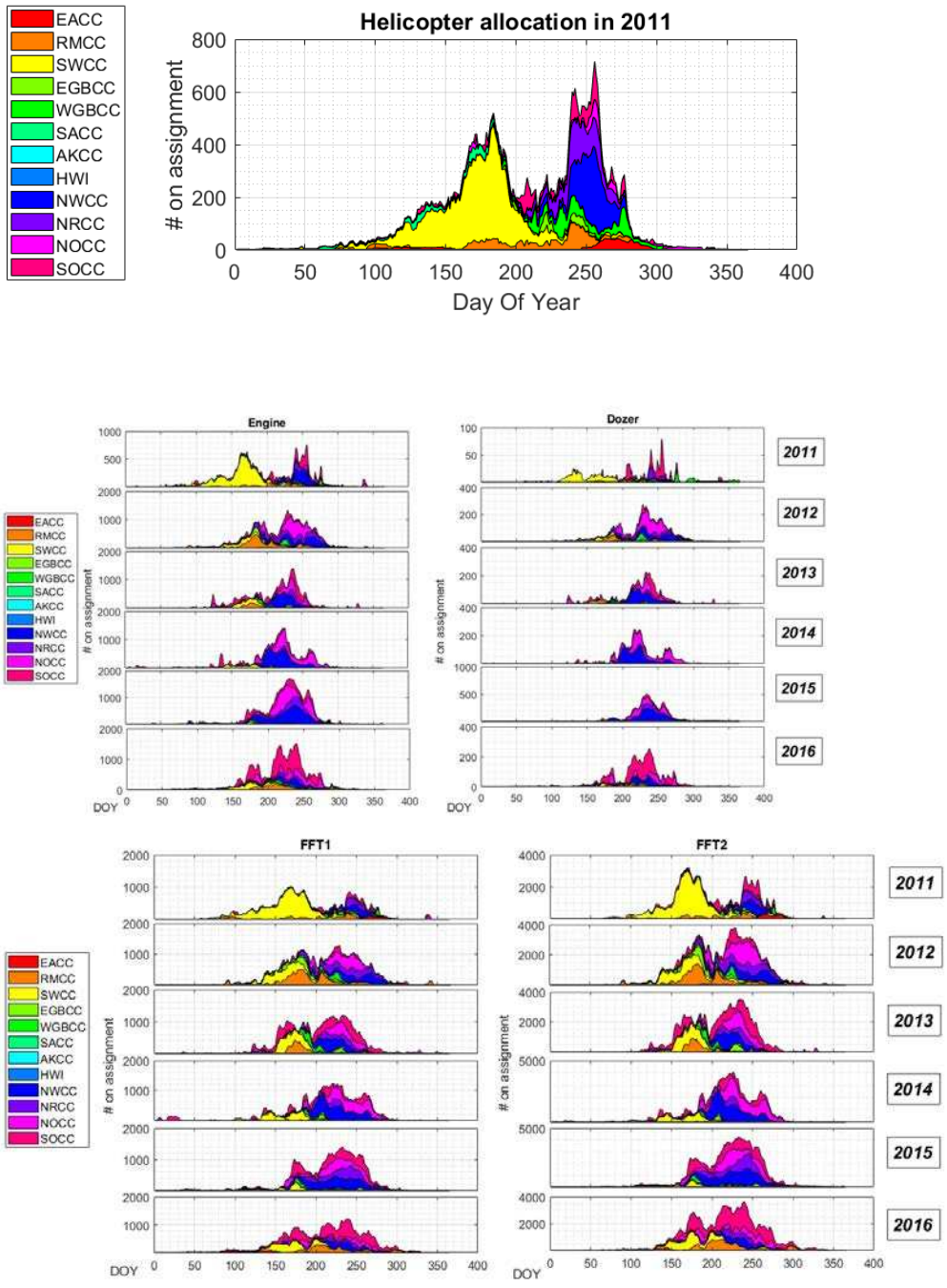

FIGURE 1.10 - ROSS request data detail, 2011-2016

Caption:

(Top) Filled requests can also help track patterns of allocation. Here the system balances early season Helicopter use in the southwestern U.S. with late season use elsewhere. (Middle and bottom) Description of ROSS levels for Engines, Dozers, FFT1s, and FFT2s.

REFERENCES FOR CHAPTER 1

Abatzoglou, John T. 2013. "Development of Gridded Surface Meteorological Data for Ecological Applications and Modelling." *International Journal of Climatology* 33 (1): 121–31. https://doi.org/10.1002/joc.3413.

Ager, Alan A., and Mark A. Finney. 2009. "Application of Wildfire Simulation Models for Risk Analysis." *Geophysical Research Abstracts. 11: EGU2009-5489.* https://www.fs.usda.gov/treesearch/pubs/42278.

Ashe, Brian, K. J. McAneney, and A. J. Pitman. 2009. "Total Cost of Fire in Australia." *Journal of Risk Research* 12 (2): 121–36. https://doi.org/10.1080/13669870802648528.

Brown, Martin C. 2006. *Hacking Google Maps and Google Earth.* Indianapolis, IN: Wiley.

Calkin, David E., Crystal S. Stonesifer, Matthew P. Thompson, and Charles W. McHugh. 2014. "Large Airtanker Use and Outcomes in Suppressing Wildland Fires in the United States." *International Journal of Wildland Fire. 23: 259-271.*, 259–71. https://doi.org/10.1071/WF13031.

Calkin, David E., Matthew P. Thompson, and Mark A. Finney. 2015. "Negative Consequences of Positive Feedbacks in US Wildfire Management." *Forest Ecosystems. 2:9. Doi: 10.1186/S40663-015-0033-8.* 2 (9). https://doi.org/10.1186/s40663-015-0033-8.

Calkin, David E., Matthew P. Thompson, Mark A. Finney, and Kevin D. Hyde. 2011. "A Real-Time Risk Assessment Tool Supporting Wildland Fire Decisionmaking." *Journal of Forestry* 109 (5): 274–80. https://doi.org/10.1093/jof/109.5.274.

Chow, Joseph Y.J., and Amelia C. Regan. 2011. "Resource Location and Relocation Models with Rolling Horizon Forecasting for Wildland Fire Planning." *INFOR: Information Systems and Operational Research* 49 (1): 31–43. https://doi.org/10.3138/infor.49.1.031.

Donovan, Geoffrey H., and Douglas B. Rideout. 2003. "An Integer Programming Model to Optimize Resource Allocation for Wildfire Containment." *Forest Science. 49(2): 331-335*. https://www.fs.usda.gov/treesearch/pubs/23594.

Duff, Thomas J., Derek M. Chong, and Kevin G. Tolhurst. 2015. "Using Discrete Event Simulation Cellular Automata Models to Determine Multi-Mode Travel Times and Routes of Terrestrial Suppression Resources to Wildland Fires." *European Journal of Operational Research* 241 (3): 763–70. https://doi.org/10.1016/j.ejor.2014.09.019.

Evans, Lawrence C. 2010. *Partial Differential Equations*. 2nd ed. Graduate Studies in Mathematics, v. 19. Providence, R.I: American Mathematical Society.

Galois, E. 1959. "On Groups and Equations and Abelian Integrals." *A Source Book in Mathematics (Ed. DE Smith). New York: Dover*, 278–285.

Giglio, Louis, Wilfrid Schroeder, and Christopher O. Justice. 2016. "The Collection 6 MODIS Active Fire Detection Algorithm and Fire Products." *Remote Sensing of Environment* 178 (June): 31–41. https://doi.org/10.1016/j.rse.2016.02.054.

Hand, Michael S., Krista M. Gebert, Jingjing Liang, David E. Calkin, Matthew P. Thompson, and Mo Zhou. 2014. "Economics of Wildfire Management: The Development and Application of Suppression Expenditure Models." *Springer Briefs In Fire. New York, NY: Springer. 71 P.* https://doi.org/10.1007/978-1-4939-0578-2.

Hand, Michael S., Matthew P. Thompson, and Dave Calkin. 2016. "Examining Heterogeneity and Wildfire Management Expenditures Using Spatially and Temporally Descriptive Data." *Journal of Forest Economics. 22: 80-102.* 22: 80–102. https://doi.org/10.1016/j.jfe.2016.01.001.

Katuwal, Hari, David E. Calkin, and Michael S. Hand. 2016. “Production and Efficiency of Large Wildland Fire Suppression Effort: A Stochastic Frontier Analysis.” *Journal of Environmental Management* 166 (January): 227–36. https://doi.org/10.1016/j.jenvman.2015.10.030.

Liang, Jingjing, Dave E. Calkin, Krista M. Gebert, Tyron J. Venn, and Robin P. Silverstein. 2008. “Factors Influencing Large Wildland Fire Suppression Expenditures.” *International Journal of Wildland Fire. 17: 650-659.* https://www.fs.usda.gov/treesearch/pubs/31571.

Lyon, Katie M., Heidi R. Huber-Stearns, Cassandra Moseley, Christopher Bone, and Nathan A. Mosurinjohn. 2017. “Sharing Contracted Resources for Fire Suppression: Engine Dispatch in the Northwestern United States.” *International Journal of Wildland Fire* 26 (2): 113–21. https://doi.org/10.1071/WF16100.

Mangeon, Stéphane, Robert Field, Michael Fromm, Charles McHugh, and Apostolos Voulgarakis. 2016. “Satellite versus Ground-Based Estimates of Burned Area: A Comparison between MODIS Based Burned Area and Fire Agency Reports over North America in 2007.” *The Anthropocene Review* 3 (2): 76–92. https://doi.org/10.1177/2053019615588790.

Ntaimo, Lewis, Julian A. Gallego-Arrubla, Jianbang Gan, Curt Stripling, Joshua Young, and Thomas Spencer. 2013. “A Simulation and Stochastic Integer Programming Approach to Wildfire Initial Attack Planning.” *Forest Science* 59 (1): 105–17. https://doi.org/10.5849/forsci.11-022.

Riley, Karin L., and Rachel A. Loehman. 2016. “Mid-21st-Century Climate Changes Increase Predicted Fire Occurrence and Fire Season Length, Northern Rocky Mountains, United States.” *Ecosphere* 7 (11): n/a-n/a. https://doi.org/10.1002/ecs2.1543.

Riley, Karin, Crystal Stonesifer, Dave Calkin, and Haiganoush Preisler. 2015. “Assessing Predictive Services’ 7-Day Fire Potential Outlook.” *In: Keane, Robert E.; Jolly, Matt; Parsons, Russell; Riley, Karin. Proceedings of the Large Wildland Fires Conference; May 19-23, 2014; Missoula, MT. Proc. RMRS-P-73. Fort Collins, CO: U.S. Department of Agriculture, Forest Service, Rocky Mountain Research Station. p. 188-195.* 73: 188–95.

Short, Martin B., P. Jeffrey Brantingham, Andrea L. Bertozzi, and George E. Tita. 2010. “Dissipation and Displacement of Hotspots in Reaction-Diffusion Models of Crime.” *Proceedings of the National Academy of Sciences of the United States of America* 107 (9): 3961–65. https://doi.org/10.1073/pnas.0910921107.

Stewart, Ian. 1998. *Galois Theory*. 2nd ed. Boca Raton: Chapman & Hall/CRC.

Stonesifer, Crystal S., Dave Calkin, Matthew P. Thompson, and Keith D. Stockmann. 2016. “Fighting Fire in the Heat of the Day: An Analysis of Operational and Environmental Conditions of Use for Large Airtankers in United States Fire Suppression.” *International Journal of Wildland Fire. 25: 520-533.* 25: 520–33.

Wei, Yu, Douglas Rideout, and Andy Kirsch. 2008. “An Optimization Model for Locating Fuel Treatments across a Landscape to Reduce Expected Fire Losses.” *Canadian Journal of Forest Research* 38 (4): 868–77. https://doi.org/10.1139/X07-162.

Westerling, Anthony LeRoy. 2016. “Increasing Western US Forest Wildfire Activity: Sensitivity to Changes in the Timing of Spring.” *Philosophical Transactions of the Royal Society B: Biological Sciences* 371 (1696): 20150178. https://doi.org/10.1098/rstb.2015.0178.

Wibbenmeyer, Matthew J., Michael S. Hand, David E. Calkin, Tyron J. Venn, and Matthew P. Thompson. 2013. "Risk Preferences in Strategic Wildfire Decision Making: A Choice Experiment with U.S. Wildfire Managers." *Risk Analysis* 33 (6): 1021–37. https://doi.org/10.1111/j.1539-6924.2012.01894.x.

Wooster M. J., Roberts G., Perry G. L. W., and Kaufman Y. J. 2005. "Retrieval of Biomass Combustion Rates and Totals from Fire Radiative Power Observations: FRP Derivation and Calibration Relationships between Biomass Consumption and Fire Radiative Energy Release." *Journal of Geophysical Research: Atmospheres* 110 (D24). https://doi.org/10.1029/2005JD006318.

CHAPTER 2 – VALUATING FIRE SUPPRESSION RISK DATA

2.1 Introduction

The United States Federal government has been investing significantly into fire suppression every year; (USDA, The Rising Cost of Wildfire Operations: Effects on the Forest Service's Non-Fire Work, 2015) explains we expect to face extended periods of elevated fire risk more frequently in the future due to factors such as climate change and rapid expansion of wildland urban interface (WUI). Where human structures are situated in forested surroundings, wildfire suppression workloads are on the rise. (USDA, 2015) finds current fire seasons are 78 days longer than in 1970. Firefighters and equipment often need to be transported long distances from home bases to fire incidents or between incidents. Suppression response alert levels are in place to describe regional and national wildfire workloads (Preparedness Levels, National Interagency Mobilization Guide, chapter 20). It is important to identify and study key factors influencing the allocation of firefighting resource, particularly during times of elevated fire activity when resources are scarce. A shortage of resources can manifest as high dollar costs from escaped fires.

Wildfires are typically sparked by lightning strikes (United States Department of Agriculture, Forest Service, 1979) or set by humans in cases of arson or accidental ignitions (Magnussen and Taylor 2012); those fire events are difficult to predict. Risk management under uncertainty is a vital element in the fire-human interaction. (Calkin et al., 2011) provides many examples of risk and costs associated with fire. Much is known about the probability of fire spread; spatial arrangement of forest fuel beds and heat transfer models facilitate fire simulation (Finney et al., 2011), (Linn et al., 2002), (Mandel et al., 2011). Our model will use historical and average fire data to assess human response to wildfire.

Fire suppression is often triggered by smoke detections or activated in response to wildfire monitoring systems. The initial response period for wildland fire ignitions is called the initial attack. Containment rates of initial attack fires are known to be high in the US; (Calkin et al., 2005) reported

between 97% and 99% successful containment. The remaining 1% - 3% escape initial attack and continue to grow as uncontained fires entering a response period called the extended attack. Large fires, those 300 ha or more in size, require a variety of management tactics that vary based on fire growth, behavior, and danger it presents to human infrastructure, and ecological values (for example, forest health and species habitat) (USDA, 2015). During periods of elevated fire activity, management may be required to oversee multiple, simultaneous fires within a region. In either initial or extended attack, a fire manager might decide to summon extra help from the national pool of resources to stop the spread of a given fire (Interagency Red Book, 2017).

We know from (Calkin et al., 2011), efficient and effective wildfire response entails system-level coordination. To request resources that are outside the local area, the manager's request must enter the Resource Ordering Status System (ROSS). Most large fire requests are processed through ROSS. Therein the request is marked as filled or remains unable-to-be-filled subject to current availability within the national pool of resources. This database is central to our analysis. As a shorthand for demand for fire suppression resources we will often write "fire demand" in this paper.

Spatiotemporal data play an integral role in this fire management research to reflect on-the-ground management concerns. Fire managers observe regional and national Preparedness Levels (PLs), which rank the overall fire activity and resource use (Preparedness Levels, National Interagency Mobilization Guide, chapter 20). The levels are 1, 2, 3, 4, and 5. They are updated daily. For example, at Preparedness Level 3:

> "Two (2) or more Geographic Areas are experiencing wildland or prescribed fire activities requiring a major commitment of National Resources. Additional resources are being ordered and mobilized through NICC [National Interagency Command Center]. Type 1 and 2 Incident Management Teams are committed in two (2) or more Geographic Areas and crew commitment national is at 50%."

PL 4 is notable for increasing the number of Geographic Areas to three (3) and 60% national commitment of crews and managers. PL 5 moves to 80% commitment and is specific to "the potential to exhaust all agency fire resources." (Preparedness Level, National Interagency Mobilization Guide, chapter 20) further explains the relaxation from PL 5 to 4, 4 to 3, and 3 to 2.

Fire weather and behavior prognostics need to be understood for this type of policy to function (Riley et al., 2015). Personal factors such as successful past collaborations or knowledge derived from experience influence managers towards their soundest possible decision (Klein et al., 2010). Dynamic weather factors also influence suppression resource assignment. This decision might be efficient or inefficient according to their superiors. For example, energy release component (ERC), burning index (BI), and wind velocity data reflect changing fire conditions (Abatzoglou, 2013) to which managers responded. Location of infrastructure tells a manager where highways and WUI areas might be at risk. They know approximately long it will take an out-of-area resource to arrive to the fire. We attempt to include all of these factors in our model. Past research has also examined resource use patterns using spatiotemporal data. Researchers have studied the effectiveness of resources once they arrive (Katuwal et al., 2016) and suppression resource movement as well (Wei et al., 2017) and (Belval et al., 2017). Other works revealed how Incident Command Teams steer fire management (Hand et al., 2017) and how decisions vary among decision makers (Wibbenmeyer et al., 2013) (Stonesifer et al., 2017).

Ordinary differential equations (ODE) models are designed to explain how a system would iterate from initial states through a series of discrete time steps according to known system dynamics. ODE systems have been developed to describe many types of spatial dynamics from the transmission of infection diseases to predator-prey interactions (Durrett and Levin, 1994). While we found no previous work of using ODE systems in fire resource allocation, some researchers have used the maximum likelihood frameworks like (Preisler et al., 2011) (Thompson et al., 2013) (Silva et al., 2014) in studying fire resource allocation. ODE model coefficients are accompanied by their statistical likelihood. An

ODE systems formulation is potentially suitable for fire suppression studies to uncover correlations among assignment data in ROSS and geographic information system (GIS) data of risk information.

In this study, we establish an inverse problem for a system of ODEs to model the complexity of interacting fire demand and risk using linear interactions among their levels and rates of change. We examine the suppression resource assignments based on resource requests from ROSS. We use the Fire Occurrence Database (FOD) (Short 2017) to examine how fire ignitions impact resource assignments. We explore the effects of extended attack on resource assignments using MODIS fire monitoring satellite data (Giglio et al., 2016). Wind velocities from (Abatzoglou, 2013) were included as both non-directional speeds and daily change in direction since both are key risks fire managers assess during initial and extend attack. Energy release component (ERC) and burning indices (BI), also from (Abatzoglou, 2013). Data for nighttime illuminance are used as a proxy for population density in the wildland urban interface. Both WUI and interstate road accessibility were build ad-hoc (Brown, 2006) in Google Earth Pro; these layers are static i.e. unchanging through time in our model. Other risks evolve through time, become known to the model, and inform resource assignments through time. See (APPENDIX 4.1) for full data listing and citation.

From a methodological standpoint this paper puts forth a math modeling approach not seen previously in the literature. We use this model to explore the impacts of fire risk information on fire demand, developing model theory and parameterizing the model using historical data. We compared fire suppression assignments along the Rocky Mountain corridor spanning Wyoming, Colorado, and New Mexico (the Rocky Mountain and Southwest Geographic Coordination Areas) with California (the Northern and Southern California Coordination Areas). Our analysis tackles a multi-faceted problem of fire suppression allocation and transportation by building ODE models grounded in current policy, processing historical data, and interpreting implications of the coefficients estimates. Identifying the drivers of resource allocation processes can inform the configuration of policies to improve the system's performance.

2.2 Solving an inverse problem for ODE model

The ODE model is for a collection of fire suppression resources being shared amongst a collection of fire management zones (FMZs). To index different types of resources, we use $R = 1,\ 2, \ldots, \#R$ for suppression resources and $G = 1,\ 2, \ldots, \#G$ for FMZs. The union of FMZs forms a multiply connected domain $\Omega = \bigcup_{G=1,\ldots,\#G} \Omega_G$. Let $U_{R,G}(t)$ denote the fire demand at time t. Our objective is to model demand data for resource R in FMZ G from some initial configuration at $t = T_0$ through $t = T_F$ based on fire risk information. To index different types of fire risk information we use $i = 1,\ 2, \ldots$ to enumerate across a set of $FACTORS$. For now, the set $FACTORS$ is general; we will show how to use specific GIS layers to describe these risks in the next section.

Risk information is denoted $D_{i,G}(t)$ and considered exogenous, i.e. external, known data. We will use a $lowercase$ typeset for parameters, coefficients, and sub-model indices. Our model equation has endogenous parameters a for risk weights, y for "reinforcing/releasing," and z for cooperative "sharing." Each parameter is specific to a resource R within FMZ G, but may be fit according to demand or risk data from the other resources and FMZs in the ODE system. We solved an inverse problem for the ODE system. In the inverse problem, exogenous demand $U_{R,G}(t)$ and risk $D_{i,G}(t)$ are sampled to find the minimum residual model across potentially non-consecutive days.

We modeled fire suppression as a gradual, day-to-day process as resource needs become known. We created a system of coupled ODEs in time t to reflect ongoing decisions to reinforce the fire suppression effort or release resources from the incident based on fire risk information. The ODE system model component equations are

$$\forall\, R = 1, \ldots, \#R \qquad \forall\, G = 1, \ldots, \#G \qquad ODE(R,G) \;:\; \frac{dU_{R,G}}{dt}(t)$$

$$= \sum\nolimits_{s \in Lag(R,G)} \left[\sum_{g=1}^{\#G} \Big(z_{R,G,g}(t-s)\, U_{R,g}(t-s) \right.$$

$$\left. + \sum\nolimits_{i \in FACTORS} z_{i,R,G,g}(t-s) D_{i,g}(t-s) \Big) + \sum_{r=1}^{\#R} z_{R,r,G}(t-s)\, U_{r,G}(t-s) \right]. \qquad (1)$$

The first line of equation (1) shows request rate data. For a given time t_0 when request rate data $\frac{dU_{R,G}}{dt}(t_0) > 0$, the FMZ G is requesting more resources of type R than in the previous time step. When $\frac{dU_{R,G}}{dt}(t_0) = 0$, the request level is constant from day to day. Some request rate data have $\frac{dU_{R,G}}{dt}(t_0) < 0$ meaning the number requests is lower than the previous time step. Risk and resource availability with influence these rates as the fire season progresses.

The second line of equation (1) introduces an outer lag sum. All parameters depend on $(t-s)$ where lag s refers to recent risk information. The set $Lag(R,G)$ is used to specify which lags to sample for $ODE(R,G)$. Within the lag sum there is a FMZ sum. Sub-index g steps through the $\#G$ FMZs in the system. Parameter $z_{R,G,g}(t-s)$ tells how request rates for resource R in FMZ G might depend on other FMZs g. Within the lag sum and the FMZ sum there is a risk $FACTORS$ sum. Parameter $a_{i,R,G,g}(t-s)$ weights the ith risk information layer for resource R in FMZ G from FMZ g.

The third line of equation (1) establishes an additional demand term. Within the lag sum there is a resource sum. Sub-index r steps through the $\#R$ resources in the system. In contrast to $z_{R,G,g}(t-s)$, the term $y_{R,r,G}(t-s)$ can be viewed as a "reinforcing/releasing" parameter for resource R based on resource r's demand data within FMZ G. It captures the propensity of current fire demand levels to influence the future fire suppression requesting. Since all FMZs share a pool of resources, we hypothesize demand in one zone may impact scarcity in another zone via one or both of these feedback

terms mechanisms. Adding r and g makes a more realistic model for how fire demand might follow risk and demand feedbacks.

To solve our model, we used finite difference methods in Matrix Laboratory (MATLAB). Given $n = 1, \dots, N$ sample times t_n we computed estimates of $a_{i,R,G,g}(t-s)$ for risks, $y_{R,r,G}(t-s)$ for release/reinforce, and $z_{R,G,g}(t-s)$ for sharing. Our procedure used sample data $U_{r,g}(t_n)$ and $D_{i,g}(t_n)$ to conclude a best-fit model across t. Limitations arise due to issues related to computer storage, run-time, and collinearity between variables. Part of the ODE system fitting method is to assemble and organize coefficient weight data into matrices $\boldsymbol{A}_{R,G}$. Request rate data form the regression data vector $\overrightarrow{\partial_t U_{R,G}}$. A best-fit ODE model to the rate data is computed by estimating a vector of unknown parameters $\overrightarrow{x_{R,G}} = \left[\, a^s_{i,R,G,g}, y^s_{R,r,G}, z^s_{R,G,g} \,\right]$ given sample data at t_n. Our research code solves sub-problems $\boldsymbol{A}_{R,G}\, \overrightarrow{x_{R,G}} = \overrightarrow{\partial_t U_{R,G}}$ by resource R and FMZ G, the structure is fixed by sub-indices i, r, and g to build the matrix. Since the resulting normal matrices $\boldsymbol{A}^T_{R,G}\boldsymbol{A}_{R,G}$ are nearly singular, we use conjugate gradient least squares (Aster, Borchers, and Thurber, 2013) to invert and declare $\hat{x}_{R,G} \approx \boldsymbol{A}^{-1}_{R,G}\overrightarrow{\partial_t U_{R,G}}$ within numerical precision. Any $\hat{at}$ above a parameter means an approximation. MATLAB script and code assemble, parse, and analyze this linear system of ODEs.

In summary, we discretized a system of $\#R \times \#G$ equations like (1) to denote a discrete time update in fire demand. $ODE(R,G)$ is similar to a moving average process. We fit a model for request rates that has three sub-models. First, fire risk information is processed with a lagged memory of past data. Second, demand can have a self-reinforcing impact demand across resources we are calling reinforce/release. Third, demand can have a cooperative impact across FMZs. We interpret the coefficients as in any linear rate model:

$$\frac{dU}{dt} \propto \text{fire risk} + \text{reinforce/release} + \text{sharing},$$

then solve the inverse problem to estimate all parameters. This report identifies the significant coefficients and interprets how they influence fire demand in the model.

Incorporating Geographic Information System (GIS) data

Now turn to the numerical aspect of preparing a numerical estimate from (1). There are many approaches to aggregate GIS data by FMZ. We chose to populate the matrix system via a smoothed quadrature procedure. Discrete input data were smoothed with the radial basis function described in (Li and Chen, 2009) according to fixed half-width radius $\kappa > 0$, before passing to the quadrature. Smoothing fabricated errors as compared to the discrete assignment count, but our model is seeking system level trends. Smoothing may have little impact if the FMZ is large. The model is biased towards simultaneous, nearby fires, but includes small disparate fires in workload calculations too.

Risk input data were either smoothed with the radial basis function, interpolated, or re-gridded. Quadrature calculations depend on spatial resolution; the smallest GIS raster grids in this study were $18\ km$ per side. We used a two-dimensional quadrature. Ignoring the elevation and curvature of Earth's surface, define spatial ordinates lx for $^\circ\ longitude$ and ly for $^\circ\ latitude$. For example, (lx, ly) might be uniformly spaced $\Delta lx = \Delta ly$ in the $NAD83$ cartographic projection. Our procedure to calculate risk data $D_{i,g}^{s}$ for each FMZ in (1) from GIS data $D_i(t-s, lx, ly)$ was:

- ☐ Apply quadrature averaging rule via approximate integration

$$\overline{\overline{D_{i,g}^{s}}}(t) \;=\; \iint\limits_{(lx,ly)\,\in\,\Omega_g} D_i\,(t-s, lx, ly)\; dlx\; dly \;\approx\; \sum_{\xi\,=\,1}^{M_\xi}\sum_{\eta\,=\,1}^{M_\eta} D_i(t-s,\xi,\eta)\;\; \Delta lx(\xi,\eta)\;\Delta ly(\xi,\eta) \qquad (2)$$

This might be interpreted as a generalized "power" level of risk information layer i within FMZ g, at lag s. Equation (2) permits unevenly spaced M_ξ-by-M_η grids where the grid widths are $\Delta lx(\xi,\eta)$ and $\Delta ly(\xi,\eta)$.

- Non-dimensionalization was performed on each risk information layer i independently. First, we scaled each quadrature estimate from (2) by the area of the FMZ

$$\overline{D_{i,g}^{s}}(t) = \frac{\overline{\overline{D_{i,g}^{s}}}(t)}{Area(\Omega_g)}, \qquad (3)$$

Then, we re-scaled to $[0,1]$ based on the extreme values across the sample and lag points:

$$D_{i,g}^{s}(t) = \left(\overline{D_{i,g}^{s}}(t) - \min_{i,g,s} \overline{D_{i,g}^{s}}(t)\right) \Big/ \left(\max \overline{D_{i,g}^{s}}(t) - \min_{i,g,s} \overline{D_{i,g}^{s}}(t)\right) \qquad (4)$$

Equations (2), (3), and (4) show how to compute for any $t \in [T_0, T_F]$, $\overline{\overline{D_{i,g}^{s}}}(t) \rightarrow \overline{D_{i,g}^{s}}(t) \rightarrow D_{i,g}^{s}(t)$. These data are input to the ODE equations in (1); $U_{r,g}^{s}(t)$ was computed from the smoothed demand maps in the same manner. Thus, all demand data and risk information layers had equal numerical footing as input to the ODE system with components (1). As GIS data resolution is typically much finer than the FMZ-level, many other options are available for performing this aggregation.

Data sampling and solution method

Knowing inversion problem size is key to understand these low rank conditions. Each best-fit $ODE(R,G)$ in (1) required the estimation of $|Lag(R,G)|(\#G(1+|FACTORS|) + \#R)$ parameters from N equations, where $|\cdot|$ gives the size of the sets. The number of parameters is the row dimension for each $\boldsymbol{A}_{R,G}$ It comes from including $|Lag(R,G)| * \#R$ reinforce/release demand coefficients $\hat{y}_{R,r,G}^{s}$, $|Lag(R,G)| * |FACTORS| * \#G$ risk coefficients $\hat{a}_{i,R,G,g}^{s}$, and $|Lag(R,G)| * \#R$ cooperative demand coefficients $\hat{z}_{R,G,g}^{s}$. We inverted low rank matrices with column dimension $O(10^2)$ unknowns and row space dimension $O(10)$ equations. This underdetermined system was sensitive to noisy data inputs so we chose an $i.i.d.$ sampling and replication method to resolve the parameter space in E experiments. Each experiment fit a sample of N time moments $t_1, \ldots, t_N$ drawn at random with replacement. Sampling can be consecutive or nonconsecutive, both work equally well. By replicating these fits some number E times we were able to assess the range, variability, and significance of the true ODE system coefficients. Our

test case descriptions mention the system and sampling sizes as $\langle \#R, \#G, N, E \rangle$. Research code assembles block-structured matrices $\boldsymbol{A}_{R,G}$ (APPENDIX 4.3), then uses them to calculate the best-fit regression.

We found ordinary least squares estimates $\hat{x}_{R,G} \approx \left(\boldsymbol{A}_{R,G}^T \boldsymbol{A}_{R,G}\right)^{-1} \boldsymbol{A}_{R,G}^T \overrightarrow{\partial_t U_{R,G}}$ required inversion of ill-conditioned regression matrices $\boldsymbol{A}_{R,G}^T \boldsymbol{A}_{R,G}$. To invert and solve under these low $rank\left(\boldsymbol{A}_{R,G}\right) = N$ and large $cond\left(\boldsymbol{A}_{R,G}^T \boldsymbol{A}_{R,G}\right) = O(10^{97})$, in the worst cases, we used two redundant inversion methods: iterative CGLS (Aster, Borchers, and Thurber, 2013) and MATLAB's bicgstab.m. CGLS is a gradient-following algorithm to minimize regression residuals in the least squares sense. In this way, $\hat{x}_{R,G}$ are known to be a maximum likelihood estimate for the parameters given data $\boldsymbol{A}_{R,G}$ and $\overrightarrow{\partial_t U_{R,G}}$. Accessing maximum likelihood parameter estimates is important to gain insight about the values of the true ODE system coefficients.

In using CGLS we are guaranteed local optimality to numerical precision of the computer because they satisfy a first order necessary condition. The bicstab.m algorithm does the same; additional steps in this algorithm are explained in (van der Horst 1992). Redundancy in matrix inversion method ensured a consistent model-fit because bicgstab.m converged within numerical tolerance to the CGLS estimates. We do not have any guarantee of global optimality via second order conditions, but the replication of coefficient fit helped us characterize weakly global minimum residuals.

Two keys to our model are first difference data and log transforms. We denote marginal first differences $\partial_t D_i(t-s, lx, ly) = D_i(t-s, lx, ly) - D_i(t-s-1, lx, ly)$, for $\Delta t = 1$, log transforms $\log D_i(t-s, lx, ly)$, and combined risk information $D_i(t-s, lx, ly) * D_{i'}(t-s, lx, ly)$ for $i \neq i'$ up front. This is done to test established fire management intuition associated with the risk information in $FACTORS$; many of these intuitions are about changes in risk information through time. Enlarging the model's parameter space up front facilitated analysis of these intuitions on the back end. By including multi-collinear $FACTORS$ we were able to make broad observations, but exact coefficient ranges and orderings needed to be scrutinized more carefully.

2.3 Test cases, U.S. data – 2011 through 2016

Our test cases include the contiguous United States, Alaska, and Hawaii from 2011 to 2016. We collected historical databases for resource demand and fire risk information layers within $\Delta t = 1\ day$ and $0.08^\circ \leq \Delta lx\ , \Delta ly \leq 0.16^\circ$, the approximate degree equivalents of 9 km and 18 km grid spacing. Test cases sample requests smoothed into demand hotspots. All GIS layers supporting U and D were computed and combined with the 2011-2016 ROSS archive for each resource R. Different types of suppression resources have been used in the past for fire suppression. We selected four types of terrestrial resources and three aerial types to build our test cases (TABLE 2.1). The United States have large FMZs organized into Geographic Area Coordination Centers (GACCs). Our interregional sharing test cases involve these regions (TABLE 2.2). Ranging from multi-state collaborations to half-state units, GACCs are important management boundaries. Incidents of fire within GACCs share certain commonalities: regional weather patterns, local suppression crews, and similar fire behaviors as fires encounter the same types of vegetation. GACCs often request resources from the shared national pool; those requests are tracked by the ROSS database.

Equation (1) is localized to the U.S. as a national sharing model with $\#G = 12$. Equations (2), (3), and (4) implement a coarse spatial aggregation, which we assemble into a matrix, then solve as an inverse problem via the methods bicgstab.m and (Aster, Borchers, and Thurber, 2013). This procedure carries the assumption that GACCs are groups of similar decision-makers. We used it to find any patterns in how these groups detect risk and generate fire demand. We designed three test cases to perform numerical and statistical analysis on equation (1).

(A) *The full ODE system was tested in all-regions*. Sampling results are available in (APPENDIX 4.5) for the data layers in (APPENDIX 4.4). As a corollary we mention computation and storage limitations of the new ODE method finding $\langle \#R = 7, \#G = 12, N = 16, E = 17 \rangle$ solvable within reasonable compute time. See (APPENDIX 4.6) for more information.

(B) Two smaller test cases were performed with $\langle \#R = 4, \#G = 2, N = 10, E = 23 \rangle$:

(B1) A risk sensitivity in demand analysis of the Rocky Mountain Area Coordination Center RMCC and the Southwestern Coordination Center SWCC. Both FMZs have a long history of cooperation because the monsoon weather patterns support more spring and early summer fires in the SWCC while the RMCC heats up in middle and late summer.

(B2) A parallel analysis between the Northern Operations Coordination Center NOCC and the Southern Operations Coordination Center SOCC, which are the regional FMZs for northern and southern California. California does order from ROSS, but also share state-level resources. It is a region that will continue to have high workloads in the future.

During preliminary analysis, we found national Preparedness Level $PL = 1,\ 2,\ 3,\ 4,$ and 5 was significant in all ordinary least squares models. As such, we elected to use national PL to partition $apriori$ the six (6) years of 2011-2016 archive data, shown in (TABLE 2.3). The archive spans 974 days. We took $Lag(R, G) = \{0,\ 1,\ 2,\ 3,\ 7,\ 14,\ 21\}$ for each $R = 1, \dots, 7$ and $G = 1, \dots,\ 12$. Other lags are testable, but we tested (1) in accordance with the 14-day shift length and 21-day maximum policies in (Preparedness Levels, National Interagency Mobilization Guide, chapter 20). Short- and long-term impacts were found in the data.

Test cases **(B1)** and **(B2)** have $\#G = 2$. They concern two GACCs apiece: $\{RMCC, SWCC\}$ and $\{NOCC, SOCC\}$ from (TABLE 2.2). They focus on the $r = 1,\ \dots,\ \#R = 4$ terrestrial resources from (TABLE 2.1). In these test cases, the ODE system has eight ODEs like (1). (TABLE 2.4) gives an example of three of these eight ODEs.

We solved an inverse problem for the ODE system by simultaneously inverting each member equation like (1). We indexed and displayed our results by lag $s \in \{0,\ 1,\ 2,\ 3,\ 7,\ 14,\ 21\}$, suppression resources R, GACCs G, and risk information $i \in FACTORS$. We analyzed significance, variability, and mean tendency of the best-fit coefficients to the ODE system in using the N-sample, E-replicate

procedure outlined in the methods section. We assumed each parameter to be normally distributed. We determine the significance of each estimate at a 95% confidence level finding p-values at $\chi^2_{E-1,0.05}$. Results are reported for the national PL23 normal workload category and for the PL45 high workload category for the archive shown in (TABLE 2.3).

Not only did the test cases help us learn about correlations in fire demand and risk data for the U.S., they also allowed us to test the intuition behind the ODE method in general. This latter was important because this approach differs from other allocation research. Instead of modeling resource movement, the ODE model was built for the changes in fire demand over time. Values for $U_{R,G}(t-s)$ must be mined from the ROSS archives and prepared according to (2), (3), and (4). A nuance of these test cases is that they assume fire demand to be efficient i.e. ROSS reflects what was actually used and needed on the fires. We filter cancelled and unable-to-fill requests using only allocation data that was filled by a resource on a fire. We included ROSS data for reassignments from incident to incident in the computations of $U_{R,G}(t-s)$. The ODE model outputs are sensitive to ordering mistakes, gaming of the system, or undue holding certain resources.

In using the ODE method, we provide statistical inferences using the samples from our test cases. While our test cases are localized to the United States, we have stated the model in general terms, so peoples from other countries can also adopt the method. Any GIS map-based risk information layer is testable in (5), but our test cases involve some 45 factors tabulated in (APPENDIX 4.4). The regression results indicate how fire demand followed risk factors according to information in the 2011-2016 archive.

2.4 Interregional resource assignment and factor data analysis

This section shows the results of Test Cases (A), (B1), and (B2). The section refers to (APPENDIX 4.4, 4.5) ; (FIGURES 2.1 - 2.6) and (TABLE 2.5). Our analyses sought out trends in central tendency and significance of the risk and demand coefficients by assuming suppression resource allocations evolve according to a system of equations like (1). Multi-collinearity commonly exists

between the factors influencing fire demand within GACC or coorperations between GACCs. (FIGURE 2.1a) demonstrates input collinearity among risk data samples for the ODE archive $D_i(t-s, lx, ly)$ and $U_{R,G}(t-s)$ post (2), (3), and (4). By assessing these sample and lag data inputs we are able to get a better idea for what the ODE model aims to fit. There may be lagged trends in these data. Risk information may be colinear. Demand for resources might coincide or be consistently higher for certain types. A detailed legend applies to all the plots and shows the GIS risk information in $FACTORS$ that were input data.

Adhering to the indexing notation in (1), we report findings in the values and significance of risk and demand coefficients. We report general results from test case **(A)**, examine the ODE system model in **(B1)**, and introduce **(B2)** to complete a comparative study between the central/southern Rockies and California.

Test Case (A)

One can see that the PL23 signficant coefficients are sparser than those at $PL45$. Full results for the best fit coefficients are given in (APPENDIX 4.5). For $PL23$ samples, cooperative sub-models with three or four significant $\hat{a}^{s}_{i,R,G,g}$ with $p < 0.01$ at the 95% level for $\chi^2_{E-1,0.05}$ were found to fit the data according to ODE system. For PL45 samples, our ODE model analysis uncovered between six and ten $p \leq 0.01$ significant coefficients. As expected the PL45 sharing databases hold a far greater level of complexity. This is an important verification.

(TABLE 2.5) summarizes the significant risk information layers in test case (A). The PL45/PL23 sparsity difference is masked in this case because we count significance across lag, but it is important to note the switching between risk information in the best fit data model between samples. (FIGURE 2.1b) shows how the lag sum in equation (1) is a model for risk processing in theory and in practice. In theory, the model can accentuate the impact of a given risk information GIS layer $i \in FACTORS$ across lags $s \in Lag(R, G)$. The plot shows how demand for the terrestrial fire suppression resources can depend on the

change in fire starts and burning index in the recent past. Instead of current risk and demand information being the most salient, information up to three weeks ago demonstrates explanatory power for mobilization data. Policy that controls resource assignment lengths to two weeks with maximum allowable overtime of three weeks may be causing these trends. In practice, we observe lagged trends in the best fit coefficients. This array of plots has large bands of uncertainty, but certain coefficients can be reported as significantly positive or negative. For example, FFT2s and engines in the SWCC have a short-term response to burning index. This makes sense as drier and drier conditions lead to more and more fire. There is also a significantly positive lag $s = 3$ coefficient on $geDIST(static) * \partial_t\, ERC(t - 3)$, which indicates FFT1s, FFT2s, and engines in the SWCC seem to be ordered a few days after seasonal drying, but in accordance with accessibility distance. Demobilization trends also exist for these three resource types in the RMCC. Significantly negative coefficients on $geDIST\ (static) * MODIS(t - 3)$ and $geDIST\ (static) * MODIS(t - 21)$ indicate release of resources when large fires go out or the maximum assignment period is reached. A 14-day assignment limit is on display in the final plot in this array because $\partial_t FOD * \partial_t BI(t - 14)$ risk information matters when ordering more FFT2s. Differences in regions are apparent in this risk coefficients as well.

Test Case (B1), central/southern Rockies

In test case (B1), we studied the demand of four resource types { FFT1, FFT2, engine, Dozer } in two GACCs { RMCC, SWCC }. The ODE method validates current research and thinking about focal roles of FFT1s and engines in large fire suppression because large fire risk information like $MODIS(t - s)$, $BI(t - s)$, and related layers have significant correlation coefficients. Results for $PL23$ and $PL45$ replicates are shown at strong $p < 0.01$ and weaker $p \in [0.01,0.045]$ in (FIGURE 2.2). Salient archive signals for both FFT1s and engines show a 14-day lag response. (FIGURE 2.2a) shows FFT1 in the SWCC demobilization trends are described by a larger number of significant coefficients than mobilization trends. While not true in every model we fit, we found in general: inflow of resources is more predictable from risk information than outflow. Demobilization happens gradually, as resources

reach the end of their 14 day shifts and as work completes on contained fires. The risk information layers in this study demonstrated certain limitations with the reinforce/release part of the ODE model.

(FIGURE 2.2b) shows the best fit risk coefficients for engines in the RMCC. Comparing FFT1 in the SWCC (FIGURE 2.2a) to engines in the RMCC reveal, at least under normal workloads and availability at $PL23$, it was common for interregional travel to occur to and from large fire incidents. The two-week work rotation policy appears to have a strong impact on the data we used. The RMCC tends to request engines from the SWCC when burning indices are resulting in more a positive coefficient for $\partial_t BI$. In contrast, significant factors $ERC(t-s)$, $WindVel(t-s)$, and related layers appear for engines in the RMCC, but are absent for FFT1 in the SWCC. (FIGURE 2.2c) shows engines in the RMCC when the national alert climbs to $PL45$. The same coefficients are still significant for engines in the RMCC, but the lag structure is not evident and other, confounding factors have entered the best fit model. On one hand, we would be surprised to uncover a 14-day lag in this case because such policy adherence might be too restrictive for effective management under national $PL45$ workloads. On the other, we are not sure why the confounding factors appear when the system is stressed. Finally, in the RMCC, quick engine ordering in response to large fire is also evident in the $PL45$ sample, but the number of strongly and weakly significant coefficients has increased from 14 to 25.

To demonstrate what this model might reveal about policy, we make an additional observation about (FIGURE 2.2c). Notice there is no delay for RMCC to order more resources at PL45 level if they discover high BI and MODIS. There is, however, a 7-day delay for the RMCC to order more resources due to the increase of fire activities at PL45. This model suggests the RMCC might pay more careful attention to escalating of fire activities with a slightly longer memory. Today's hot fire behavior and last week's both inform demand for this critical fire suppression resource.

Next, we go into more detail about the risk models. Each ODE model has the capacity to select among all 45 risk information data layers. These are the $FACTORS$. (FIGURE 2.3) shows all

coefficients, even ones that are not significant or show mean tendency near 0. These plots show variability of risk coefficients across-samples and reveal fit outliers, but cannot indicate significance.

We have highlighted the following observations for lag $s = 0$ coefficients in (FIGURE 2.3a):

(a) Today's large fire behavior metrics $MODIS(t)$ satellite fire radiative power and $BI(t)$ drive engine ordering in the RMCC,

(b) Similarly, outliers in the $\partial_t MODIS(t)$ coefficients at the ± 0.04 level indicate changes in large fire activity can precipitate substantial mobilization and demobilization of engines in the RMCC,

(c) Moreover, engine mobilization in the RMCC is conditioned on hot fires near the WUI because combined layers $\log LSNITE * MODIS(t)$ and $\log LSNITE * BI(t)$ have variable signals. See (APPENDIX 4.4) for more information about combined layers and the WUI metric $\log LSNITE$ used in our study.

Large fire metrics are also salient in the 14-day lag coefficients, but $ERC(t - 14)$ also plays a role. We have highlighted some more observations for lag $s = 14$ coefficients in (FIGURE 2.3b):

(d) $p < 0.01$ When $noise(t - 14)$ is significant it means none of the other risk information layers are successfully explaining the mobilization of engines in the RMCC,

(e) Resource release according to the 14-day limit from fires near the WUI might supersede other risks,

(f) Seasonal drying of fuels in $ERC(t - 14)$, $\partial_t ERC(t - 14)$, and combined $\log LSNITE$ data drive engine allocation in the RMCC,

(g) Changes in regional alert levels seem to matter most when combined with the accessibility of an incident to interstate highways as evidenced by high variability in the model fit.

engine mobilization in the SWCC exhibits similar 0- and 14-day patterns with $MODIS(t)$ and $BI(t)$ driving the process, especially on WUI fires. (FIGURE 2.3c) looks at 1-day lag patterns in the risk

information fit for engines in the SWCC. Wind and fire starts have higher variability than those for 1-day large fire indicators. We have highlighted the following observations in (FIGURE 2.3c):

(h) $BI(t-1)$ has a strong signal probably because of the possibility for large fires to produce ordering the day after a spike in fuel flammability,

(i) Our $\partial_t WindVel(t-1)$ layer captures a change in wind direction and shows strong signal in the best fit engine model for the SWCC; changing winds often correspond to increased fire activity as the heat might be steered towards new beds of unburned fuels,

(j) High winds speeds near the WUI have a strong signal for the engine SWCC model because of the threat posed to structures under these conditions,

(k) Many layers include yesterday's fire starts $FOD(t-1)$, but this hybrid metric of $\partial_t FOD * \partial_t ERC(t-1)$ is particularly interesting because it supports rapid changes in fuel moisture as a critical factor for fire starts.

(FIGURE 2.4) echos FFT1 versions of each plot in (FIGURE 2.3). The same trends (a) – (k) are present in the FFT1 results. Furthermore, FFT1 coefficients in the SWCC share the characteristic 1-day lag switch from large fire response, to anticipating large fire in wind and fire starts.

Impacts of demand

We found self-reinforcing and cooperative demand impacts in (3) are specific to a given resource. Our model for FFT1s and engines in the RMCC and SWCC indicates how these impacts change within the GACC over time. (FIGURE 2.5) transmits our findings. In (FIGURE 2.5a) we see engine use at national $PL23$ is indicative of the rest of the self-reinforce during fire suppression because fire demand for FFT1s in RMCC seems to follow mobilization of engines within the past couple of days and FFT1 release seems to follow demobilization of engines on a 14-day lag. In (FIGURE 2.5b) this feedback manifests for engines as compared with mobilization other engines in the SWCC.

All demand coefficients exhibit a common time signature. It applies to both the self-reinforcing impact of demand in $\hat{y}^{s}_{R,r,G}$ and the cooperative impact of demand in $\hat{z}^{s}_{R,G,g}$. In terms of the cooperative coefficients, we found a central tendency for $\hat{z}^{0}_{R,G,g} > 0$ meaning today's orders are filled tomorrow in rate data $\frac{dU}{dt}$ for { FFT1, FFT2, engine, Dozer } ROSS data. For lag $s = 1$ we found $\hat{z}^{-1}_{R,G,g} < 0$ indicating it is rare to order the same resource to the same GACC two consecutive days in a row. This makes sense because orders are typically filled in the order they arrive.

Test Case (B2), California intercomparison ODE model

We report test case (B2) in order to compare and contrast { FFT1, FFT2, engine, Dozer } use in { NOCC, SOCC } with their use in { RMCC, SWCC }. The bottom panel of (FIGURE 2.5) shows self-reinforcing demand impact at normal alert levels for FFT1s and engines in NOCC and SOCC. In contrast to the top panel of (FIGURE 2.5) internal coordination within California is stronger than within the central/southern Rockies. The data suggest California coordinates FFT1 allocation in the short-term and FFT2 allocation in the long-term since many of the reinforce/release parameters are significant.

(FIGURE 2.6) echoes (FIGURE 2.2) showing the best fit risk models for FFT1s in the SOCC at national $PL23$, engines in the NOCC at national $PL23$, and engines in the NOCC at national $PL45$. They share an emphasis on current changes in regional PL in $\partial_t regionalPL(t)$ as well as both accessibility and WUI layers see (APPENDIX 4.1) for more information about $static$ and dynamic GIS data. Both GACC pairs change their sharing practices according to the national PL, with $PL45$ resulting in noisier ODE output models. Lagged coefficients with long memory play a role in the best fit models for both test cases (B1) and (B2) and (FIGURE 2.6) also reflects greater complexity in demobilization models as compared with mobilization models.

Key differences in the best fit ODE models are:

- (FIGURE 2.6a) shows the 14-day lag is only prevalent $noise(t-14)$. California sharing is not so centered on lag information, but rather 2- to 7-day risk response. FFT1s have a much sparser mobilization model in the SWCC as compared with SOCC.
- (FIGURE 2.6b) California has different risk models than the central/southern Rockies. A national $PL23$ model for engines in the RMCC (FIGURE 2.2b) as compared with engines in the NOCC. Closer coordination is evident in demobilization for { NOCC, SOCC } as compared with { RMCC, SWCC}.
- (FIGURE 2.6c) Elevated risk brings large fire data into focus in the RMCC, but not so in NOCC.

To conclude our findings for test case **(B2)** consider that California has the largest set in the nation of state-managed resources, including engines and FFT1s. So, any sharing linkages between the NOCC and SOCC might be appreciably stronger than those between the RMCC and SWCC. We think California state ownership of resources might impact their ROSS requesting as well. Habits might be apparent in the data. Further information about standard response in each of these two-GACC models might further explain these differences. If either region has a stronger tendency to mobilize with a standard response, regardless of how threatening the fire is, risk signals in the ODE models would be appreciably weaker.

2.5 Conclusion and discussion

Our work tested a new method based on ODEs. We showed in theory and practice how to distill resource assignment and risk factor data into a set of linear models. We populated the models with time series data via a smoothed quadrature across individual FMZs. Solutions of our test cases demonstrated how input data covariance in time series GIS data results in noisy parameter estimates. The regression is extremely ill-conditioned in certain models. Despite this issue, we used redundant matrix inversion methodologies based on CGLS to verify the parameter estimates. All our fit results have weakly global minimum residuals for the samples and replicates. We reported best fit risk coefficients and interpreted their possible meanings for the inverse data problem. Our findings also quantified the impact of self-

reinforcing demand within a GACC across fire suppression resources in the U.S. and cooperation between GACCs when sharing a single type of resource from the national pool. We used three test cases to verify the model detects known allocation patterns, especially firefighter and engine use on large fires.

The system of ODEs was developed to reveal when and where spatiotemporal correlation occurs in allocation data. Our best-fit models differentiate between mobilization and demobilization. Our findings from ROSS data support the conclusion that mobilization is more readily explainable by risk information than demobilization. Another finding was a stark contrast between fire demand at national $PL23$ and at national $PL45$. Elevated fire activity seems to worsen the ability of a few coefficients to explain ordering preferences. We are seeing the stress explained in (Klein et al., 2010) manifest quantitatively as more difficult tradeoffs in the best fit risk model to $PL45$ data than to $PL23$ data. Indeed, between 2 and 3 times the number of risk information GIS layers were often needed to achieve the same quality of model fit when sampling fire days with higher level of resource scarcity $(PL45)$ as compared with normal days $(PL23)$. We are left wondering, is this the best way to manage fire risk? Whatever chaotic effect is causing output noise and model mismatch in our ODE system, it is augmented when the system is on high alert. A pressing question for future policy is: should this circumstance be opposite? Under conditions of high alert and scarce availability ODE models for the allocation data become more complicated. Perhaps a national threat response system to specify which risk information layers should be most salient by region, lag, and layer would make for efficient allocation in which all GACCs get a fair share. Our method was verified by showing known suppression resource movement trends emerge, despite noise in model outputs. Our research objective was to quantify risk preferences expressed in fire demand data.

We have noted the extent to which this inverse problem is ill-conditioned. The CGLS-based inversion method is robust in this regard and trends emerge despite issues in model noise and data mismatch. Even though all results in this paper have been reported from CGLS solutions and deemed weak global least squares minimizer, we found different fit results using Kaczmarz's algorithm, which

makes sense since (Aster, Borchers, and Thurber, 2013) note this algorithm tends to suffer when tradeoffs in matrix column-data are particularly close. Correlated risk information layers and fire demand data that were central to our paper's study of daily and weekly lags, different firefighting resource types, and collaborative interregional sharing resist Kaczmarz's algorithm. Ordinary least squares would not estimate the low-rank inversion even based on singular value decomposition. Since ODE systems are standard math models, these findings suggest a true complexity to the fire allocation problem.

We elaborated a novel data processing method for resource allocation in multiply connected domains based on a system of ODEs. This paper shows how processing noisy data through the assimilation model leads to noisy results. However, the strongest signals surpass the noise and validate prior thinking about FFT1s and engines (Belval et al., 2017; Lyon et al., 2017). Allocation for extended attack on large fires follows the management intuition we expect because MODIS fire radiative power data (Giglio et al., 2016) is often best suited for the fits in our test cases. Stating the model's component equations in general terms, helped define specific test cases from the abstract theory. We carried out between $E = 1$ and $E = 23$ experiments by inverting ill-conditioned matrices and applying $\chi^2_{E-1,0.05}$ statistics to determine significant trends. FIGURES 2.1b, 2.2 and 2.6 report both strong $p < 0.01$ and weak $p \in (0.01,0.045)$ signals. FIGURES 2.1a, 2.3, 2.4 and 2.5 explain the advantages we found with the lag and risk sub-models in equation (1). It is a productive model to account for resource use that follows a required 14-day shift.

Given multicollinearity of inputs, we conjecture a pre-conditioner on the matrix system might help us to better avoid accidental significance. This model so far does not account for the impact of forecast risk information layers. Mechanically, the ODE system of equations like (1) can function with an augmented Lag set, call it $Lag^* = \{+1,\ 0, -1, -2, -3, -7, -14, -21\}$. Forecast risk weights could be found for $+1$. GIS data for forecasts were not available during development, butwe tested within the archive using a fog-of-war style pseudo-forecasts. Our statistical work is descriptive of data trends, but forward prediction remains in prototyping. For this model, we do not expect to meet any forward

modeling limitation using MATLAB's ode45.m algorithm. It is an accurate, stable, and fast numerical solver (Dormand and Prince, 1980). Applying ode45.m's Runge-Kutta method would follow-up to this data-fitting project.

Communicating the model to an end user group of fire managers would rely on the visuals to convey all findings. This research does much to illuminate which indices matter and future work to streamline its interpretability are attractive. A second-stage linear model could start with a smaller number of input risks perhaps including only a few maps from (APPENDIX 4.1). We could use the significant factors we found to be significant in this paper – like $\partial_t MODIS * \partial_t BI$, $regionalPL$, $geDIST * WindVel$, etc. – to make more reliable and informative coefficient estimates.

Recent consolidation of nonlinear AIMD (Additive Increase Multiplicative Decrease) algorithms in (Corless, 2016) show promise for the ODE system framework established here. Risk heuristics are also appropriate to test. Adding a directional aspect to this problem is topic of current research into partial differential equation (PDE) systems. (Short et al., 2010) demonstrate PDE systems are capable of distinguishing risk-contouring versus risk-following dynamics in a similar demand potential framework. MATLAB PDE software is currently being explored as a finite element method solver on triangular meshes. This would afford simulation en masse and a better understanding of these parameters. Other applications for smoothing and averaging of spatial areas are possible.

TABLES 2.1, 2.2, 2.3 –

TABLES 2.1, 2.2, and 2.3 summarize our test cases.

TABLE 2.1

Fire Suppression Resources

$R =$	**Terrestrial**	$R =$	**Aerial**
1	Firefighter Type 1 $(FFT1)$	5	$(Helicopter)$
2	Firefighter Type 2 $(FFT2)$	6	$(Airtanker)$
3	Types 1-6 $(Engine)$	7	Smokejumper $(SMKJ)$
4	Types 1-3 $(Dozer)$	$(\cdots)$ *ROSS archive data mining strings*	

TABLE 2.2

U.S. Geographic Area Coordination Centers (GACCs)

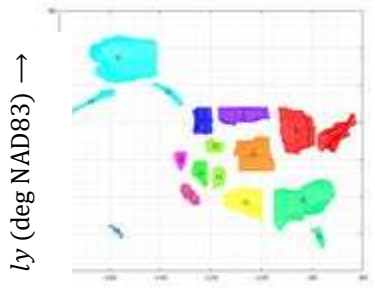

Domain partition: $\Omega = \bigcup_G \Omega_G$

$G \neq g \implies \Omega_G \cap \Omega_g = 0$

$G = 1$	Eastern Area Coordination Center, $EACC$ (2 sub-zones)
2	Rocky Mountain Coordination Center, $RMCC$
3	Southwestern Coordination Center, $SWCC$
4	Eastern Great Basin Coordination Center, $EGBCC$, (2 sub-zones)
5	Western Great Basin Coordination Center, $WGBCC$
6	Southern Area Coordination Center, $SACC$, (2 sub-zones)
7	Alaskan Coordination Center, $AKCC$, (3 sub-zones)
8	Hawaii, as part of $NOCC$
9	Northwestern Coordination Center, $NWCC$
10	Northern Rockies Coordination Center, $NRCC$
11	Northern Operations (N. California), $NOCC$
12	Southern Operations (S. California), $SOCC$

TABLE 2.3

Preparedness Level archive partition

Daily (# of records) for $2011 - 2016$ archive

Workloads:	**High**	**Normal**	**Low**
Resource use:	*Scarce*	*Normal*	*Abundant*

	$PL45$	$PL23$	$PL1$*
$(N_{archive}) =$	(151)	(405)	(505)

*No tests on $PL1$ are reported in this paper

TABLE 2.4 –

In the top-left box, $Engines$ use identical demand data $U_{3,2}(t-s)$ and yet linear fit coefficients $\hat{z}^{S}_{3,2,2}$ and $\hat{z}_{3,2,3}$. We test the two-sided alternative $H_0 : \hat{z}^{S}_{3,2,2} \neq \hat{z}_{3,2,3}$ to see if the RMCC and SWCC respond differently to the same fire demand they are seeing. It tests the assumption that RMCC ordering might account for ordering and resource use in the SWCC and visa-versa. In the bottom-right box, the SWCC uses identical mustering data sources. Here we have modeled a potential cooperative impact as the muster of personnel occurs day-to-day.

(TABLE 4) ODE Equation Coupling $(R, G) = (3,2)\ ;\ (3,3)\ ;\ (4,3)$

	Sharing	Risk	Mustering
Engine, RMCC $\frac{dU_{3,2}}{dt}(t) =$	$\hat{z}^{s}_{3,2,2}\ U_{3,2}(t-s) + \hat{z}^{s}_{3,2,3}\ U_{3,3}(t-s)$	$+\sum_{i=1}^{L}\left(\hat{a}^{s}_{i,3,2,2}\ D_{i,2}(t-s) + \hat{a}^{s}_{i,3,2,3}\ D_{i,3}(t-s)\right)$	$+\hat{y}^{s}_{3,1,2}\ U_{1,2}(t-s) + \hat{y}^{s}_{3,2,2}\ U_{2,2}(t-s) + \hat{y}^{s}_{3,3,2}\ U_{3,2}(t-s) + \hat{y}^{s}_{3,4,2}\ U_{4,2}(t-s)$
Engine, SWCC $\frac{dU_{3,3}}{dt}(t) =$	$\hat{z}^{s}_{3,3,2}\ U_{3,2}(t-s) + \hat{z}^{s}_{3,3,3}\ U_{3,3}(t-s)$	$+\sum_{i=1}^{L}\left(\hat{a}^{s}_{i,3,3,2}\ D_{i,2}(t-s) + \hat{a}^{s}_{i,3,3,3}\ D_{i,3}(t-s)\right)$	$+\hat{y}^{s}_{3,1,3}\ U_{1,3}(t-s) + \hat{y}^{s}_{3,2,3}\ U_{2,3}(t-s) + \hat{y}^{s}_{3,3,3}\ U_{3,3}(t-s) + \hat{y}^{s}_{3,4,3}\ U_{4,3}(t-s)$
Dozer, SWCC $\frac{dU_{4,3}}{dt}(t) =$	$\hat{z}^{s}_{4,3,2}\ U_{4,2}(t-s) + \hat{z}^{s}_{4,3,3}\ U_{4,3}(t-s)$	$+\sum_{i=1}^{L}\left(\hat{a}^{s}_{i,4,3,2}\ D_{i,2}(t-s) + \hat{a}^{s}_{i,4,3,3}\ D_{i,3}(t-s)\right)$	$+\hat{y}^{s}_{4,1,3}\ U_{1,3}(t-s) + \hat{y}^{s}_{4,2,3}\ U_{2,3}(t-s) + \hat{y}^{s}_{4,3,3}\ U_{3,3}(t-s) + \hat{y}^{s}_{4,4,3}\ U_{4,3}(t-s)$

TABLE 2.5 –

Significant risk information layers (ANY LAG) for resource/region within all-GACC model

	PL45/PL23 **X** = $p < 0.01$ **-** = $p \geq 0.01$ *2011-2016* *# of assignments & reassignments per year* [median] max, min	constant	MODIS	ERC	FOD	BI	regionPL	WindVel	geDIST (static)	log LSNITE (static)	COST	*# of factors*
Dozers												
- EGBCC	[57] 393, 3	**-/-**	**X/-**	**X/X**	**X/X**	**X/-**	**-/-**	**-/X**	**-/X**	**-/-**	**-/X**	*4/5*
- WGBCC	[390] 1034, 66	**-/X**	**X/X**	**X/-**	**X/X**	**X/X**	**-/X**	**X/X**	**X/X**	**X/-**	**X/X**	*8/8*
FFT2s												
- EGBCC	[6366] 22182, 397	**-/-**	**-/-**	**X/X**	**X/-**	**X/X**	**X/X**	**-/-**	**-/-**	**-/-**	**-/-**	*4/3*
- WGBCC	[8081] 15102, 42	**-/-**	**-/X**	**-/X**	**X/X**	**-/X**	**-/-**	**-/-**	**-/-**	**-/X**	**-/-**	*1/5*
FFT1s												
- NOCC	[18405] 26965, 2910	**X/X**	**X/X**	**-/X**	**X/X**	**X/-**	**-/X**	**X/X**	**-/X**	**X/X**	**-/-**	*6/8*
- SOCC	[23431] 46199, 7251	**-/-**	**-/-**	**X/-**	**X/-**	**X/-**	**-/-**	**X/-**	**X/-**	**-/-**	**-/-**	*5/0*
engines												
- NOCC	[20115] 31616, 3051	**X/-**	**-/X**	**X/-**	**-/X**	**X/-**	**-/-**	**X/-**	**-/-**	**-/-**	**-/-**	*4/2*
- SOCC	[14679] 42249, 7827	**-/-**	**-/-**	**-/-**	**-/X**	**-/X**	**X/-**	**-/-**	**-/-**	**-/-**	**-/-**	*1/2*
- RMCC	[3992] 17629, 971	**X/-**	**-/X**	**-/X**	**-/-**	**X/X**	**X/X**	**X/X**	**X/-**	**X/-**	**-/X**	*6/6*
- SWCC	[72985] 22893, 2740	**X/-**	**X/-**	**X/-**	**-/-**	**-/-**	**X/-**	**X/-**	**X/-**	**X/X**	**-/-**	*7/1*

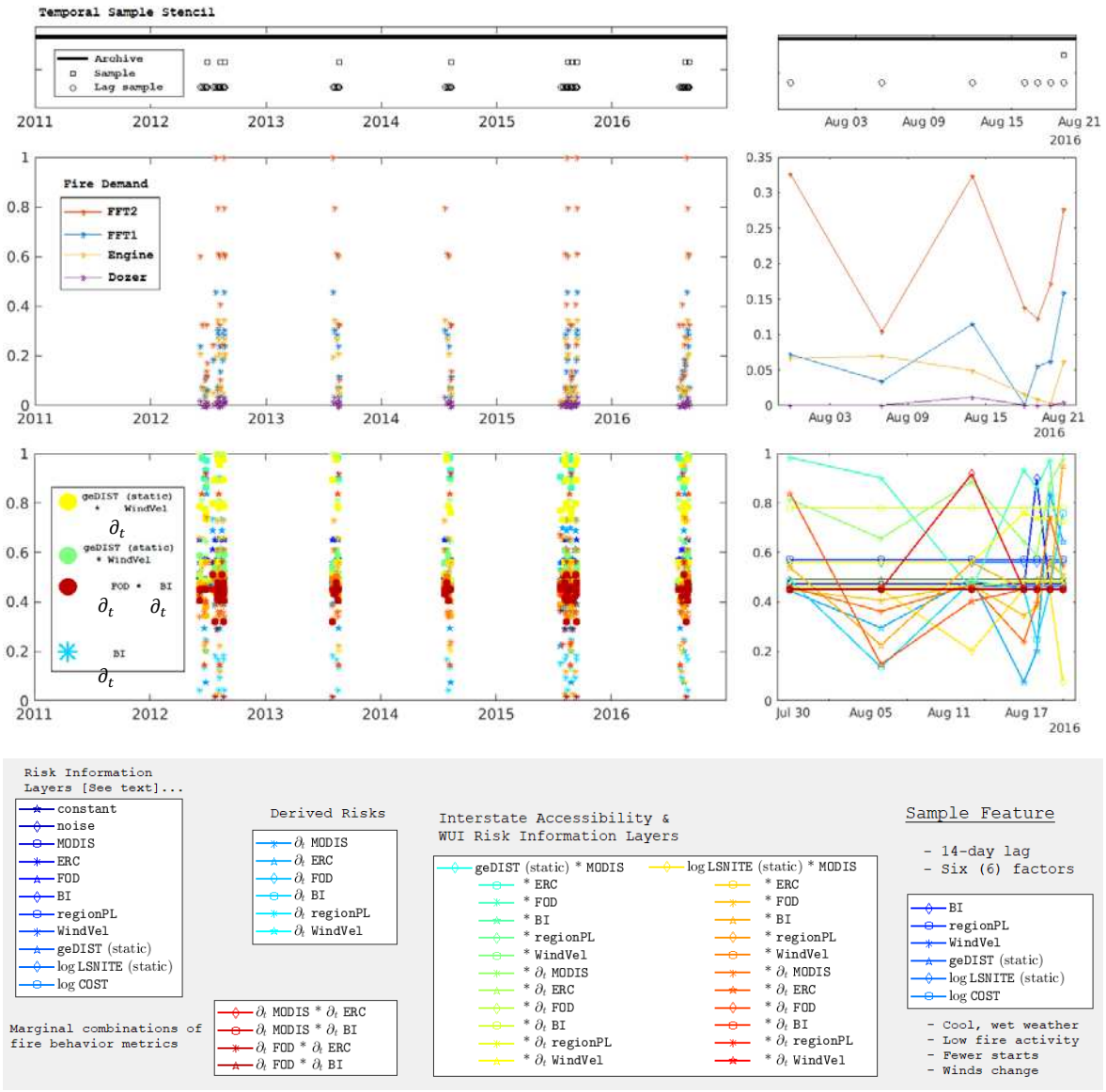

FIGURE 2.1a - ODE method input data *(full sample LEFT PANEL) (single sample at RIGHT PANEL)* Legend in gray

Caption:

[LEFT PANEL] Top plot, N-day, E-replicate sample structure. Middle plot, central tendency of risk data in sample is near 0.5. Bottom plot, some input statistics from which the visual estimate of mean μ and variance σ^2: $geDIST\ (static) * \partial_t WindVel\ (t-s) \sim \boldsymbol{N}(\mu = 0.80, \sigma^2 < 0.14)$; $geDIST\ (static) * WindVel\ (t-s) \sim \boldsymbol{N}(\mu = 0.59, \sigma^2 < 0.14)$; $\partial_t FOD * \partial_t BI\ (t-s) \sim N(\mu = 0.47, \sigma^2 < 0.01)$; and lastly any recent changes in Burning Index $\partial_t BI(t-s) \sim N(\mu = 0.25, \sigma^2 < 0.14)$

[RIGHT PANEL] Top plot, within sample. Middle plot, a correlated surge of demand for firefighters on August 15th, a period of lower demand, followed by a spike in fire demand coinciding with the August 21st sample. Bottom plot, bundles of lines move together, multicollinearity in inputs.

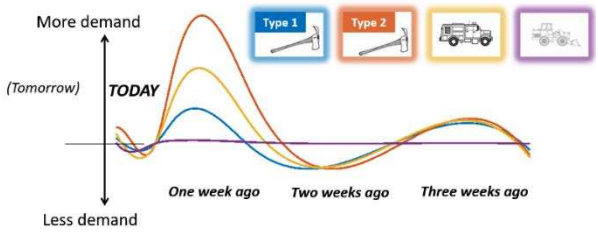

(i)

(ii) $A.$ $B.$
$C.$ $D.$

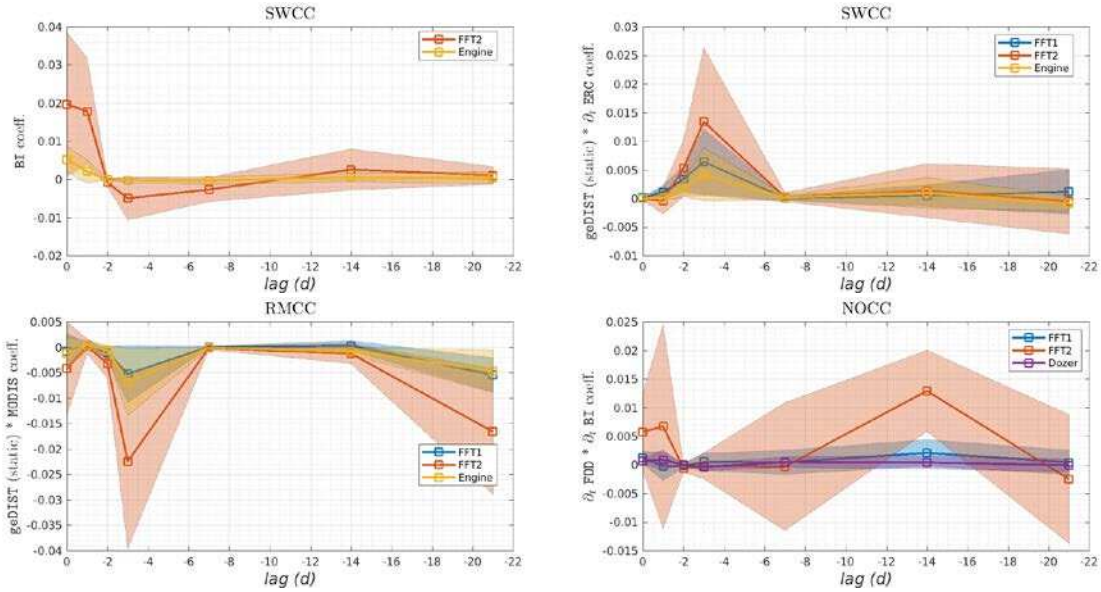

FIGURE 2.1b - Lag structure in theory and practice

Caption:

(i) Demand response to $\partial_t FOD * \partial_t BI(t-s)$ - Lag structure in (2) fits data in a logical fashion. Instead of current risk and demand information being the most salient, information up to three weeks ago demonstrates explanatory power for mobilization data. Policy that controls resource rotations to two weeks with maximum allowable overtime of three weeks is evident.

(ii) Practice – ODE coefficient panel labels

A. Short term lag prevalence in SWCC FFT2s engines on $BI(t-s)$
B. SWCC { FFT1s FFT2s engines } strong sensitivity to short term lag data for $geDIST(static) * \partial_t ERC(t-3)$
C. Demobilization trends on a sub-weekly up to a 21-day lag $p < 0.01$
D. NOCC FFT2 rotation according to 14-day assignment limit $p < 0.01$

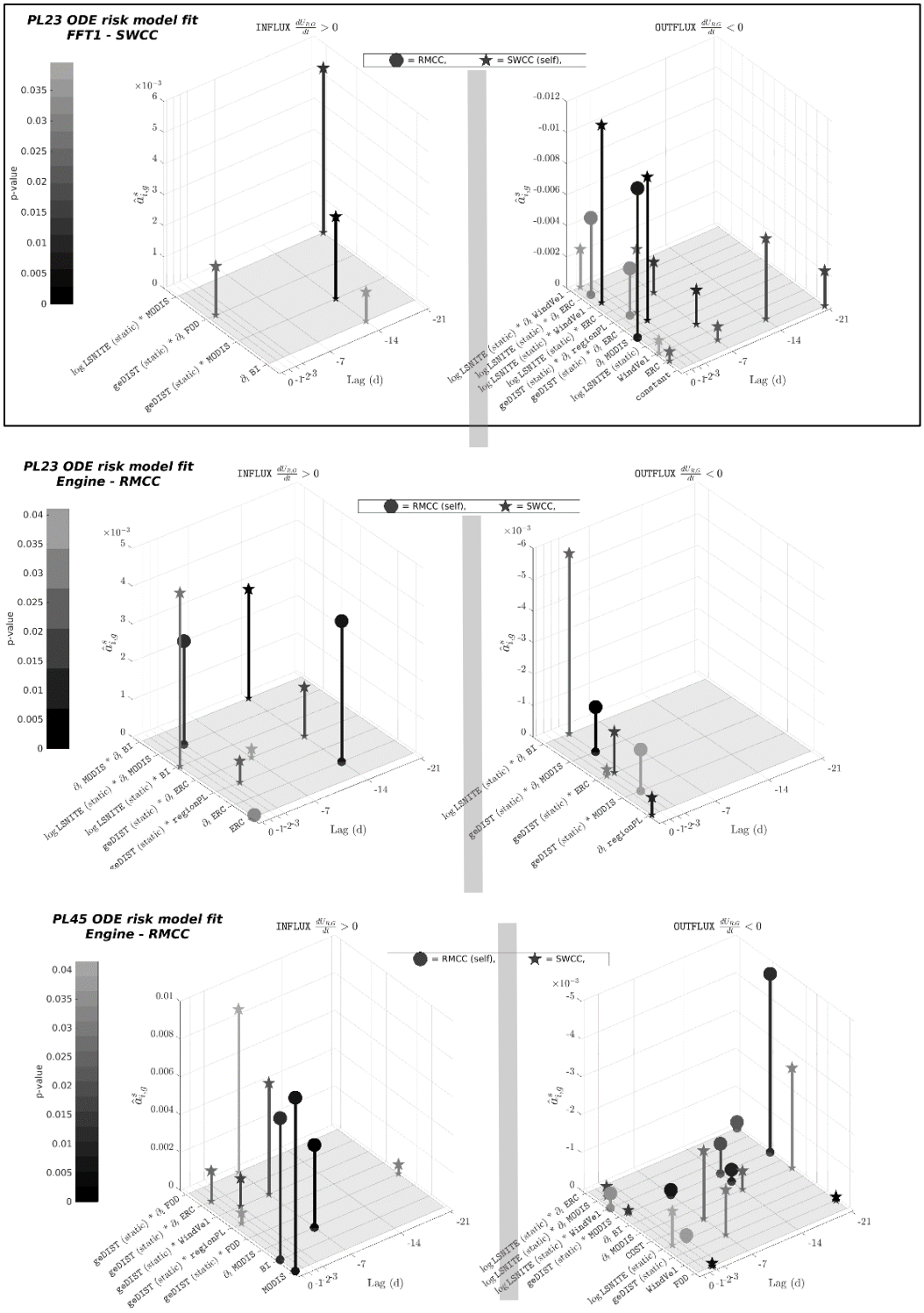

FIGURE 2.2a, 2.2b, 2.2c - shown in order… *(MobETA LEFT PANEL) (MobETD RIGHT PANEL)*

Caption:

Foreground axes are for Lag and $FACTORS$. Vertical axes are for the coefficient's mean value over E replicates. The left plot shows mobilization to incidents in the GACC. The right plot has its axes reversed to display release or demobilization from incidents in the GACC. Dots and markers specify the coefficient belongs to the same (self) GACC or the other GACC in these two-region sharing models. A bar at the left gives the significance of the coefficient within our two ranges $p < 0.01$ and $p \in (0.01,0.0435]$. Each plot set is specific to the PL sample, RESOURCE, and GACC in the ODE model being fit i.e. in the above instance $PL23$ sample results for FFT1 in the RMCC.

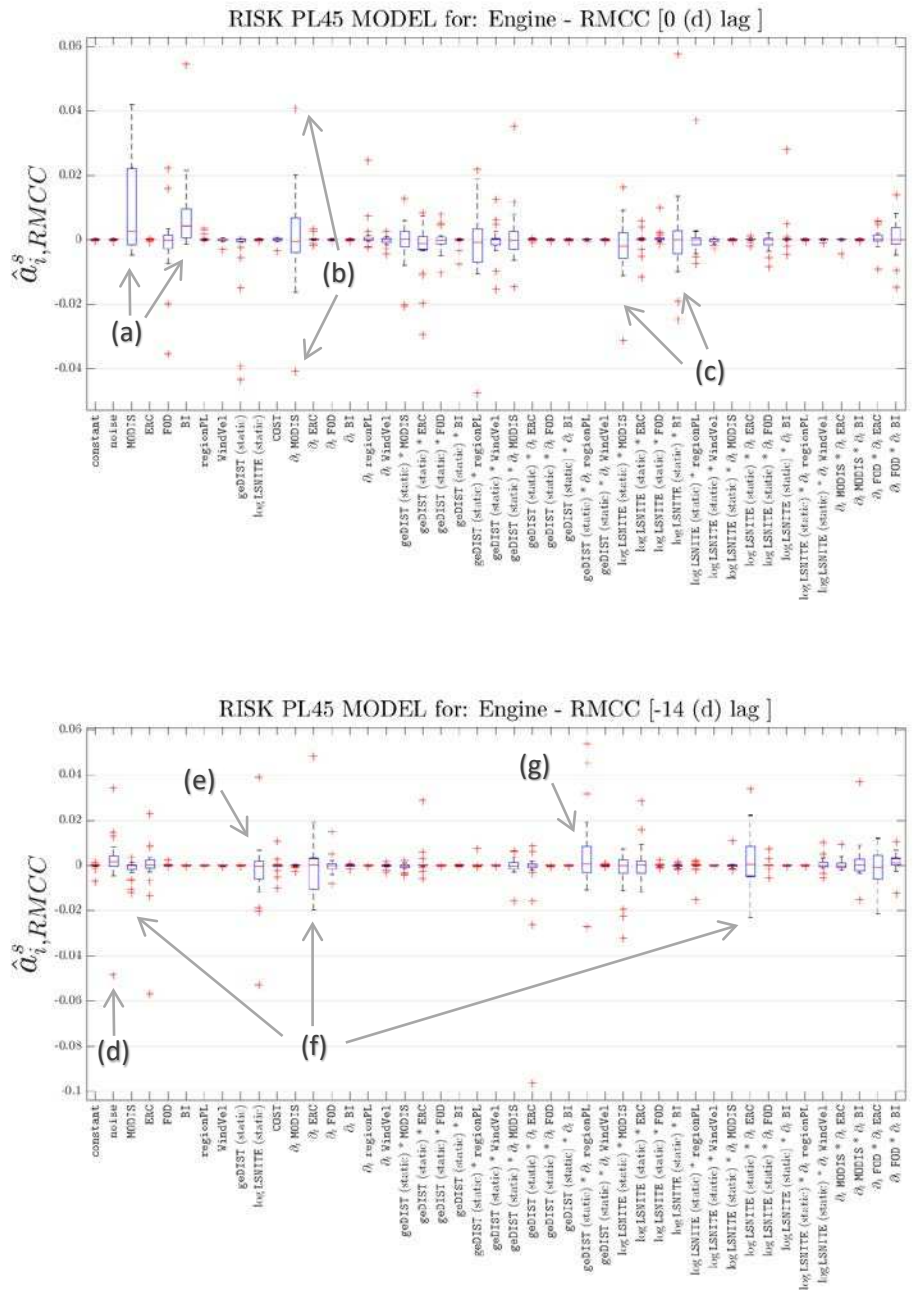

FIGURE 2.3 - Variability of ODE model coefficients

Caption:

Vertical boxplots across E replicates for best fit risk coefficients to t_n sample. Comments (a) – (f) in text explain how we interpret the variability and outliers.

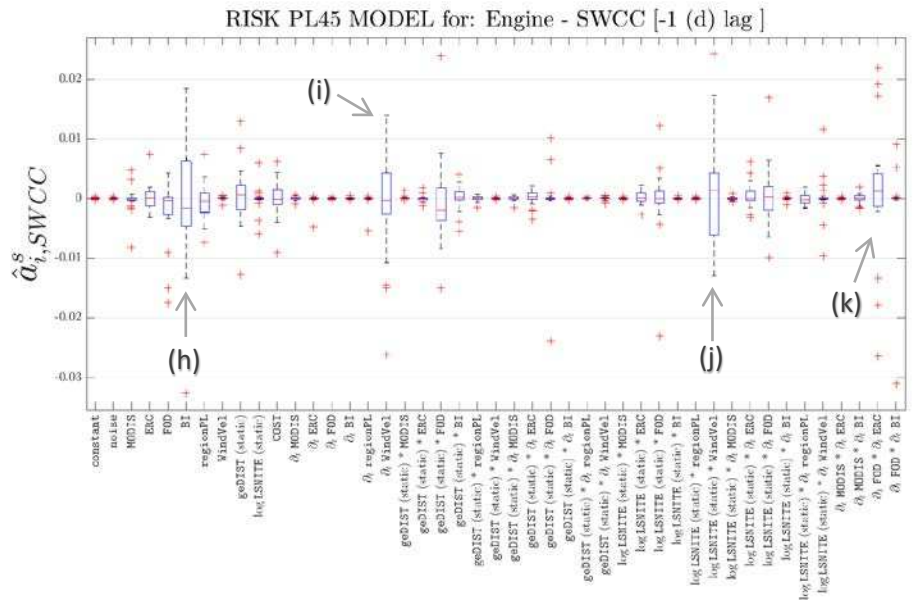

FIGURE 2.3 - Variability of ODE model coefficients

Caption:

All GIS layer fit display. Comments (h) - (k) in text. *Interpreting the plot as variability instead of significance.

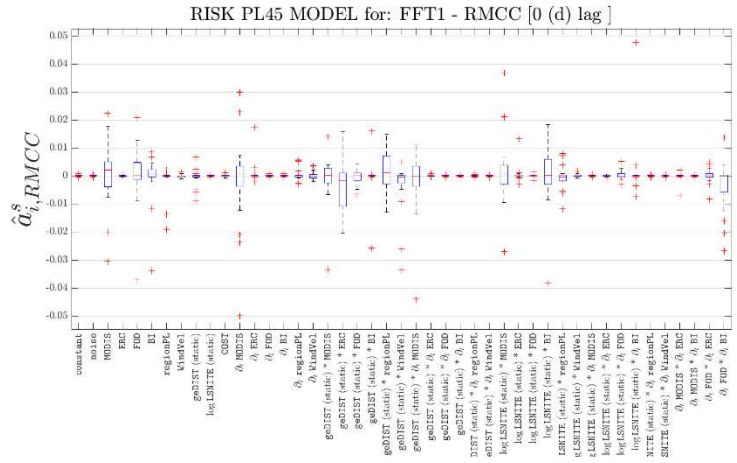

FIGURE 2.4a

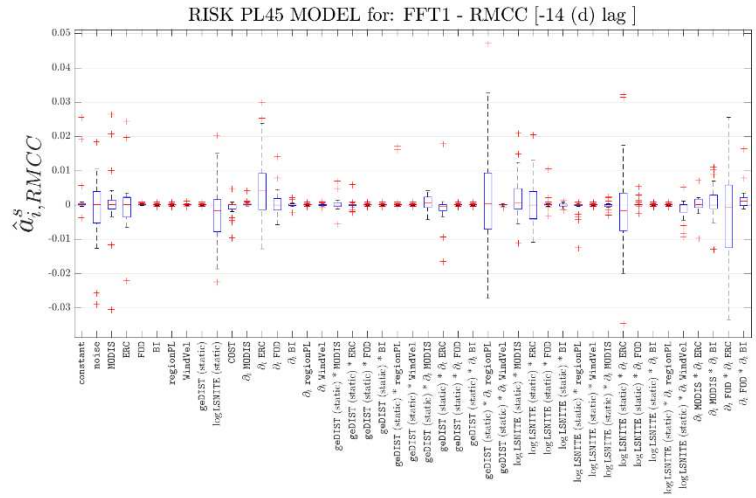

FIGURE 2.4b

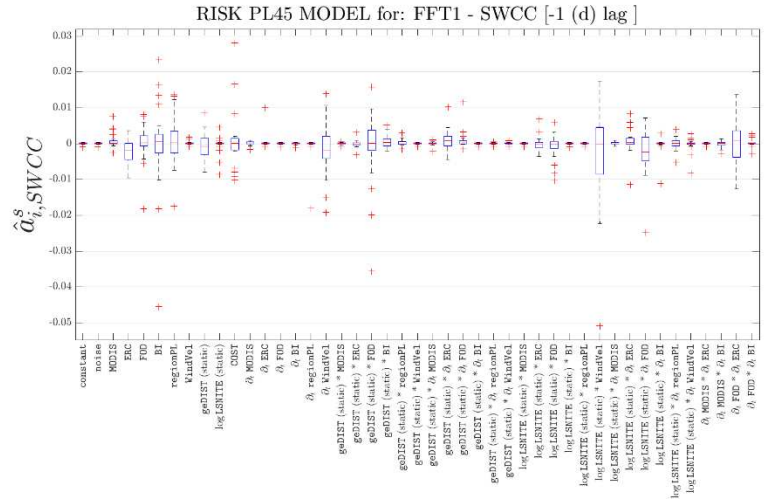

FIGURE 2.4c

FIGURE 2.4 - Variability of ODE model coefficients

Caption: All GIS layer fit display.

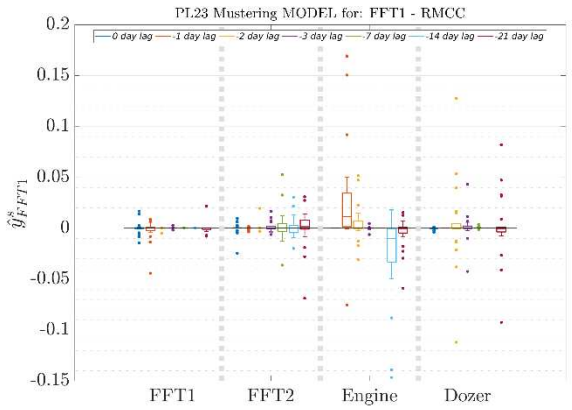

2.5a

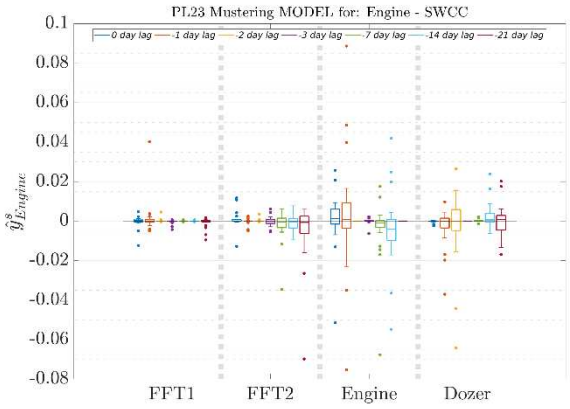

2.5b

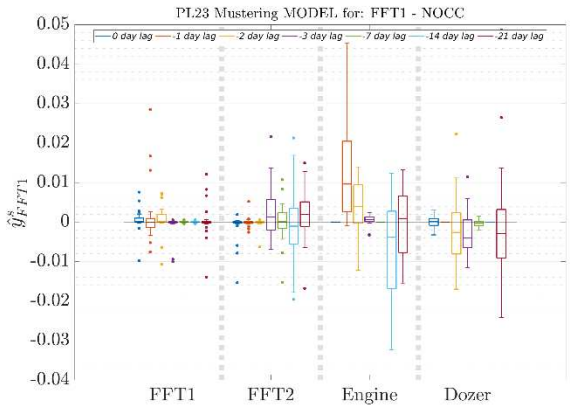

2.5c

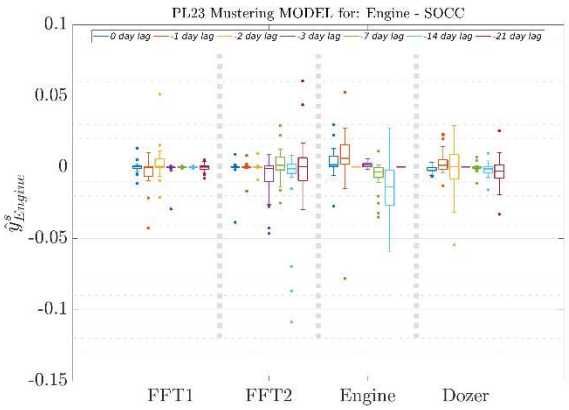

2.5d

FIGURE 2.5a, 2.5b, 2.5c, 2.5d - Cooperative demand impact panel

Caption:

Reinforce/release demand patterns in our data. Interpret as variability. Positive/negative significance is known when the box is bounded away from zero. Vertical box plots across E replicates for colored lags across resource types on the horizontal axis. See text for our observations.

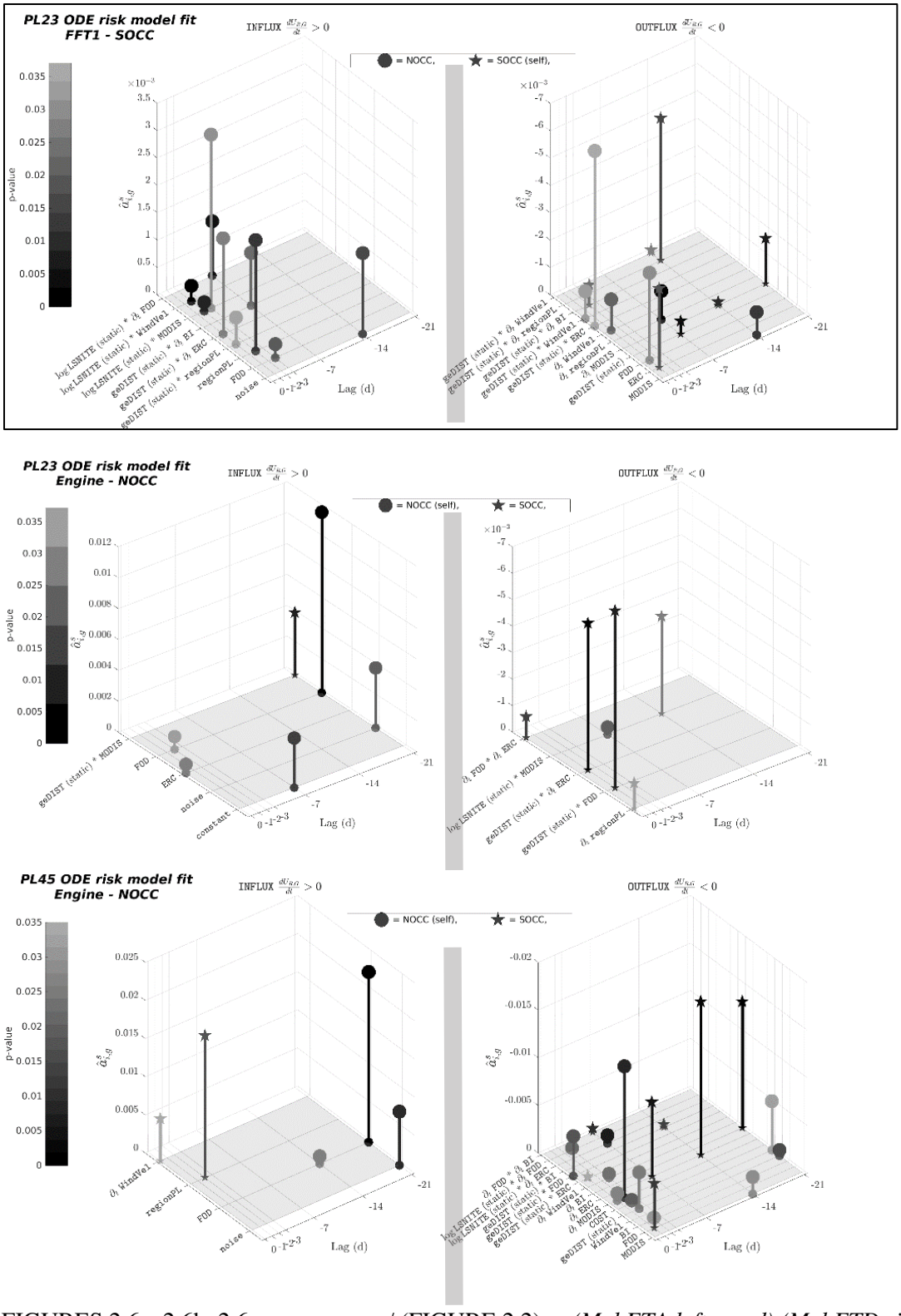

FIGURES 2.6a, 2.6b, 2.6c - compare w/ (FIGURE 2.2)… *(MobETA left panel) (MobETD right panel)*

Caption: California risk results for test case (B2).

REFERENCES FOR CHAPTER 2

Abatzoglou, J.T., 2013. Development of gridded surface meteorological data for ecological applications and modelling. Int. J. Climatol. 33, 121–131. https://doi.org/10.1002/joc.3413

Aster, R.C., Borchers B., and Thurber, C.H., 2013. Parameter estimation and inverse problems, 2nd ed. ed. Academic Press, Waltham, MA.

Belval, E.J., Wei, Y., Calkin, D.E., Stonesifer, C.S., Thompson, M.P., Tipton, J.R., 2017. Studying interregional wildland fire engine assignments for large fire suppression. Int. J. Wildland Fire 26, 642–653. https://doi.org/10.1071/WF16162

Brown, M.C., 2006. Hacking Google Maps and Google Earth. Wiley, Indianapolis, IN.

Calkin, D.E., Gebert, K.M., Jones, J.G., Neilson, R.P., 2005. Forest service large fire area burned and suppression expenditure trends, 1970-2002. J. For. 1034 179-183.

Calkin, D.E., Thompson, M.P., Finney, M.A., Hyde, K.D., 2011. A Real-Time Risk Assessment Tool Supporting Wildland Fire Decisionmaking. J. For. 109, 274–280. https://doi.org/10.1093/jof/109.5.274

Corless, M.J., 2016. AIMD dynamics and distributed resource allocation, Advances in design and control. Society for Industrial and Applied Mathematics, Philadelphia.

Dormand, J.R., Prince, P.J., 1980. A family of embedded Runge-Kutta formulae. J. Comput. Appl. Math. 6, 19–26. https://doi.org/10.1016/0771-050X(80)90013-3

Durrett, R., Levin, S., 1994. The Importance of Being Discrete (and Spatial). Theor. Popul. Biol. 46, 363–394. https://doi.org/10.1006/tpbi.1994.1032

Giglio, L., Schroeder, W., Justice, C.O., 2016. The collection 6 MODIS active fire detection algorithm and fire products. Remote Sens. Environ. 178, 31–41. https://doi.org/10.1016/j.rse.2016.02.054

Hand, M., Katuwal, H., Calkin, D.E., Thompson, M.P., 2017. The influence of incident management teams on the deployment of wildfire suppression resources. Int. J. Wildland Fire 26 615-629 26, 615–629. https://doi.org/10.1071/WF16126

Katuwal, H., Calkin, D.E., Hand, M.S., 2016. Production and efficiency of large wildland fire suppression effort: A stochastic frontier analysis. J. Environ. Manage. 166, 227–236. https://doi.org/10.1016/j.jenvman.2015.10.030

Klein, G., Calderwood, R., Clinton-Cirocco, A., 2010. Rapid Decision Making on the Fire Ground: The Original Study Plus a Postscript. J. Cogn. Eng. Decis. Mak. 4, 186–209. https://doi.org/10.1518/155534310X12844000801203

Li, J., Chen, Y.-T., 2009. Computational partial differential equations using MATLAB, Chapman & Hall/CRC applied mathematics and nonlinear science series. CRC Press, Boca Raton.

Lyon, K.M., Huber-Stearns, H.R., Moseley, C., Bone, C., Mosurinjohn, N.A., 2017. Sharing contracted resources for fire suppression: engine dispatch in the Northwestern United States. Int. J. Wildland Fire 26, 113–121. https://doi.org/10.1071/WF16100

Preisler, H.K., Westerling, A.L., Gebert, K.M., Munoz-Arriola, F., Holmes, T.P., 2011. Spatially explicit forecasts of large wildland fire probability and suppression costs for California. Int. J. Wildland Fire 20, 508–517. https://doi.org/10.1071/WF09087

Riley, K., Stonesifer, C., Calkin, D., Preisler, H., 2015. Assessing predictive services' 7-day fire potential outlook. Keane Robert E Jolly Matt Parsons Russell Riley Karin Proc. Large Wildland Fires Conf. May 19-23 2014 Missoula MT Proc RMRS-P-73 Fort Collins CO US Dep. Agric. For. Serv. Rocky Mt. Res. Stn. P 188-195 73, 188–195.

Short, M.B., Brantingham, P.J., Bertozzi, A.L., Tita, G.E., 2010. Dissipation and displacement of hotspots in reaction-diffusion models of crime. Proc. Natl. Acad. Sci. U. S. A. 107, 3961–3965. https://doi.org/10.1073/pnas.0910921107

Silva, F.R. y, Martínez, J.R.M., González-Cabán, A., 2014. A methodology for determining operational priorities for prevention and suppression of wildland fires. Int. J. Wildland Fire 23, 544–554. https://doi.org/10.1071/WF13063

Stonesifer, C.S., Calkin, D.E., Hand, M.S., 2017. Federal fire managers' perceptions of the importance, scarcity and substitutability of suppression resources. Int. J. Wildland Fire 26 598-603 26, 598–603. https://doi.org/10.1071/WF16124

Thompson, M.P., Calkin, D.E., Finney, M.A., Gebert, K.M., Hand, M.S., 2013. A risk-based approach to wildland fire budgetary planning. For. Sci. 591 63-77 63–77.

Wei, Y., Belval, E.J., Thompson, M.P., Calkin, D.E., Stonesifer, C.S., 2017. A simulation and optimisation procedure to model daily suppression resource transfers during a fire season in Colorado. Int. J. Wildland Fire 26, 630–641. https://doi.org/10.1071/WF16073

Wibbenmeyer, M.J., Hand, M.S., Calkin, D.E., Venn, T.J., Thompson, M.P., 2013. Risk Preferences in Strategic Wildfire Decision Making: A Choice Experiment with U.S. Wildfire Managers. Risk Anal. 33, 1021–1037. https://doi.org/10.1111/j.1539-6924.2012.01894.x

Contemporary Policy Documents

(Interagency Red Book, 2017) Interagency Coordination and Cooperation: Interagency Standards for Fire and Fire Aviation Operations, NFES 2724 edition, January 2017.

(Mobilization Guide, 2016) National Interagency Mobilization Guide: Geographic Areas. NFES 2092. 1-29; 31-53; 55-56; 81-87, March 2016.

(Preparedness Levels, National Interagency Mobilization Guide, chapter 20) National Preparedness Level Definitions, [Available]: https://www.nifc.gov/fireInfo/fireinfo_prepLevels.html Accessed: 2/27/18

CHAPTER 3 – PDE-CONSTRAINED ALLOCATION

3.1 Why PDEs? What is being constrained? Fire management background

This chapter outlines the framework for a partial differential equation (PDE) system model to add to the technological toolkit for fire management analyses. We have applied PDEs to personnel movement in the fire suppression allocation problem because PDEs have been used in the past to provide mathematically rigorous descriptions of chaotic dynamics. In addition, we develop a mixed binary-linear math program to examine the performance of the PDEs under an optimal control framework. The PDEs can express both temporal and spatial variation in a dependent scalar or vector variable, which is an important trait in modeling wildland fire resource allocation.

We identified a parabolic, heat-type PDE model based on trends in time series data, patterns in raster spatial data, and requirements of near-term forecasting. Parabolic, heat-type PDEs are linear. The PDE model identified in this paper can be solved numerically but is not solved analytically. Our framework is a PDE-constrained optimization where the PDE constraints are coupled parabolic equations of vector and scalar potentials. This chapter will explain the physics principles of potential, system energy, and statistical mechanics we see as important to the fire suppression management problem.

Fire suppression involves ground based resources to build fire line and provide point protection (i.e., firefighters, engines, dozers) and aerial support to drop slurry and water on advancing flames (i.e., helicopters and airtankers). In addition, managers are needed to orchestrate on-the-ground resource response including fire suppression strategy, organization of fire camp, mobilization and demobilization of resources, and interaction with the media; these

managers are typically part of the Incident Command Teams. We assume those managers have access to fire risk information. Probabilistic fire behavior models and their data inputs would be an example of key burn projections the command team might have (Finney et al., 2011), (Linn et al., 2002), (Mandel et al., 2011).

3.2 Literature Review

PDEs were a fast-growing numerical field through the 1980s, 1990s, and continue to find use in countless models of physical flows (Brezis and Browder 1998; Evans 2010; Farlow 1993). Our dynamic modeling goals are similar to those of statistical mechanics on many-particle systems. Statistical mechanics uses limiting arguments about the sheer number of particles to establish macroscopic measures from microscopic behavior via ensembles. The complexity of the fire suppression management problem can be an issue when drawing analogies between our model and physical flow problems directly. First, even though we model the motion of tens of thousands of people and their equipment, the limiting arguments from statistical mechanics do not hold. While there are a large number of firefighting resources in action, there are not as many as a molecular system. Physical systems are much larger and therefore afford some continuous limits we cannot take. Continuum models work best when there are large numbers of particles in the system or there exists some natural spatial constraint that can reduce the spatial dimension of their dynamics. Second, using a realistic number of risk information input data can lead to combinatorically-large approximation spaces. Sorting non-optimal solutions during parameter identification can generate big data in intermediate and output model results.

(FIGURE 3.1) shows the variety of time scales over which PDEs and fire models have occurred in the past. This examination of literature helped us narrow down candidate PDEs. We reviewed math models of traffic flow, heat transport in real media, and crime hotspot formation

from the literature. Traffic models continuize car-by-car dynamics using a change of state space to continuous density and flux. (Holmes 2009) shows how parabolic, transport-type PDE equations are derived from such assumptions. Single cars are anonymous and only macroscopic metrics matter to control traffic. Researchers use tracking data on road network configurations to find patterns in driver behavior (Fan and Seibold 2012; Helbing 2001). Simple spatial control elements like traffic circles have been shown to create patterned behavior in drivers (Sugiyama et al. 2008). Traffic models find success, in part, because vehicle flow proceeds in a well-defined direction. A one-dimensional assumption is reasonable. Fire management has a topographic North-South-East-West context, bumping our spatial domain of interest to two dimensions.

We found two (or greater) dimensional heat-type PDE models have been tested with real tracking data for animals including skipjack tuna (Sibert et al. 1999), locusts (Topaz et al. 2012), and elk (Brillinger 2007). Transport phenomena, random/Brownian motion, and source/sink dynamics can all be simulated numerically. PDEs apply to human movement too. In the one dimensional case (Protopopescu, Santoro, and Dockery 1989). This paper is about troops marching. The paper uses a first order convolution spatial model with advection, diffusion, and reaction, from the fifth equation therein:

$$u_t = (D_1 u_x)_x + (C_1 u)_x + u\big(a_1 + b_1 u + \int c_1(x-y)v(y)\,dy\big) + d_1 v + e_1$$
$$v_t = (D_2 v_x)_x + (C_2 v)_x + c\big(a_2 + b_2 v + \int c_2(x-y)u(y)\,dy\big) + d_2 u + e_2$$

It is a first order, coupled integral equation sometimes called the Lanchester equations. Instead of enumerating the parameters, we make two theoretical notes of the model form. A of all, the variable u is coupled to the variable v. B of all, the spatial derivatives are in a self-adjoint form, which appear in this paper as well. Results of march simulations show a realistic, albeit, one-

dimensional head-to-head, pass-through, and pursuit modes. As well as the jostling one would expect as individuals maintain their space within the column. Overall, it is nice to compare a math model of combat with the fire management problem.

In the two dimensional case PDEs can model how human movements exhibit transport and random walking; (González, Hidalgo, and Barabási 2008) provide a comprehensive summary of how mobility field parameters of PDEs can describe human walking paths. Given tracked data, the inverse problem for the PDE is to estimate a mobility field.

(Short et al. 2010) used urban burglary data to show how background crime risk interacts with dynamic risk and policing in more than 2 spatial dimensions. Their model accounted for variation in criminal density in time and space. Their model for criminal behavior included law enforcement crackdowns as well as parameters for criminal movement from the database. Researchers noticed rings and hot-spots forming in their criminal density model output and performed a nuanced pattern analysis classifying the persistence of hot-spots as sub-critical or super-critical. They learned the policing pattern could be changed to break the stability of hot-spots and reduce crime in the city. Just as policing policy benefited in this case from modeling criminals, PDEs may help us learn nuances in the wildfire suppression system.

Looking further in (Short et al. 2010) we found reaction is like a dynamic pressure. The analogy to draw is to a heat sink or source. In wildfire allocation, directionally mobilized resources will no longer diffuse randomly, but be drawn towards the reaction site. This is analogous to criminals being attracted to victims and avoiding police in crime modeling. At its core, the crime hotspot formation is a coupled PDE model that includes reaction, diffusion, and source/sink features. The equations for this model are:

$$\frac{\partial B}{\partial t} = \eta D\vec{\nabla}^2 B - \omega B + \kappa\rho A$$
$$\frac{\partial \rho}{\partial t} = D\vec{\nabla} \cdot \left[\vec{\nabla}\rho - 2\rho\vec{\nabla}\ln A\right] - \rho A + \gamma$$

The independent variables are time t and space x. These are continuous in the model with time steps of one day and a scope of about one year in the simulations. Spatial resolution is high enough for convergence and the scope is neighborhood in Los Angeles, California – the extent of the burglary data. The endogenous dependent variables are: environmental risk $A(t, x)$ describing the level of background crime risk, dynamic risk $B(t, x)$ describing the fluctuations above and below background, and density of criminal agents $\rho(t, x)$ describing the relative density of criminal offenders. The exogenous parameters are:

- The diffusion coefficient $\eta\ D$ has two components $\eta \in [0,1]$ and $D > 0$. These work together to control the $\vec{\nabla}^2$ diffusion term, which the authors mention as a "near-repeat phenomenon." Criminals tend to victimize multiple people in the same 2000 meter-radius area, albeit randomly within this domain, over time.
- A risk decay factor $\omega \geq 0$ describes how spikes in dynamic risk B decay to the background risk A over time,
- An attractive force parameter $\kappa \geq 0$ tells to what extent criminal agent density ρ interacts with environmental risk A to cause dynamic risk to increase,
- And the criminal introduction rate $\gamma \geq 0$ describes how criminals move into the area.

The paper uses a technical, but primarily qualitative, technique to study the reaction/ diffusion and predator/prey dynamics. They are able to examine large perturbations that drive the density of criminal agents to zero as law enforcement makes arrests. Areas where there was no crime suppression tend to serve as a sink for criminals. Hot spot patterns form around the suppression

areas that seem to spread risk in an undesirable way, generating more crime areas by dispersed criminals. However, these negative effects can be ameliorated in a second round of suppression or by varying the duration of the suppression effort. Differentiating between sub-critical and super-critical hot spots is one of the model's contributions that can lead to sustainable reduction of crime. Both the crime model and our wildfire suppression model are in terms of human agents. When those agents make decisions, unintended consequences can arise. We are looking for similar optimal control switches in this study.

In contrast to PDEs, operations research methodology have been extensively applied to fire suppression problems. To review them all is beyond the scope of this work. Instead we postulate the methods in (Xun et al. 2013) could be applied to our model as well. Close analogs to the PDE problem in wildfire management are found in (Preisler and Westerling 2007) and a temporal characterization of the interregional sharing problem in general is analyzed for Canadian provinces in (Magnussen and Taylor 2012).

Suppose some process called $\mathcal{G}$, connects fire risk information to the allocation decision output. In our visualizations of ROSS data, we can see $\mathcal{G}$ in action. Could a PDE model this behavior? Certainly, if the drivers for demand potential Φ and supply potential $\overrightarrow{\Phi}$ were known and the model were identified. (Klein, Calderwood, and Clinton-Cirocco 2010) and (Sharkey and Davis 2008, Hard Work) shows establishing an ad hoc set of rules that correctly follow this human-driven system is impossible. Such human-based problems tend to suffer from Np-hardness. We turn to continuous time-space linear PDEs to attempt to describe $\mathcal{G}$.

3.3 PDE Model Specification

Our theoretical model varies in continuous time t. However, our numerical model varies across discrete times t_n, like snapshots or samples taken from some longer time interval $[T_0, T_F] \subset \mathbb{R}$. Similarly, our theoretical model varies across a simply connected domain $x \in \Omega \subset \mathbb{R}^{\dim \geq 2}$ while our numerical model varies across structured grid points $\xi \in \mathbb{Z}^{\dim \geq 2}$. Domain boundaries will be called $\partial\Omega$. Domain Ω is partitioned into subunits $\Omega = \bigcup_g \Omega_g$ that have boundaries $\partial\Omega_g$. We write ordered time-space pairs like (t, x) for continuous independent variables. Superscript ^{n} for sample time t_n and subscript $_\xi$ for grid points ξ. (TABLE 3.1) gives a conceptual diagram of the process. It emphasizes that risk state spaces might be large and discrete. So we assume continuous risk update information comes in kernels of GIS time series data indexed $= 1,\ 2, \ldots$. Our test case optimizes a self-adjoint PDE with advection, diffusion, and reaction commonly found in the literature.

We are looking to identify a hidden process model $\mathcal{G}$ to interact wildfire risk with demand for fire suppression resources. We start by defining continuous/discrete exogenous variable $\mathcal{R}_i(t, x)/\mathcal{R}_{i,\xi}^n$ as a risk assessment. These are expressed risk weights or components in an additive mental model on GIS risk information layers (continuous: risk map as in (Calkin et al. 2011) /discrete: binary, decimal, percentage, etc.) This studies single component risk models and multi-component risk models using GIS data. In our theory, we assume risk sub-models with linear components:

$$\text{linear scalar field } \mathcal{R}(t, x) = \sum_{i=1}^{45} \alpha_i R_i(t, x) \qquad (1)$$

$$\text{linear gradient field } \vec{\mathcal{R}}(t,x) = \sum_{i=1}^{45} \beta_i \vec{\nabla} R_i(t,x) \qquad (2)$$

In our test cases, there were at most 45 risk factor weights, but any number are possible.

Next, we define demand and supply as continuous potentials:

$\Phi_D(t,x)/U_\xi^n$ scalar demand potential,

$\Phi_D(t,x)$ part of the physics model, and U_ξ^n a smoothed count density metric

*In test cases, U is stored as adaptive vector data. Data size depends on model localization: national, regional, local, grid resolution, etc.

$\vec{\Phi}_S(t,x)/\vec{a}_\xi^n$ is the same, but for a vector potential,

$\vec{\Phi}_S(t,x)$ part of physics model, and $\vec{a}_\xi^n$ a vector of parameters we fit

*In test cases, $\vec{a}$ is fit as a model parameter. It is a vector field related to the optimal allocation direction. We will use MATLAB to draw the vector fields in different ways

GIS input data resolution has been tested at $9km$, $18km$, $36km$, and $44km$ grid side and found to give consistent results.

Our approach is to assume a general PDE form for $\left[\Phi_D, \vec{\Phi}_S\right] = \mathcal{G}\left(\mathcal{R}, \vec{\mathcal{R}}\right)$ and perform two specific approximations. First, approximate the field $\vec{a}_\xi^n$ based on demand data U_ξ^n and some assumptions about α_i in the risk data sub-model equation (1). Second, calibrate the risk models based on an inversion $\left[\mathcal{R}, \vec{\mathcal{R}}\right] = \mathcal{G}^{-1}\left(\Phi_D, \vec{\Phi}_S\right)$. This is a nonlinear inverse problem involving scalars and vectors. Projecting the PDE onto these data kernels reveals spatial correlation.

Identifying a best-fit PDE process model for $\mathcal{G}$ will constrain the optimal control to solutions that have admissible dynamics. For now, $\mathcal{G}$ can be assumed to exist. Fire managers express their risk preferences in ordering, but patterns in these actions might be difficult to isolate. The goal is to learn risk coefficients α_i or even β_i for risk gradients in equation (2) from historical allocation data. The size and complexity of working with $\mathcal{G}^{-1}$ depends on the extent and detail of $i\ , \xi, n, \omega$, and the grid resolution.

Common PDE parameters are shown in (TABLE 3.2). We use them to state $[PDEsys]$ as an initial boundary value problem:

$$
\begin{cases}
\frac{\partial \Phi_D}{\partial t}(t,x) = \vec{\Phi}_S \cdot \vec{\nabla}\Phi_D(t,x) + b\,\vec{\nabla}\cdot\vec{\nabla}\,\Phi_D(t,x) + c\,\Phi_D(t,x) + f \quad \text{demand evolution} \quad (3a) \\
\frac{\partial \vec{\Phi}_S}{\partial t}(t,x) = \vec{v}\cdot\vec{\nabla}\Phi_D(t,x) + \vec{w}\times\vec{\nabla}\,\Phi_D(t,x) \quad \text{allocation strategy} \quad (3b) \\
ICs\colon \begin{cases} \Phi_D(t_0,x) = U_0(x) & \text{initial demand potential} \quad (4a) \\ \vec{\Phi}_S(t_0,x) = \vec{A}_0(x) & \text{initial supply potential} \quad (4b) \end{cases} \\
EBCs\colon \begin{cases} \left\|\vec{\Phi}_S(t,x_0)\right\|_p \geq Q_0(t) \quad \forall\, x_0 \in \Omega_0(t) & \text{drawdown resources } (5a) \\ \frac{\partial \Phi_D}{\partial \hat{n}}(t,x) = 0 \quad x \in \partial\Omega \text{ bndy } \Omega & \text{conservative domain } (5b) \end{cases} \\
NBC\colon \left\{\frac{\partial \vec{\Phi}_S}{\partial t}\left(t, x \in \partial\Omega_g\right) = h_g(t) \quad \forall x \in \partial\Omega_g \right. \quad \text{supply fluxes } (6)
\end{cases}
$$

Equations (3) – (6) represent a coupled system of PDEs; our theoretical model for allocation dynamics:

$(3a)$ Heat PDE governs the ebb and flow of demand potential,

$(3b)$ Supply potential is coupled to the demand heat PDE as a vector allocation strategy,

$(4a)$ At time t_0, known initial conditions $U_0(x)$ for the scalar potential

$(4b)$ $\vec{A}_0(x)$ for initial vector potential,

$(5a)$ Lower fixed bound on supply to represent a holding amount,

$(5b)$ No-slip boundary condition using $\hat{n}$ for outward unit normal to $\partial\Omega$ means no demand generates across boundary and therefore supply will not be allocated in these directions,

(6) Data-driven boundary condition $H_g(t)$ along connected subdomain boundaries $\partial\Omega_g$

This initial boundary value problem facilitates our study of approximate numerical solutions. We will not solve the entire system, but rather several key pieces. An additional note on the boundaries is warranted here:

- PDEs need boundary and initial conditions to converge numerically. In the fire allocation system, such boundaries include where resources are held or drawn down and FMZ boundaries. Our model is particularly sensitive to activity near the borders of FMZs. These are flux boundary conditions. (Holmes 2009) explains how boundary layer analysis helps assuage difficulties along boundaries.

The next section poses a grand allocation problem in order to understand what our work with the risk sub models and PDEs will tell us. Without the framework, there are too many contingencies in the model. It is common to associate a given PDE with an optimization problem via principles of conservation of energy and of mass (Brezis and Browder 1998; Evans 2010; Farlow 1993). We assume the number of fires suppression resources in the available pool is constant.

3.4 Optimization Framework

Process $\mathcal{G}$ suffers an imbalance of information with many risks to choose from in $\mathcal{R}(t,x)$ as compared to limited supply and demand data. Optimal control of this system is taken by proposing an objective function involving GIS risk submodels (1) and (2), the scalar demand

potential $\Phi_D(t,x)$, and the vector supply potential $\overrightarrow{\Phi}_S$. The associated optimization framework for interregional resource sharing and allocation is:

$$\Upsilon\left(\Phi_D, \overrightarrow{\Phi}_S\right) \mapsto \text{extremum} \quad (7)$$

$$subject\ to:$$

$$\begin{cases} \mathcal{G}\left(\mathcal{R}, \vec{\mathcal{R}}\right) = \left[\Phi_D, \overrightarrow{\Phi}_S\right] & (8) \\ \psi\left(\Phi_D, \overrightarrow{\Phi}_S\right) = \mathbf{0} & (9) \end{cases}$$

$$where\ \mathcal{R}, \vec{\mathcal{R}}, \Phi_D, \overrightarrow{\Phi}_S\ depend\ on$$

$$(t,x) \in [T_0, T_F] \times (\Omega \cup \partial\Omega) \subset \mathbb{R}^{1+\dim \geq 2} \quad (10)$$

Explanation of terms

(7) Objective function $\Upsilon \in \mathbb{R}$ is the quantity to minimize or maximize. Different demand potential Φ_D and supply potential $\overrightarrow{\Phi}_S$ configurations can be penalized or encouraged,

(8) Nonlinear process model $\mathcal{G}$ will depend on the risks and deliver the demand and supply; we have hypothesized a general parabolic, heat-type PDE,

(9) ψ is a sharing network to route dispatched resources from supply to demand, we do not model this sharing network in a normative model, see Chapter 1 for a descriptive treatment via Dijkstra's classic algorithm, for more information about the network see (Alderson 2008), for key principles behind minimum arrival time algorithms see (Mees 1986), and recent refinements in (Duff, Chong, and Tolhurst 2015)

(10) Continuous domain statement using set notation

This framework can be compared to previously formulated optimal control frameworks for physical problems (Zlotnik, Chertkov, and Backhaus 2015; Jourdain, Le Bris, and Lelièvre 2005). A key insight for the fire management problem is to reduce the network ψ's complexity.

By tackling the continuous potentials in (8), we lower the dimensionality of this problem by avoiding nodal evaluation of risk in equation (9). The framework helps make the Np-hardness of discrete node evaluation tractable using continuous time-space PDEs. We discuss the objective function (7) in the following sub-section.

3.4.1 Continuous Objective Functions

We define error norms here as they were important in model regularization and fitting. Let z be a vector. The spatial p-norm of interest is $\|z\|_p = \sqrt[p]{\sum z^p}$ where $p = \infty$ indicates the max norm and $p = 1$ is the sum of the absolute values of the components of z. On a continuous domain this is an integral measure $\left(\int_{\Omega \cup \partial\Omega} [z(x)]^p \, dx\right)^{1/p}$. We work with square integrable functions L_2 – GIS data surfaces. We used integration quadrature taking a root mean square error $\sqrt{RME}$ to measure model error $\epsilon_{model}(t) = \left\|\mathcal{G}\left(\mathcal{R}, \vec{\mathcal{R}}\right) - data\right\|_2$; $data$ is a placeholder for the smoothed potentials and parameter estimation in $\left[\Phi_D, \vec{\Phi}_S\right]$. In essence, the p-norm is a spatial averaging of GIS data.

Spatial average in hand, our temporal objective function $\Upsilon(z) = \min_z \int_{T_0}^{T_f} \| z\,(t)\|_p \, dt$ integrates the control function z over time. The functional $\Upsilon : \left(T_0, T_f\right) \times (\Omega \cup \partial\Omega) \mapsto [0,1]$, has decimal values in the range $[0,1]$. So for a best fit on the interval $[T_0, T_F]$ we might take residual minimization $\Upsilon\left(\epsilon_{model}(t)\right) = \min_z \int_{T_0}^{T_F} \epsilon_{model}(t) \, dt$. For regularization of model error take the total variation procedure $\left\|\mathcal{L}(\mathcal{R}, \vec{\mathcal{R}})\right\|_1$ described in (Aster, Borchers, and Thurber 2013) so as to not overfit the data with the PDE model. An objective could involve multiple goals with customizable penalties λ:

- λ_0 Fit the data, a penalty on model residuals $\epsilon_{model}(t)$,
- λ_{advect} Advection penalty on the allocation direction,
- λ_{smooth} Interpretability of model, balance between model and data,
- λ_{UNMET} Penalty for unmet demand,
- $\lambda_{gas\ mileage}$ Hypothetical penalty for supply variability.

The continuous version of $[PDEsys - LP]$'s objective function:

$$\Upsilon(\Phi_D.\vec{\Phi}_S) = \min \int_{T_0}^{T_F} \left(\lambda_0\, \epsilon_{model}(t) + \lambda_{advect} \left\| \vec{\Phi}_S \cdot \vec{\nabla} \Phi_D \right\|_1 + \lambda_{smooth} \left\| \mathcal{L}(\mathcal{R}, \vec{\mathcal{R}}) \right\|_1 + \lambda_{UNMET} \|\Phi_D\|_\infty \right.$$

$$\left. + \lambda_{gas\ mileage} \left\| \frac{\partial \vec{\Phi}_S}{\partial t} \right\|_2 \right) dt \quad (*)$$

The functional $(*)$ is very general. Our focus is $\lambda_0 = 1, \lambda_{smooth} = \lambda_{UNMET} = \lambda_{gas\ mileage} = 0$. We will explore some risk factor models with $\lambda_{advect} = \gamma \neq 0$. Discretization of such a function is shown in the p-norm sense in (Chong and Żak 2013). Also in this reference are general descriptions of Banach space optimization. We are doing some sequential Banach space projection here. First, onto the linear PDE operator space and then the linear risk sub-model space. Next, we move to the discretization of (10).

3.4.2 Grid Transformation Procedure

To generate structured grids for GIS data we synthesized techniques from (Barrera-Sanchez et al., 2009), (Ivanenko, 1998), and (Vianey Villamizar, 2007). Our grids, shown for the United States at right, conformed to the boundaries $\partial\Omega_g$ of each Geographic Area Coordination Center. Our grid construction method resembles transfinite interpolation, which is a parametric boundary deformation. A bijective grid transformation $\mathcal{T} : (lx, ly) \leftrightarrow (\xi, \eta)$ was used to wrangle

NAD83 latitudes lx and longitudes ly into rectangles with unit spacing indexed by $\xi = 1, \dots, X$ and $\eta = 1, \dots, Y$. As recommended in (Ivnenko, 1998), grid post-optimization was performed to minimize convexity violations where the grids overlap. Although adaptive gridding is possible, $\mathcal{T}$ does not depend on time in this paper. Each point in the X-by-Y rectangular grid (ξ, η) maps to a certain GIS map point (lx_0, ly_0) via a matrix multiplication

$$\begin{pmatrix} \boldsymbol{J_{11}}(\xi,\eta) & \boldsymbol{J_{12}}(\xi,\eta) \\ \boldsymbol{J_{21}}(\xi,\eta) & \boldsymbol{J_{22}}(\xi,\eta) \end{pmatrix} \begin{bmatrix} \xi \\ \eta \end{bmatrix} = \begin{bmatrix} lx_0 \\ ly_0 \end{bmatrix} \quad (11)$$

Where $\boldsymbol{J}(\xi, \eta)$ a numerical grid Jacobian of interest to the PDE formulation. The numerical grid Hessian: $\begin{pmatrix} \boldsymbol{H_{11}}(\xi,\eta) & \boldsymbol{H_{12}}(\xi,\eta) \\ \boldsymbol{H_{21}}(\xi,\eta) & \boldsymbol{H_{22}}(\xi,\eta) \end{pmatrix}$ (12) also appears when following such a transformation through diffusion calculations.

3.4.3 Adjoint Version of PDE and Finite Difference Methods

We want to approximate the field $\vec{a}^n_{\xi,\eta}$ based on demand data $U^n_{\xi,\eta}$ and some assumptions about α_i in the risk data sub-model. So our first goal will be to fit an adjoint parabolic PDE:

$$\frac{\partial U}{\partial t}(t,\xi,\eta) = \vec{\nabla} \cdot \left(a \, \vec{\nabla} \, U(t,\xi,\eta) \right) + \mathcal{R}(t,\xi,\eta), \qquad [PDE]$$

where a is an adjoint fit function that contains advective and diffuse information. The advantage of an adjoint problem is to ensure a stable scheme. Equation $[PDE]$ is a candidate model for $\mathcal{G}$, now the task is to fit its parameter a. Our optimization is subject to the PDE constraint. In discrete difference form for the central difference gradient approximation

$$z^{n+1}_{\xi,\eta} - z^n_{\xi,\eta} = \epsilon + a\xi^n_{\xi,\eta} \frac{\left(z^n_{\xi+1,\eta} - z^n_{\xi-1,\eta}\right)}{2} + a\eta^n_{\xi,\eta} \frac{\left(z^n_{\xi,\eta+1} - z^n_{\xi,\eta-1}\right)}{2} + b^n_{\xi,\eta} \Delta_{disc.} z^n_{\xi,\eta} \quad (**)$$

This is an explicit averaging scheme. Discrete difference equation $(**)$ shows how to do the averaging in a first-order accurate scheme. A second-order accurate scheme uses a hybrid implicit/explicit finite difference method. We use implicit schemes to further our knowledge of what fields $\vec{a}_{\xi,\eta}^{n}$ look like and how they behave over time.

In two dimensions, an implicit computational stencil is a useful discrete data spatial differencing tool. We used it in this study to make finite difference approximations to first- and second-order partials with a North-South-East-West stencil.

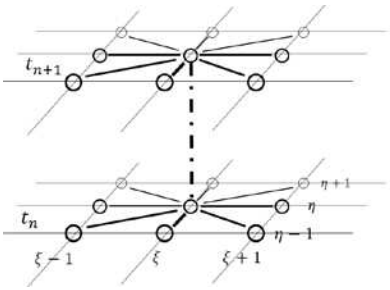

First-order effect ∂_ξ (shown), ∂_η (similar)

$$\frac{\partial \Phi}{\partial \xi}(t_n,\xi,\eta) \approx \frac{1}{2}\left[\frac{1}{2}\left(\Phi(t_{n+1},\xi+1,\eta)-\Phi(t_{n+1}\xi-1,\eta)\right)\right.$$
$$\left.+\frac{1}{2}\left(\Phi(t_n,\xi+1,\eta)-\Phi(t_n\xi-1,\eta)\right)\right] \qquad (13)$$

*where Φ stands for Φ_D or $\vec{\Phi}_S(t,x)$

Second-order effects $\partial\xi\partial\eta$ (shown), ∂_ξ^2 and ∂_η^2 (similar)

$$\frac{\partial^2 \Phi}{\partial \xi\, \partial \eta}(t_n,\xi,\eta) \approx \frac{1}{4|\aleph|}\sum_{\tilde{n}\in\aleph}\left(\Phi^{\tilde{n}}_{\xi+1,\eta+1}-\Phi^{\tilde{n}}_{\xi+1,\eta-1}-\Phi^{\tilde{n}}_{\xi-1,\eta+1}+\Phi^{\tilde{n}}_{\xi-1,\eta-1}\right) \qquad (14)$$

Second-order effect detection is important to distinguish between diffusive and advective behavior in data. Notice how the risk stencil samples time step t_n and t_{n+1}. Boundary conditions can be seamlessly incorporated in the finite difference computational stencil by using the values of $h_g(t)$ from equation (6) in the following way. On a rectangular grid $\xi = 1, \dots, X$ and $\eta = 1, \dots, Y$ with spacing $\Delta x = \frac{1}{X}$ and $\Delta y = \frac{1}{Y}$ we get boundary conditions for boundary flux data

$H^n_{\xi,\eta}$, a sample of $h_g(t)$ at grid points along the edges. It is most convenient to use a ghost point technique to straddle each of the four boundaries and use the known flux to express

$$\begin{aligned} u^n_{\xi,0} &= u^n_{\xi,2} - 2\,\Delta y\, H^n_{\xi,1} \quad \forall\, \xi \in [2, X-1] \subset \mathbb{Z} \\ u^n_{X+1,\eta} &= u^n_{X,\eta} + 2\,\Delta x\, H_{X,\eta} \quad \forall\, \eta \in [2, Y-1] \subset \mathbb{Z} \\ u^n_{\xi,Y+1} &= u^n_{X,Y} + 2\,\Delta y\, H^n_{\xi,Y} \quad \forall\, \xi \in [2, X-1] \subset \mathbb{Z} \\ u^n_{0,\eta} &= u^n_{2,\eta} - 2\,\Delta x\, H^n_{1,\eta} \quad \forall\, \eta \in [2, Y-1] \subset \mathbb{Z} \end{aligned} \tag{15}$$

Then, central differences apply with these corrective reflections of the computational stencil. At corners a scaling of $\sqrt{2}/2$ applies as two arms of the stencil must reflect. The ghost nodes are on the left-hand-side of equations (15). Diagonal connectors compute mixed derivative estimates in MATLAB software.

When stencils overlap it transmits spatial autocorrelation. We found it useful to apply the finite difference method to study spatiotemporal autocorrelation in terms of risk information type, firefighting resource type, nodes in a grid, or even sub-regions. The two-step stencil is a classic tool to analyze this type of PDE because it leads to stable Crank-Nicholson type discrete schemes. More information about working with finite time differences: $\frac{\partial \Phi}{\partial t}(t_n, \xi, \eta) \approx \frac{1}{2}\big(\Phi(t_{n+1}, \xi, \eta) + \Phi(t_n, \xi, \eta)\big)$ (16) consult references for finite differences (Benito, Ureña, and Gavete 2007).

3.4.4 Inverse Problem for Nodal PDEs

A stable scheme helps find the best-fit model because it gives a guarantee that the numerical solution is close to the theoretical solution. This is a property called model convergence. Model convergence is most difficult at spatial domain boundaries, where we know much of the allocation data tends to fall. To obtain the best convergence in our model we

carefully meshed the domain into subregions Ω_g and their boundaries $\partial\Omega_g$. In this way we could model any subregion. Wildfires happen inside the domains Ω_g and resources are sometimes shared across the boundaries $\partial\Omega_g$ throughout the season. Although international sharing occurs inside the domain Ω, it is limited, and our model assumes a no-slip boundary conditions $\frac{\partial \Phi_D}{\partial \hat{n}}\Big|_{\partial\Omega} = 0$ for conservation of overall resources where $\hat{n}$ is the unit normal to a counter clockwise oriented boundary $\partial\Omega$.

Our inverse problem fits nodal PDEs

$$\begin{Bmatrix} \begin{pmatrix} H1(\xi,\eta)\,\partial_\xi U(t,\xi,\eta) + H2(\xi,\eta)\,\partial_\eta U(t,\xi,\eta) + J1(\xi,\eta)\,\partial_\xi^2 U(t,\xi,\eta) \\ + J2(\xi,\eta)\,\partial_\eta^2 U(t,\xi,\eta) + 2\,J3(\xi,\eta)\,\partial_{\xi\eta}^2 U(t,\xi,\eta) \end{pmatrix} \\ \vdots \\ J1(\xi,\eta)\partial_\xi U(t,\xi,\eta) + J3(\xi,\eta)\partial_\eta U(t,\xi,\eta) \\ \vdots \\ J3(\xi,\eta)\partial_\xi U(t,\xi,\eta) + J2(\xi,\eta)\partial_\eta U(t,\xi,\eta) \end{Bmatrix}^T \begin{Bmatrix} b(t,\xi,\eta) \\ \vdots \\ a\xi(t,\xi,\eta) \\ \vdots \\ a\eta(t,\xi,\eta) \end{Bmatrix} = RHS(t,\xi,\eta) \quad (17a)$$

where

$$RHS(t,\xi,\eta) = \epsilon(t,\xi,\eta) + \partial_t U(t,\xi,\eta) - \gamma U(\xi,\eta) + \mathcal{R}(t,\xi,\eta) \quad (17b)$$

The goal is to estimate diffusive parameter $b(t,\xi,\eta)$ and the two vector basis directions of the adjoint fit function, $a\xi(t,\xi,\eta)$ and $a\eta(t,\xi,\eta)$. Parameter $\gamma \in [-1,1]$ will be explored in this scheme as well. In this case error can accrue over both time and space. The sources are $\epsilon = \epsilon_{model} + \epsilon_{data} + \epsilon_{trunc}$, model error is caused my parameter mismatch, data error is unavoidable, and truncation error is controlled by grid size in these application (Farlow 1993). The main idea behind scheme convergence is to choose high enough resolution data so that ϵ_{trunc} is negligible. For our transformed $\Delta\xi = \Delta\eta = 1$ grids ϵ_{trunc} was expected to produce no more than ±1.7% relative error at the 18-km resolution. Model error ϵ_{model} is important to track

carefully. Data error for ϵ_{data} will enter this system through miss entry or miss-time stamping, miss-allocation (i.e. an incorrect mobilization), and transposition of incident numbers.

To solve an inverse problem for the PDE model we use redundant linear algebra methods. Non-iterative SVD eigenvalue methods and conjugate gradient least squares can be used to carry out the inversion. Both are standard and covered in (Aster, Borchers, and Thurber 2013). Via high resolution data control we used software objects for smoothed demand grid data `U(xi,eta);` risk sub-model data at different lags `D(ii).risk.lagstr.`

3.4.5 Calibration and Forecast Theory

The PDE equality constraint in our model leads to non-convex linear programs. A binary relaxation helps resolve this issue.

This argument is abstracted to vector $\vec{w}$. The goal is to formulate estimates of cross product terms. A nonlinearity results from substituting linear risk sub-model (1) and (2) into $[PDE]$.To demonstrate a small part of this calculation, again in $\mathbb{R}^2$, consider a linear gradient field $\vec{\mathcal{R}}(t,\xi,\eta)$ from (2) in vector $\vec{w} = \langle w_\xi, w_\eta \rangle$

$$\vec{w} \times \vec{\nabla}\, u(t,\xi,\eta) \approx w_{\xi,k}\mathcal{R}_k \frac{\partial u}{\partial \eta} - w_{\eta,k}\mathcal{R}_k \frac{\partial u}{\partial \xi} \approx w_{\xi,k}\mathcal{R}_k \delta_\eta[u(t,\xi,\eta)] \; - w_{y,k}\mathcal{R}_k \delta_\xi[u(t,\xi,\eta)]$$

$$= \widehat{w_{\xi,k}}\mathcal{R}_k u(t,\xi,\eta+1) - \widehat{w_{\xi,k}}\mathcal{R}_k u(t,\xi,\eta-1) - \widehat{w_{\eta,k}} u(t,\xi+1,\eta) + \widehat{w_{\eta,k}} u(t,\xi-1,\eta),$$

where the vector cross product definition, centered finite difference proxy, and transformations $\widehat{w_\xi} = \frac{1}{2} w_\xi$ as well as $\widehat{w_\eta} = \frac{1}{2} w_\eta$ have all been applied.

Mixed products crop up and beyond the initial configuration at t_0, the $[PDEsys - LP]$ must resolve both terms. Even under grid-transformation (11) $\begin{pmatrix} \boldsymbol{J}_{11} & \boldsymbol{J}_{12} \\ \boldsymbol{J}_{21} & \boldsymbol{J}_{22} \end{pmatrix}$ it can be shown via the

chain rule directly on the transformed (ξ, η) grids that mixed products are a nonlinearity within a full calibration:

$$\boldsymbol{J}_{11}(\xi,\eta)\,\alpha_i(t,\xi,\eta)\,\frac{\partial \mathcal{R}_i}{\partial \xi}(t,\xi,\eta)\,\frac{\partial \mathcal{R}}{\partial \xi}(t,\xi,\eta) \text{ or } \boldsymbol{J}_{21}(\xi,\eta)\,\alpha_i(t,\xi,\eta)\,\mathcal{R}_i(t,\xi,\eta)\frac{\partial^2 u}{\partial \eta^2}(t,\xi,\eta)$$

These are the mixed products of risk coefficients and fire demand. We approached this nonlinearity in both direct and indirect ways, see APPENDIX 4.8.

Model calibration will be demonstrated with $[PDEsys - LP]$ goal and a forward scheme will prototype prediction in August 2012. By calibration we mean choosing the best coefficients with full information (including all future demand). Prediction has no access to future knowledge or forecasts. We now have a consistent model capable of risk assessment statistical analysis.

In $\mathbb{R}^2$, parameters $\vec{A} = \left(A_x, A_y\right), B, C, F, \vec{V} = \left(V_x, V_y\right)$, and $\overrightarrow{W} = \left(W_x, W_y\right)$ are used to fit the forward model. Ultimately, the $[PDEsys - LP]$ solves (3) - (6) as in similar models for physical flows (Zlotnik, Chertkov, and Backhaus 2015; Jourdain, Le Bris, and Lelièvre 2005). We implement and tested $[PDEsys - LP]$ using CPLEX as a solver.

3.5 Results of the Adjoint PDE constrained $\dim = 2$ Optimization Model

All results are for a least squares model fit to predict in forward time $t > 0$ $\epsilon_{model}(t) = \left\|\mathcal{G}\left(\mathcal{R}, \vec{\mathcal{R}}\right) - data\right\|_2 \approx \|u(t) - U(t)\|_2$ least squares framework problem:

$$\Upsilon\left(\epsilon_{model}(t)\right) = \min_{z} \int_{T_0}^{T_F} \epsilon_{model}(t)\, dt \; + \gamma \left\| \vec{\nabla} a \cdot \vec{\nabla} u \right\|_1 (\mathrm{t}_n) \qquad [OBJ]$$

$$subject\ to:$$

$$\begin{cases} \dfrac{\partial u}{\partial t}(t,\xi,\eta) = \vec{\nabla} \cdot \left(a\, \vec{\nabla}\, u(t,\xi,\eta) \right) + \mathcal{R}(t,\xi,\eta), \quad [PDE] \\ \dfrac{\partial\, \vec{\nabla} a}{\partial t}(t,\xi,\eta) = \vec{v} \cdot \vec{\nabla} u\,(t,\xi,\eta) + \vec{w} \times \vec{\nabla}\, u\,(t,\xi,\eta) \quad \text{[coupled PDE]} \\ ICs: \begin{cases} u(t_0,\xi,\eta) = U_0(\xi,\eta) & \text{initial demand potential} \quad [IC1] \\ \vec{\nabla} a(t_0,\xi,\eta) = \vec{A}_0(\xi,\eta) & \text{initial supply potential} \quad [IC2] \end{cases} \\ EBCs: \begin{cases} \left\| \vec{\nabla} a(t,\xi_0,\eta_0) \right\|_p \geq 0 \quad \forall\, (\xi_0,\eta_0) \in \mathcal{T}(\Omega) & \text{NO DRAWDOWN} \\ \dfrac{\partial u}{\partial \hat{n}}(t,x) = 0 \qquad x \in \mathcal{T}(\partial\Omega) & \text{[conservative domain]} \end{cases} \\ \text{NO NBC of supply fluxes} \end{cases}$$

$[PDEsys - LP]$ is the relaxation of this problem as described in this chapter. See (APPENDIX 4.7)

Explanation of terms

[OBJ] is the model fit objective. The γ gives weight to allocation mismatch in direction. We will compute this by hand for clarity. [PDE] is the adjoint form under scrutiny for $\mathcal{G}$; [coupled PDE] is also a prototype treated in the $[PDEsys - LP]$. Initial data conditions [IC1] and [IC2] are known and the domain is conservative. We will see figures and data experimentation in $\dim = 2$ to convey the supply response patterns. We have discretized this smaller problem according to the methods in this paper.

What is missing?

Compared with the physical set-up of the gas dynamics through pipes model in (Zlotnik et al. 2015), a lot… We have analyzed $\psi\left(\Phi_D, \overrightarrow{\Phi}_S\right) = \mathbf{0}$ elsewhere in the dissertation and reviewed current research to understand this part without innovating anything. There are no resource capacity restrictions in place anywhere in the domain, so no drawdown nodes in $(5a)$. This study considers Ω without any partition by regional boundaries $\partial\Omega_g$. Although our patterns

show that is regional boundaries do appear in the data. We simply assume the no-slip, conservative condition i.e. no fire engines drive off into the ocean.

Thus, we accessed a limited, but useful set of solutions to the optimization in (7) - (10). In particular we look at risk sub models from (1) with a small number of equally weighted α_i factors. Nodal PDE estimation as in (17) is quick and the redundant matrix inversion methods agree to numerical precision.

We summarized the results of the PDE model using some of the visualization techniques outlined in the previous chapter. Such mapping can facilitate understanding in the fire community at large. In this section we will report the results from:

- ✓ Solved the inverse problem for $[PDE]$ stated in (17), (FIGURE 3.2)
- ✓ Applied objective function (7) to 44km resolution grid (TABLE 3.3)
- ✓ Visualized $\mathcal{G}$ in an intraregional resource demobilization scenario (FIGURE 3.4)
- ✓ Calibrated $[PDEsys - LP]$ and used it to predict demand, see (FIGURE 3.5)

The results in (TABLE 3.3) use the best fit model to apply a penalty term $\vec{\Phi}_S \cdot \vec{\nabla}\Phi_D$ to a complete list of six different allocation options among the fires. How do we compare and contrast alternatives for re-allocating resources on August 16, 2012? One option is to use the model fit to different risk layers. Then compute, work-against-field penalties for each grid box in the allocation. Here we show how to do diffusive and advective penalty computations for (FIGURE 3.2) and (FIGURE 3.3). $i = 1$ for MODIS, $i = 2$ for PL, $i = 3$ for LSNITE, $i = 4$ for NOISE. Hypothetical allocation penalties are computed using

Equation 0 : $\sum_{\xi}\sum_{\eta} \boldsymbol{b}_i(\boldsymbol{\xi}, \boldsymbol{\eta})$

Equation 1: $(-1) * \sum_{\xi} \sum_{\eta} \left|\vec{\nabla} \boldsymbol{a_i}\right| \cos\left(\omega_i(\xi,\eta) - \theta_k(\xi,\eta)\right)$ where $\omega_i(\xi,\eta) - \theta_k(\xi,\eta) \in (-\pi, \pi]$

Equation 0 penalizes each movement based on the diffusive parameter for $i = 1$ and $i = 2$ within each cell it traverses. LSNITE is static so no diffusive penalty applies and the NOISE values have no meaningful interpretation. Instead, Equation 1 gives a penalty an advective parameter mismatch. The difference between the allocation angle from north through the cell $\theta_k(\xi,\eta)$ and the best-fit field angle of $\langle a\xi, a\eta \rangle$ from north $\omega_k(\xi,\eta)$ is penalized in Equation 1. The penalty is smallest and equal to -1 when the risk lines up with allocation. The penalty is largest and equal to $+1$ when the allocation is contrary to the risk direction. If the manager were to follow the model recommendations, then they would incur the lowest penalty.

The situation is a toss-up in terms of diffusive term penalties, but the advective penalty describes the true allocation. We know twelve Type I firefighters and ten Type 3 engines were reallocated from the Holloway Fire on August 16, 2012 to the Rush Fire. It looks like the most salient risk metric in this case was the proximity to WUI layer with an allocation penalty of -2.9.

We also explored the optimization framework reporting some large perturbations to allocation equilibrium in the 2011-2016 data archive, see (FIGURE 3.6).

Many agencies and stakeholders are involved in national level allocation of wildland fire resources. As input, $[PDEsys - LP]$ is expecting weights or binary on/off preference of information layers. A national group might be represented by varying the value of risk information.

This paper also provided a risk description of fire demobilization phase. A particular three-fire scenario in August 2012 in the western United States. We predicted a Northwest

advection of fire risk, a persistence of demand away from peak useage, and observed skewed prediction $\sqrt{RME}$ errors. (TABLE 3.4) gives some fast facts about the Rush, Barry Point, and Holloway Complex wildfires in 2012, the demobilization phase August 15-21 is featured to tell the story.

It is a national level scenario of interest because resources are on boundaries, competing risk descriptions apply, and there could be significant reallocation. Interagency coordination is conducted in times of high fire workloads by a National Multi-Agency Coordination Group (NMAC). Gaming out different normative allocation strategies using historical data is a future avenue of this work.

Single factor forcing functions lead to different demand potential configurations. A regional discrete measure like the Preparedness Level (PL) will accentuate the regional boundaries. On August 15, 2012 Nevada was holding onto resources. When MODIS large fire detection or energy release component (ERC) drives the border is less to the supply field. ERC is notably more heterogenous within region than is MODIS. A more realistic risk sub-model would fit a weighted average of MODIS, PL, and ERC. This might be what happens in a fire manager's risk assessment anyhow. The resulting field has boundary behavior, but not so strongly as when PL is driving the system alone. Allocation in this context can be characterized in terms of work the resource must do against or with the field.

In the sequence of risk maps there are several trends. The FOD fire starts data shows a dark-colored, advective wave of ignitions being detected from Northwest to Southeast during August 15-20, 2012. This would be critical information for regional managers as there may be both initial and extended attack work required. Would it be optimal to allocation from the Southeast toward the Northwest to help out? The MODIS large fire layer does little more than

reveal the large perturbations to the system that Rush, Barry Point, and Holloway fires caused. From August 19 and 20 it seems there is a large fire in central Oregon that may be drawing demand potential too. Using forecast information in the national level scenarios might involve consulting special risk layers:

- Accessibility and dryness indicates the fire in central Oregon, the Barry Point fire, and the ongoing Rush fires might be in dry wilderness areas. Any personnel allocated to these areas may have to a great distance off the interstate highway to arrive to the incidents.
- The strongest fire start and burning index layer shows a situation developing in central Washington as well. While parts of central Washington might be getting some moisture, it looks like some of the FOD fire starts line up with increases in the burning index.
- Rush seems to be cooler today than yesterday. Northwestern California may be a great place to demobilize from a large fire to address other nearby incidents.
- There are few fire starts August 19 as compared to August 20 in western Oregon and Washington. The Norwest to Southeast fire start trend may be about to repeat itself.
- The ERC metrics near the super-complex show drying, so even though these fires are well along the way to containment, caution should be taken. Contouring resources around this area would keep them close to these incidents in case an emergency situation grows demand again.

3.6 Conclusion and Discussion

This paper has identified physical mechanisms of advection and diffusion at length and interpreted them as components of an the risk mental model we identified. Based on our analyses of risk information data, our findings indicate advective, diffusive, reactive, rotational, feedback, and random error are all descriptive of allocation processes.

This paper proposed a data testing scheme for a complex math model. The application area is wildland fire management. Data processing in preparation for fitting a PDE model produced some illuminating visuals. Our PDE test cases involved a super-complex of three-fires on which risk tradeoffs were present. Our theoretical finding is a continuous statement of the problem that is consistent with data. We solved an inverse problem for a simple version the PDE constraint and demonstrated it on an interregional scenario. After analyzing a few fire suppression system large perturbations, we better determine the major factors that influence mobilization in ROSS data. By describing the drivers of different allocation modes and processes we take a step towards configuring policies to improve the system's performance. Moreover, these equations establish a test-bed to move from a descriptive visualization methodology towards a normative one on a chaotic data set.

Limiting this study are the following. Statistical analyses of the prediction problem remain. Visualizations are on short samples only. Statistics will be needed to give more concrete evidence about wildfire risk response. We did not treat the value of future information, which is important (Riley et al. 2015). As a parabolic, heat-type PDE, dynamic programs can provide numerical solutions (Short et al. 2010; Brillinger 2007; Sibert et al. 1999; Bellomo and Soler 2012), but suffer long run times in dynamic programming. Equality constraints make the problem non-convex. We identified a PDE candidate for nonlinear process $\mathcal{G}$, simplified from the (Zlotnik et al. 2015) physical coupled equation optimization framework. Binary risk indicators are easy to work with and explain. A GIS layer can be part of an average or in a go/no-go type reaction in the mental risk models of fire managers.

3.7 Future work

This type of PDE technology might be exciting to apply to the management of simultaneous fires, defined here as super-complexes. Our model for $\mathcal{G}$, the fire suppression management problem (Martell 2015), is complex, but not inapproachable when continuizing discrete data, removing risk evaluation from the network model, and casting the optimization framework $[PDEsys - LP]$ as in (Zlotnik, Chertkov, and Backhaus 2015). Calibration of these methods is ongoing, but this paper reassures the model is consistent in many useful ways.

Future work will repeat the calibration using the full $[PDEsys]$ and apply prediction. Our limited optimization demonstration shows promise to measure efficient and effective wildland fire response.

TABLE 3.1 – Nonlinear process detail

expressed RISK	$\mathcal{G}$	DEMAND & SUPPLY
$\mathcal{R}_{i,\xi}^{s}$	:	U and $\vec{a}$
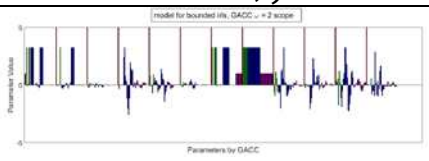 Example model space	↑ software: ALOC8/ dir matlab = … GIS feature data: import.py	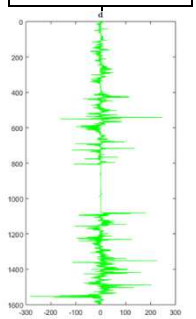 Example data space
Definition of expressed RISK – (n.) External action taken according internal size-up of a situation.		

TABLE 3.2a – PDE constraint mechanisms

Here are the advecive, diffusive, reactive (source/sink), and feedback dynamics in $\mathcal{G}$

Advection	$\vec{a}(t,x)^{[*]}$	Risk alignment causes demand to flow	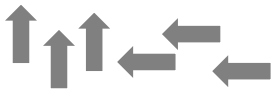 (vector bases) Scenarios A & B - Northwest risk
Diffusion	$b(t,x)$	Independent local action - Spreads demand, - Brownian motion,	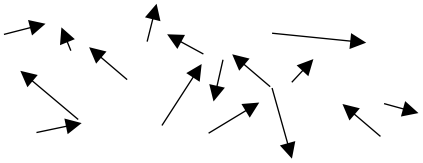
Reaction	$f(t,x)$	Exogenous forcing - External factors	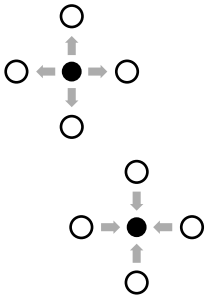
Feedback	$c(t,x)$	Consecutive request days - Ramp-up and ramp-down patterns	*Further information available in ICS-209 or "Situation Reports"*

TABLE 3.2b –

There are two possible spatial allocation strategies that might fit $\mathcal{G}$

Directional allocation	$\vec{v}(t,x)^{[*]}$	Risk-following allocation - Head into the heat!	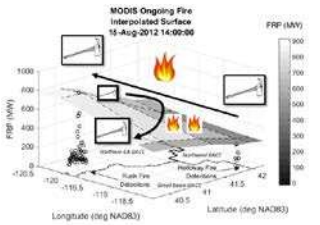
	$\vec{w}(t,x)^{[*]}$	Risk-cooperative allocation - Pre-position for future action	*... see Figure 1.8 (full size)*

**Can be vectors in $\mathbb{R}^d$ i.e. $\mathbb{R}^2$ would have $\vec{a}(t,x,y) = \left(a\xi(t,\xi,\eta), a\eta(t,\xi,\eta)\right)$ and $\mathbb{R}^3$ would have $\vec{v}(t,\theta,\phi,\rho) = \left(v_\theta(t,\theta,\Phi,\rho), v_\phi(t,\theta,\Phi,\rho), v_\rho(t,\theta,\Phi,\rho)\right)$

TABLE 3.3 – Reallocation metric penalties by hand

These numbers can be verified applying equations 0 and 1 in text to (FIGURE 3.2) by measuring angles. The true allocation was $Q = 3$ in this case

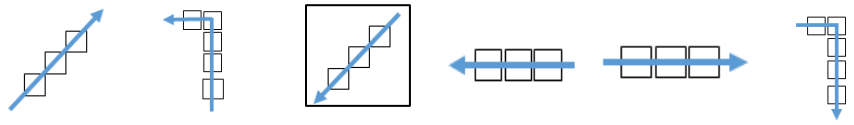

	$Q = 1$	$Q = 2$	$Q = 3$	$Q = 4$	$Q = 5$	$Q = 6$
Origin:	Rush	Rush	Holloway	Holloway	Barry Point	Barry Point
Destination:	Holloway	Barry Point	Rush	Barry Point	Holloway	Rush
Diffusive penalty Equation 0	MODIS = 0 PL = 0	MODIS = 0 PL = 0	MODIS = 0 PL = 0	MODIS = +0.5 PL = +0.5	MODIS = +0.5 PL = +0.5	MODIS = 0 PL = 0
Advective penalty Equation 1	MODIS − 0.97 PL − 0.97 LSNITE + 2.8 NOISE + 0.82	MODIS + 3.04 PL + 3.04 LSNITE − 2.7 NOISE − 3.6	MODIS + 0.92 PL + 0.92 LSNITE − 2.9 NOISE − 0.93	MODIS + 1.95 PL + 1.95 LSNITE − 2.6 NOISE − 2.6	MODIS − 2.8 PL − 2.8 LSNITE + 1.3 NOISE + 1.3	MODIS − 2.2 PL − 2.2 LSNITE + 0.7 NOISE + 0.7

TABLE 3.4

Locations, names, durations, fire expenditures, and final burned acres

Northern CA	**NV border**	**Lakeview, OR**
Rush Fire	Holloway Complex	Barry Point Fire
August 13 – September 4	August 5 – August 24	August 5 – September 22
$15.2 *million*	$9.2 *million*	$23.2 *million*
315,577 *acres*	460,850 *acres*	93,070 *acres*

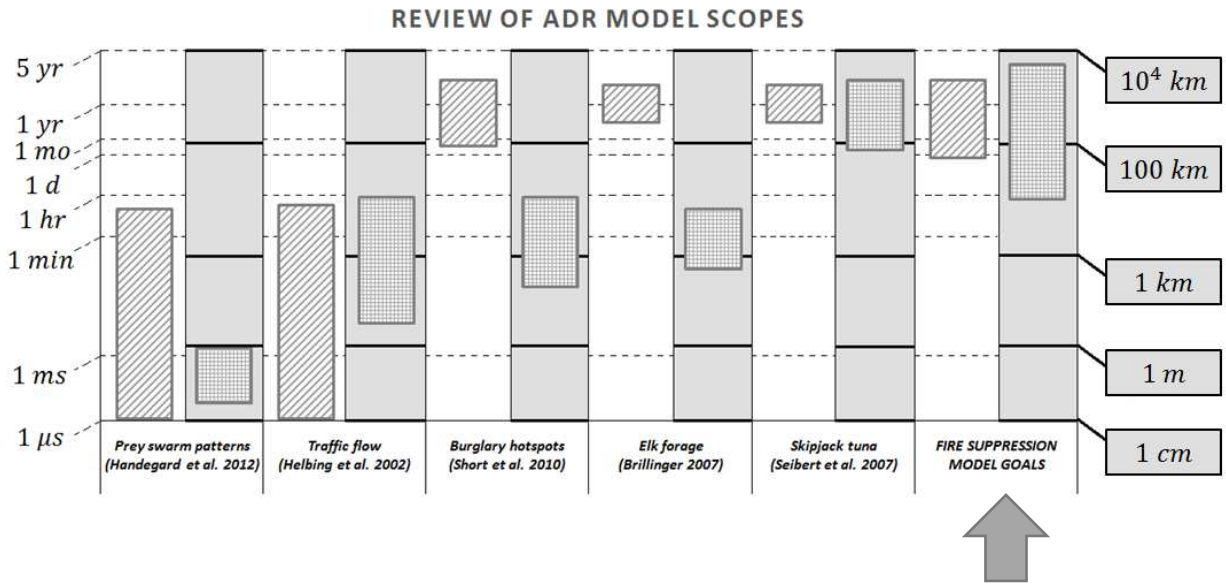

FIGURE 3.1 - Advective, diffusive, reactive (ADR) literature review

Caption:

Model scaling considerations from literature review across bottom axis. Our model spatiotemporal scaling goals are indicated with the arrow at right. Temporal scale is on the striped, left axis with dotted lines and white background. Spatial scale is on the hatched, right axis with bold lines and filled background. It summaries extents we expected to see in our model as compared with other models.

A macroscopic versus microscopic trend is on display from agent-based models in (Handegard et al. 2012) that would be more microscopic systems. Traffic flow and the burglary hotspots model smooth data. These models adopt aspects of both the microscopic and macroscopic ends. Species work in (Brillinger 2007) and (Seibert et al. 2007) are very much vector based and benefit from diffusion-dominated estimation to detect spatial patterns.

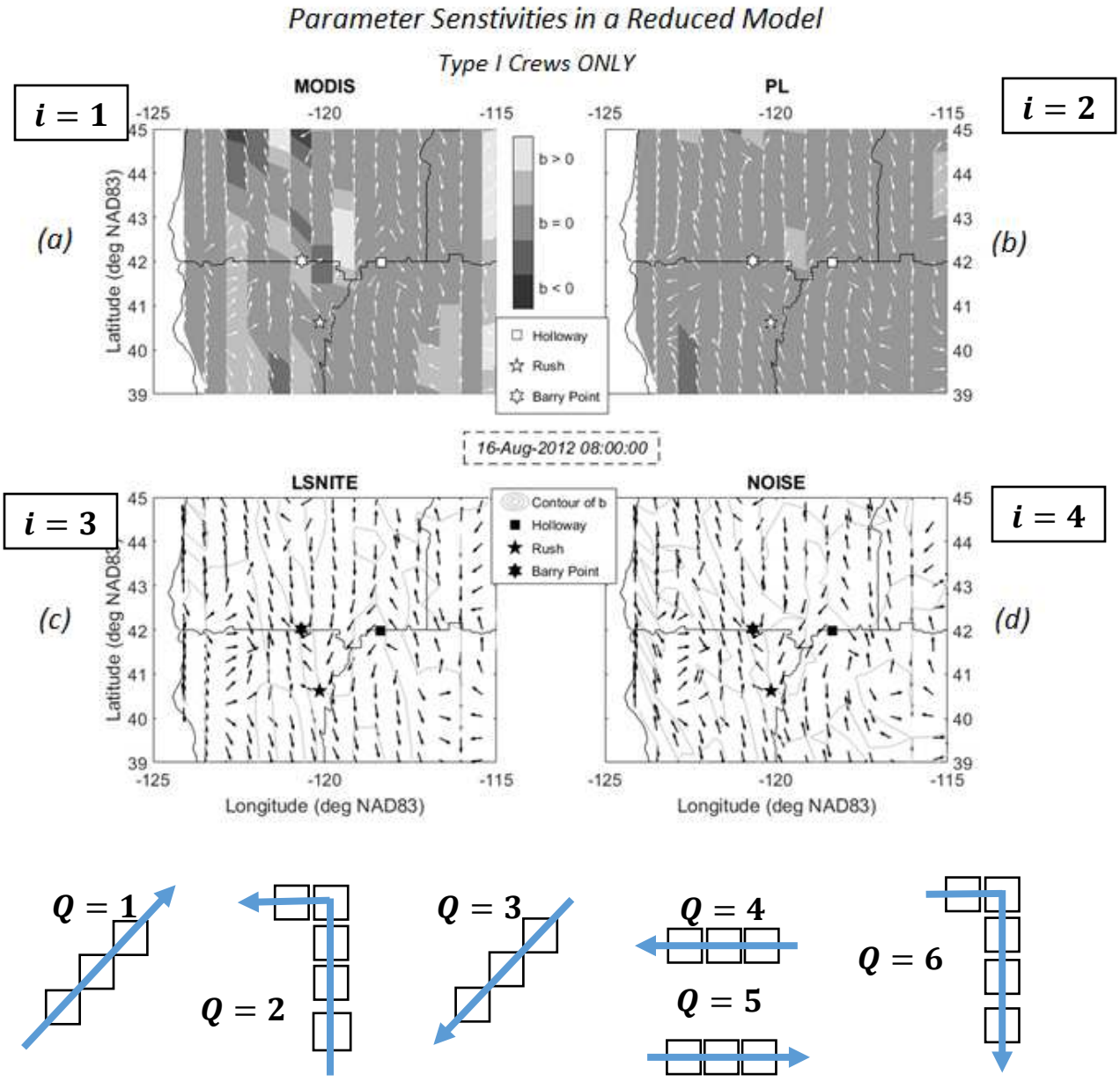

FIGURE 3.2 Estimates for diffusion $b(t,\xi,\eta)$ and advection $\langle a\xi, a\eta\rangle$ parameters

Model fit results for adjoint PDE. Post-optimization done by hand. Results are shown for best fit nodal PDEs to $\mathcal{R}_i$ single factor models. $(i = 1)$ MODIS fire radiative power, $(i = 2)$ preparedness level PL, $(i = 3)$ population density and $(i = 4)$ i.i.d. nodal noise. A key difference we learned from this model is between advective and diffusive allocation penalties.

What is the best reallocation among these fires at this time? Penalizing supply in the objective function $\left\|\vec{\Phi}_S \cdot \vec{\nabla}\Phi_D\right\|_1$ and taking $\vec{\Phi}_S \approx \langle a\xi, a\eta\rangle$ leads to different allocation from population density and the rest. A known re-allocation on this day was from the Holloway Complex to the Rush fire. Population density in $i = 3$ LSNITE shows how population density was a critical factor in this decision. See (TABLE 3.5) for full calculations of options $Q = 1, \ldots, 6$

$\mathcal{R} = \mathcal{R}_i =$ MODIS PL ERC

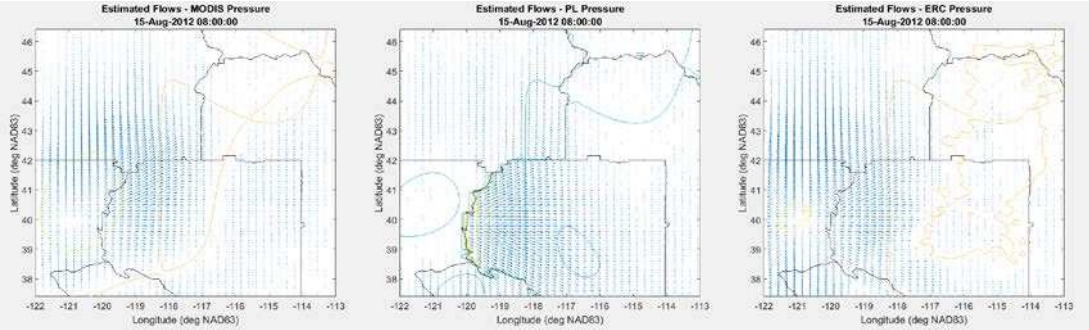

$\mathcal{R} = \frac{1}{3}$ MODIS $+ \frac{1}{3}$ PL $+ \frac{1}{3}$ ERC

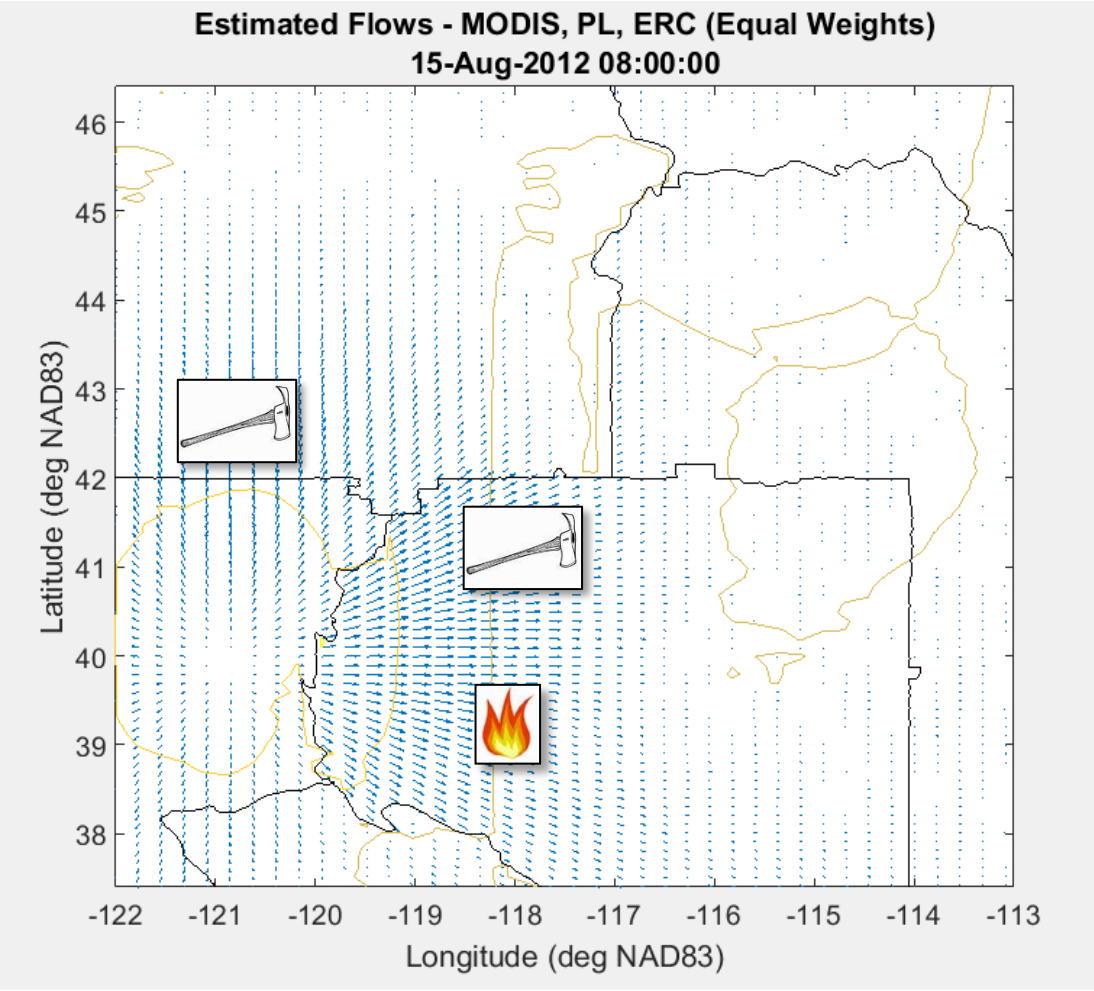

FIGURE 3.3 - Estimated vectors $\langle a\xi, a\eta \rangle$ across numerical grids on August 15, 2012

Sequence: August 15, 2012 16 17 18 19 20

FOD

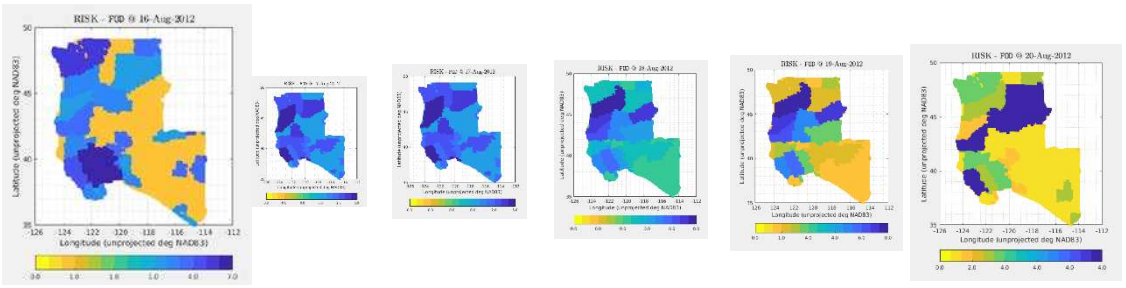

MODIS

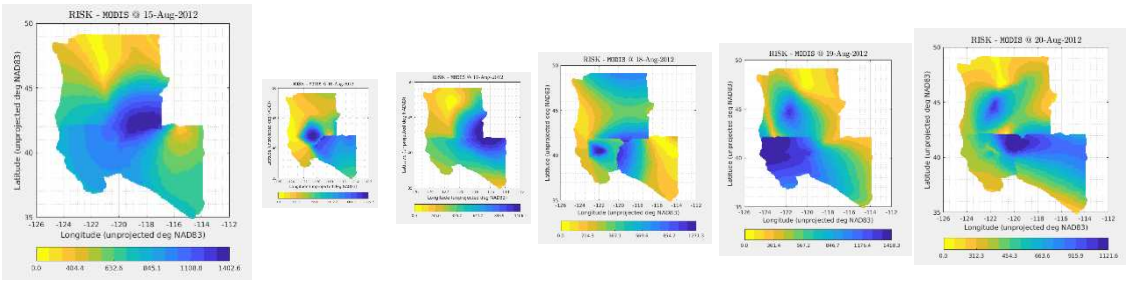

Forecast information from August 20, 2012

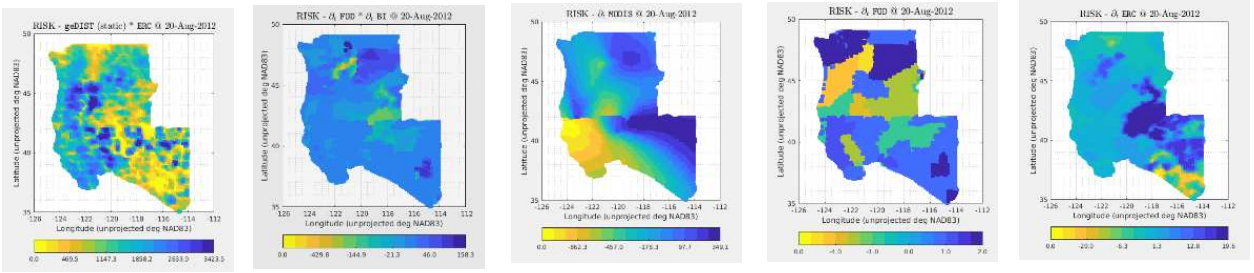

FIGURE 3.4 - Demobilization scenario

Displaying Fire Occurrence Database (FOD) data (Short 2017) and our interpolation of large fires from (Giglio 2016)

Caption

The most important MATLAB technique to map and store this data entails structure-based storage. Interacting structures directly is quickest. In order to run our experiment and learn prediction mismatch norms, vectors were preferable to the raster GIS input. Zeros were trimmed in a column-based decomposition. Our software contributes a discrete threshold version of scatter3.m (shown) to plot vectors directly and save time. Vector storage turns Gb of data on simply connected Ω regions into sleek national archives with Mb of data and kb of visuals. Full risk archives available upon request.

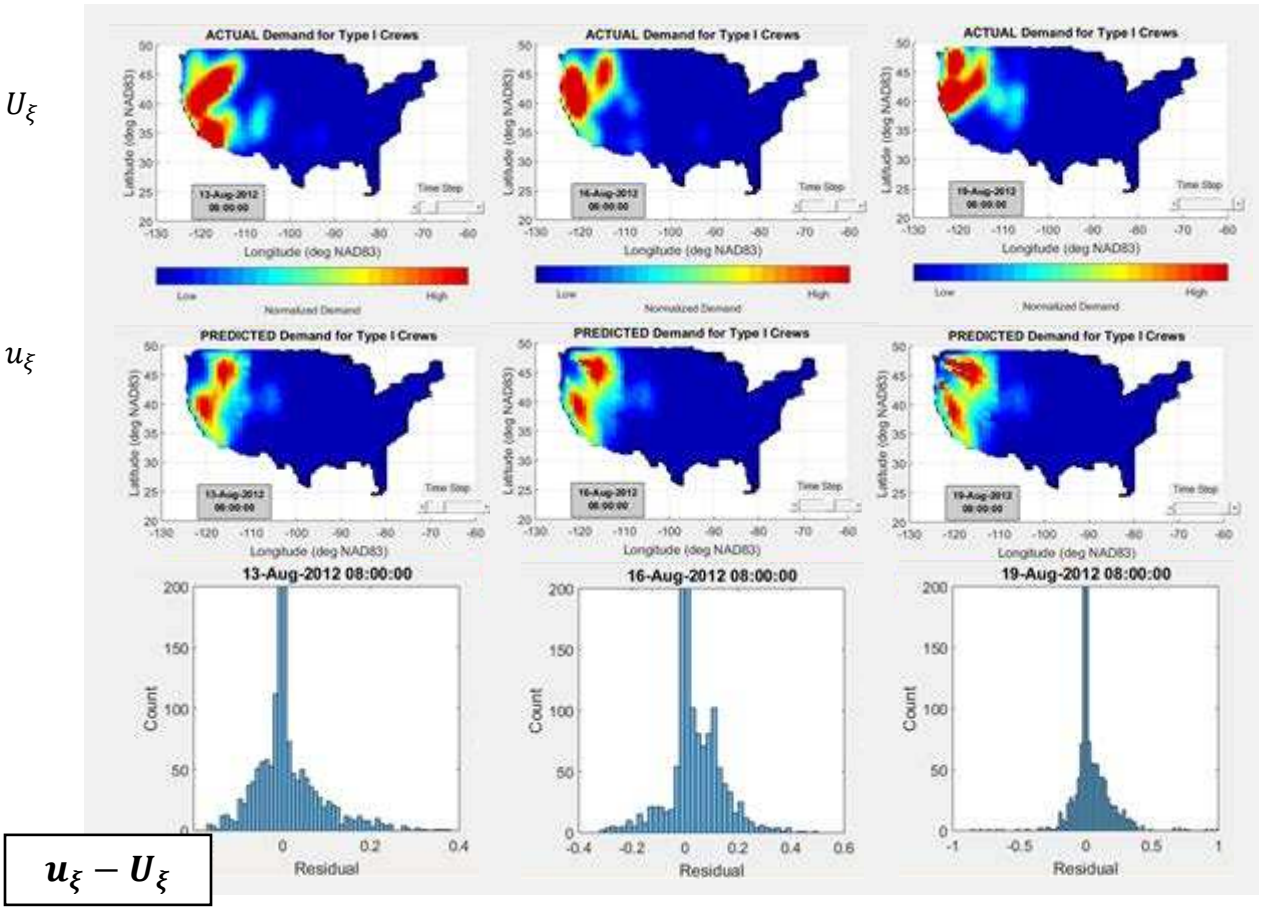

FIGURE 3.5 - Predicting $n+1$, $n+3$, and $n+6$ for Type 1 firefighters, fixed $r = 1$

Caption:

Forecasting prototype. Following the $[PDEsys - LP]$ calibration on all data leading up to and including August 12, 2012

(columns) Predictions for August 13, 16, and 19.

(rows) First, ACTUAL for the smoothed archive demand. Second, PREDICTED by forward finite difference Crank-Nicholson scheme. Produced on the $[PDEsys - LP]$ calibrated result. Third, decimal % relative error, binned by value across all nodes. A residual of 0.125 means $+12.5\%$ excess of actual demand was predicted. Similar for deficits. All plots seem skewed indicating the advection mechanism leads to error. Broadening is natural as diffusion clouds future information. Observe worse case $+40\%$ nodal error for $n+1$, worse case $+60\%$ for $n+3$, and $\pm 100\%$ for $n+6$. A more modest critique gives $\sqrt{RME} \approx 0.088$ for $n+1$, $\sqrt{RME} \approx 0.125$ for $n+3$, and $\sqrt{RME} \approx 0.225$ for $n+6$.

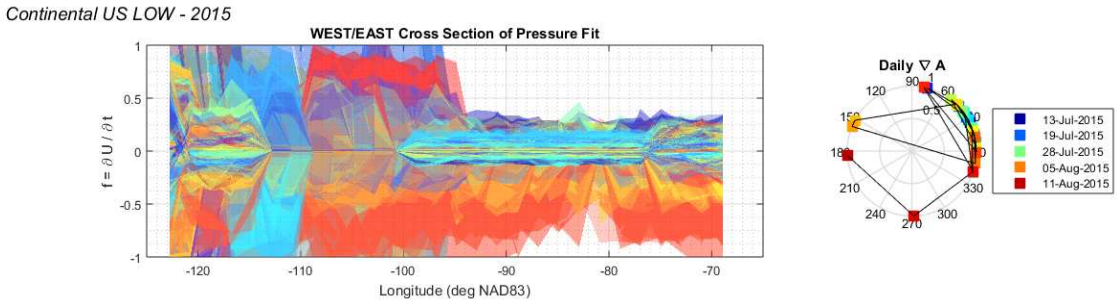

FIGURE 3.6 - Large perturbation detection, colored by day July - August 11, 2015

Caption:

Large perturbations to system equilibrium. Lots of mobilization towards Northern Rockies demand on August 11, 2015. Days are separating into colors. Shows as a switch in demand flow average direction from orange to red hues. The horizontal axis is a west to east relief of the United States. The vertical axes show demand rate model. Positive + readings for inflow and − for outflow. Superimposed, transparent colors by day of 2015 in legend. Also, in the legend is a diagram showing substantial departure from usual directions as the Northern Rockies fire activity was about to ramp up for the year.

We could use this figure to quantitatively define large perturbations, compute the number of large perturbations per year, and compare across years. This would be an informative system level measure. Would we see an increase or decrease? Do large perturbations form more readily for certain types of resources over others? Why are the patterns different?

REFERENCES FOR CHAPTER 3

Alderson, David L. 2008. “Catching the ‘Network Science’ Bug: Insight and Opportunity for the Operations Researcher.” *Operations Research* 56 (5): 1047–65.

Aster, Richard C., and Clifford H. Thurber. 2013. *Parameter Estimation and Inverse Problems*. 2nd ed. Waltham, MA: Academic Press.

Bellomo, N., and J. Soler. 2012. “ON THE MATHEMATICAL THEORY OF THE DYNAMICS OF SWARMS VIEWED AS COMPLEX SYSTEMS.” *Mathematical Models and Methods in Applied Sciences* 22 (supp01): 1140006. https://doi.org/10.1142/S0218202511400069.

Benito, J.J., F. Ureña, and L. Gavete. 2007. “Solving Parabolic and Hyperbolic Equations by the Generalized Finite Difference Method.” *Journal of Computational and Applied Mathematics* 209 (2): 208–33. https://doi.org/10.1016/j.cam.2006.10.090.

Brezis, Haïm, and Felix Browder. 1998. “Partial Differential Equations in the 20th Century.” *Advances in Mathematics* 135 (1): 76–144. https://doi.org/10.1006/aima.1997.1713.

Brillinger, D. R. 2007. “Learning a Potential Function From a Trajectory.” *IEEE Signal Processing Letters* 14 (11): 867–70. https://doi.org/10.1109/LSP.2007.900032.

Calkin, David E., Matthew P. Thompson, Mark A. Finney, and Kevin D. Hyde. 2011. “A Real-Time Risk Assessment Tool Supporting Wildland Fire Decisionmaking.” *Journal of Forestry* 109 (5): 274–80. https://doi.org/10.1093/jof/109.5.274.

Chong, Edwin Kah Pin, and Stanislaw H. Żak. 2013. *An Introduction to Optimization*. Fourth edition. Wiley Series in Discrete Mathematics and Optimization. Hoboken, New Jersey: Wiley.

Duff, Thomas J., Derek M. Chong, and Kevin G. Tolhurst. 2015. “Using Discrete Event Simulation Cellular Automata Models to Determine Multi-Mode Travel Times and Routes of Terrestrial Suppression Resources to Wildland Fires.” *European Journal of Operational Research* 241 (3): 763–70. https://doi.org/10.1016/j.ejor.2014.09.019.

Evans, Lawrence C. 2010. *Partial Differential Equations*. 2nd ed. Graduate Studies in Mathematics, v. 19. Providence, R.I: American Mathematical Society.

Fan, Shimao, and Benjamin Seibold. 2012. “A Comparison of Data-Fitted First Order Traffic Models and Their Second Order Generalizations via Trajectory and Sensor Data.” *ArXiv:1208.0382 [Physics]*, August. http://arxiv.org/abs/1208.0382.

Farlow, Stanley J. 1993. *Partial Differential Equations for Scientists and Engineers*. Dover Books on Advanced Mathematics. New York: Dover Publications.

González, Marta C., César A. Hidalgo, and Albert-László Barabási. 2008. “Understanding Individual Human Mobility Patterns.” *Nature* 453 (7196): 779–82. https://doi.org/10.1038/nature06958.

Helbing, Dirk. 2001. “Traffic and Related Self-Driven Many-Particle Systems.” *Reviews of Modern Physics* 73 (4): 1067–1141. https://doi.org/10.1103/RevModPhys.73.1067.

Holmes, Mark H. 2009. *Introduction to the Foundations of Applied Mathematics*. 2009 edition. Dordrecht ; London: Springer.

Jourdain, Benjamin, Claude Le Bris, and Tony Lelièvre. 2005. “Coupling PDEs and SDEs: The Illustrative Example of the Multiscale Simulation of Viscoelastic Flows.” In *Multiscale Methods in Science and Engineering*, 149–168. Springer.

Klein, Gary, Roberta Calderwood, and Anne Clinton-Cirocco. 2010. “Rapid Decision Making on the Fire Ground: The Original Study Plus a Postscript.” *Journal of Cognitive Engineering*

and Decision Making 4 (3): 186–209. https://doi.org/10.1518/155534310X12844000801203.

Magnussen, Steen, and Stephen W. Taylor. 2012. "Inter- and Intra-Annual Profiles of Fire Regimes in the Managed Forests of Canada and Implications for Resource Sharing." *International Journal of Wildland Fire* 21 (4): 328–41.

Martell, David L. 2015. "A Review of Recent Forest and Wildland Fire Management Decision Support Systems Research." *Current Forestry Reports* 1 (2): 128–37. https://doi.org/10.1007/s40725-015-0011-y.

Mees, Romain. 1986. "Locating Suppression Resources by Travel Times to Wildfires | Northern Rockies Fire Science Network." 1986. http://www.nrfirescience.org/resource/11472.

Preisler, Haiganoush K., and Anthony L. Westerling. 2007. "Statistical Model for Forecasting Monthly Large Wildfire Events in Western United States." *Journal of Applied Meteorology and Climatology* 46 (7): 1020–30. https://doi.org/10.1175/JAM2513.1.

Protopopescu, V., R. T. Santoro, and J. Dockery. 1989. "Combat Modeling with Partial Differential Equations." *European Journal of Operational Research* 38 (2): 178–83. https://doi.org/10.1016/0377-2217(89)90102-1.

Riley, Karin, Crystal Stonesifer, Dave Calkin, and Haiganoush Preisler. 2015. "Assessing Predictive Services' 7-Day Fire Potential Outlook." *In: Keane, Robert E.; Jolly, Matt; Parsons, Russell; Riley, Karin. Proceedings of the Large Wildland Fires Conference; May 19-23, 2014; Missoula, MT. Proc. RMRS-P-73. Fort Collins, CO: U.S. Department of Agriculture, Forest Service, Rocky Mountain Research Station. p. 188-195.* 73: 188–95.

Sharkey, Brian J., and Paul O. Davis. 2008. *Hard Work: Defining Physical Work Performance Requirements*. Champaign, IL: Human Kinetics.

Short, Martin B., P. Jeffrey Brantingham, Andrea L. Bertozzi, and George E. Tita. 2010. "Dissipation and Displacement of Hotspots in Reaction-Diffusion Models of Crime." *Proceedings of the National Academy of Sciences of the United States of America* 107 (9): 3961–65. https://doi.org/10.1073/pnas.0910921107.

Sibert, John R, John Hampton, David A Fournier, and Peter J Bills. 1999. "An Advection–diffusion–reaction Model for the Estimation of Fish Movement Parameters from Tagging Data, with Application to Skipjack Tuna (Katsuwonus Pelamis)." *Canadian Journal of Fisheries and Aquatic Sciences* 56 (6): 925–38. https://doi.org/10.1139/f99-017.

Sugiyama, Yuki, Minoru Fukui, Macoto Kikuchi, Katsuya Hasebe, Akihiro Nakayama, Katsuhiro Nishinari, Shin-ichi Tadaki, and Satoshi Yukawa. 2008. "Traffic Jams without Bottlenecks—experimental Evidence for the Physical Mechanism of the Formation of a Jam." *New Journal of Physics* 10 (3): 033001. https://doi.org/10.1088/1367-2630/10/3/033001.

Topaz, Chad M., Maria R. D'Orsogna, Leah Edelstein-Keshet, and Andrew J. Bernoff. 2012. "Locust Dynamics: Behavioral Phase Change and Swarming." *PLOS Computational Biology* 8 (8): e1002642. https://doi.org/10.1371/journal.pcbi.1002642.

Xun, Xiaolei, Jiguo Cao, Bani Mallick, Arnab Maity, and Raymond J. Carroll. 2013. "Parameter Estimation of Partial Differential Equation Models." *Journal of the American Statistical Association* 108 (503): 1009–20. https://doi.org/10.1080/01621459.2013.794730.

Zlotnik, Anatoly, Michael Chertkov, and Scott Backhaus. 2015. "Optimal Control of Transient Flow in Natural Gas Networks." In *Decision and Control (CDC), 2015 IEEE 54th Annual Conference On*, 4563–4570. IEEE.

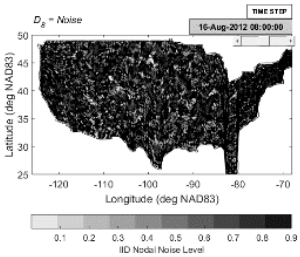

We performed a coefficient fit with 11 GIS layers as well as 34 derived and mixed layers.

A constant layer helped diagnose unwanted drifts during development.

Noise type $i.i.d.$ uniform

$MODIS$ Fire radiative power, units: $(megawatts)$

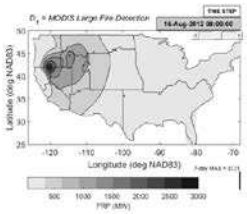

Moderate Resolution Imaging Spectroradiometer satellite fire detection, *MODIS MCD14ML 2011-2016*

Filtered for confidence $> 80\%$ and actively burning pixels $\geq 2.02\ km^2$.

Interpolation: scatteredInterpolant.m splines to max of $\sim 30\ km$ detection cluster radius

Further info: *(Roberts et al. 2005); (Mangeon et al. 2015); (Giglio 2016)*

ERC Energy release component of fuels, units: $(index\ 25-110)$

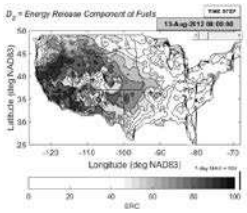

BI Burning index flammability metric, units $(index\ 0-110+)$

Seasonal trend in fuel dryness potential. *UofI METDATA 2011-2016,*

Interpolation: scatteredInterpolant.m splines re-gridded ERC from 585×1386 lat/lon

Further info: *(Lindley et al. 2015); [Abatzoglou 2013]*; (Deeming et al. 1977)

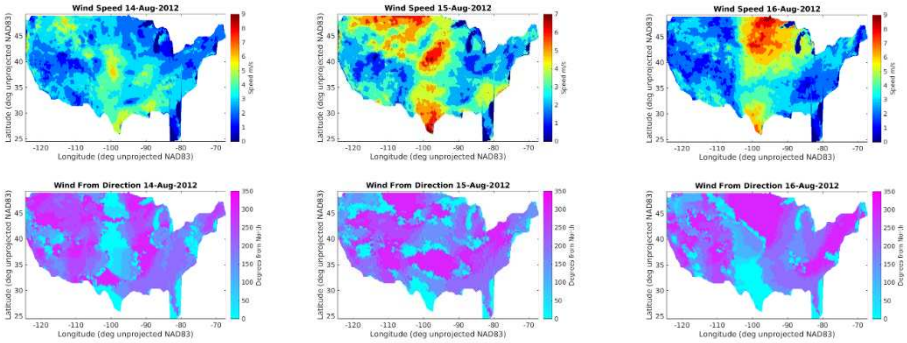

Also from (Abatzoglou 2013) $WindVel$ magnitude of wind velocity, units $\left(\frac{m}{s}\right)$; $\partial_t WindVel$ wind direction in units of degrees from North

FOD Fire occurrence database, units: $(\#\ discoveries\ per\ PSA)$ *2016 PSA config.

Data collection 2011-2016 (Short 2017), aggregated by PSA boundaries
Interpolation: scatteredInterpolant.m nearest neighbor to discovery count

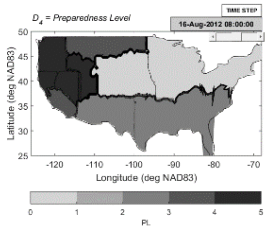

$regionPL$ Preparedness Level by GACC, units $(category: 1,\ 2,\ 3,\ 4,\ 5$ and 0 for no data) *IMSR NIFC 2011-2016*

Interpolation: scatteredInterpolant.m nearest neighbor to PL category, boundaries - jump discontinuities

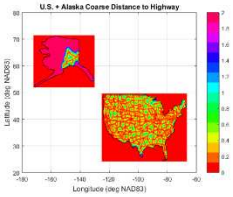

$geDIST\ (static)$ Google Earth distance, units
$(normalized\ access\ distance\ 0.0 - 2.0)$

Google Earth 2016, ad hoc selection of interstate and regional roads, gridded computation of distances, roughly scaled for curvature of earth, static

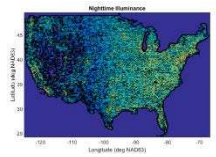

$\log LSNITE\ \ (static)$ log-transformed LandScan, units:
$(\log nightime\ illuminance\ /km^2\ )$

Re-gridded high resolution layer to 9 km per side, within grid cell sample median illuminance scaled from brightest to darkest, static

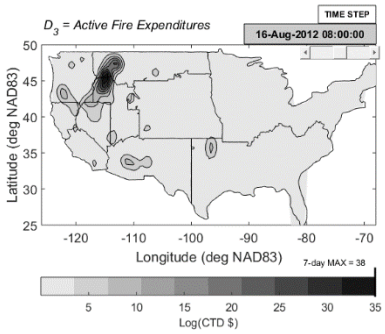

$COST$ Smoothed Ongoing fire expenditures to date, units: $(\log \$)$

ICS-209 NIFC 2011-2014, 2015-2016 corrupt, Grouped by incident, transformed with log function,

Interpolation: exponentialBumpGenr8r.m to incident log cost levels

Cost was very rarely among the best fit parameters. Either expenditure data is accumulated post-fire so as to not be a true risk factor, or cost is not a strongly expressed risk preference in ROSS ordering data.

- ∂_t derived layers were applied to $\partial_t MODIS$, $\partial_t ERC$, $\partial_t FOD$, $\partial_t BI$, $\partial_t regionPL$, and $\partial_t WindVel$ was change in wind direction from north

Pre-combined layers were

	$MODIS$	ERC	FOD	BI	$regionPL$	$WindVel$
	$\partial_t MODIS$	$\partial_t ERC$	$\partial_t\ FOD$	$\partial_t BI$	$\partial_t\ regionPL$	$\partial_t\ WindVel$
$geDIST\ (static)$	*	*	*	*	*	*
	*	*	*	*	*	*
$logLSNITE\ (static)$	*	*	*	*	*	*
	*	*	*	*	*	*
$\partial_t MODIS$	n/a	n/a	n/a	n/a	n/a	n/a
	n/a	*	n/a	*	n/a	n/a
$\partial_t FOD$	n/a	n/a	n/a	n/a	n/a	n/a
	n/a	*	n/a	*	n/a	n/a

APPENDIX 4.2 – WILDFIRE SUPER-COMPLEXES

DEFINTION wildfire super-complexes

multiple, nearby incidents of managed wildfire, shown below with $\mathbb{R}^2$ smoothing:

Large regional demand introduces greater bias in GIS demand average $U_{R,G}$ than smaller regional demand.

Super-complexes form

Adjacent fire incidents super-impose demand

Isolated incidents of fire add into $U_{R,G}$ as well.

Each caries a smoothing bias according to $\kappa > 0$.

Theoretically, this smoothing is an approximation to Dirac-δ bumps. Radially symmetric basis functions help share the information about super-complexes.

<u>Smoothing based on full-width-half-max κ:</u>

For fixed time step t_n, suppose request coordinates at (lx_0, ly_0),

Smooth bump with $U(t_n, lx_0, ly_0) = 1$ and decay $U(t_n, lx, ly) = e^{-\left[(lx-lx_0)^2+(ly-ly_0)\right]^2/\kappa}$,

Suppose $k = 1, \ldots, K$ additional requests at (lx_k, ly_k)

$$U(t_n, lx, ly) = U(t_n, lx, ly) + \sum_k e^{-\left[(lx-lx_k)^2+(ly-ly_0)^2\right]^2/\kappa}$$

This procedure can be implemented in the following lines of code:

```
function z = expBumpGenr8r(xq,yq,xIN,yIN,SLIM)
% expBumpGenr8r.m Smooths discrete information into continuous surface
%   INPUTS:
%       xq, yq = double arrays of two dimensional mesh (fine scale)
%       xIN, yIN = double vectors of request points (may repeat)
%       SLIM = double bump width parameter (increase for sharper bumps)
%           *tested in range 4.562 to 9.998
%   OUTPUT:
%       z = double array of size(xq) of smoothed surface

% One exponential bump at (x0,y0)
fxn = @(xi,eta,a,b,k) 1.0*exp(-k*(( xi-x0*ones(size(xi)) ).^2...
        + ( eta-y0*ones(size(eta)) ).^2));
% Grab memory to match spatial mesh size
z = zeros(size(xq));
% Given a list of requests
numRequests = numel(xIN);
% Superimpose exponential bumps
for kk = 1:numRequests
    z = z + fxn(xq,yq,xIN(kk),yIN(kk),SLIM);
end

end %end function
```

(Remark) As $\kappa \to 0$ ($SLIM = 1/\kappa \to \infty$ in code), there is a Dirac-δ spike at each (lx_k, ly_k) for $k = 0,\ 1,\ \ldots,\ K$. As $\kappa \to \infty$ the model is oversmoothed and we lose the request locations. We set κ to be slightly smoothing ($SLIM \in [2.25,9.998]$ in code) so that spikes are distinguishable, but clusters of requests can aggregate as a model for urgency in super-complexes.

Finite difference code is as one would expect. Algebraic manipulation is part of learning how these schemes work and necessary to prove they converge. Our use of a scheme stencil helped us to focus on the application area. Elements of graduate semesters on Numerical Analysis I & II and PDE I & II (Evans 2010) have helped throughout.

Sample code and further linear algebra vector gradient $\vec{\nabla}$ are available upon request…

APPENDIX 4.3 – BLOCK ASSEMBLY OF REGRESSION MATRICES/VECTORIZATION

The index mapping is a string sort algorithm to connect single index k with the seven-tuple $(r, s_1, i, g_1, s_2, g_2, s_3)$ to pin down which demand or risk coefficient is in row k in the matrix inversion

$$\{\, k : x_k \in \vec{\boldsymbol{x}} \,\} \iff \left\{\, (r_1, s_1) : \hat{y}_{r_1}^{s_1} \in \vec{\boldsymbol{y}} \,\right\} \cup \left\{\, (i, g_1, s_2) : \hat{a}_{i,g_1}^{s_2} \in \vec{\boldsymbol{a}} \,\right\} \cup \left\{\, (g_2, s_3) : \hat{z}_{g_2}^{s_3} \in \vec{\boldsymbol{z}} \,\right\} \quad (A.1)$$

The block regression inversion system for these "mYAZ" models:

$$\boldsymbol{A}_{R,G}\,\vec{\boldsymbol{x}} \coloneqq \begin{bmatrix} \overrightarrow{\boldsymbol{U}_{r,G}^{s}}^{\boldsymbol{T}}(T_0) & \overrightarrow{\boldsymbol{D}_{i,g}^{s}}^{\boldsymbol{T}}(T_0) & \overrightarrow{\boldsymbol{U}_{R,g}^{s}}^{\boldsymbol{T}}(T_0) \\ \vdots & \vdots & \vdots \\ \overrightarrow{\boldsymbol{U}_{r,G}^{s}}^{\boldsymbol{T}}(t_n) & \overrightarrow{\boldsymbol{D}_{i,g}^{s}}^{\boldsymbol{T}}(t_n) & \overrightarrow{\boldsymbol{U}_{R,g}}^{\boldsymbol{T}}(t_n) \\ \vdots & \vdots & \vdots \\ \overrightarrow{\boldsymbol{U}_{r,G}^{s}}^{\boldsymbol{T}}(T_F) & \overrightarrow{\boldsymbol{D}_{i,g}^{s}}^{\boldsymbol{T}}(T_F) & \overrightarrow{\boldsymbol{U}_{R,g}^{s}}^{\boldsymbol{T}}(T_F) \end{bmatrix} \begin{Bmatrix} \vec{\boldsymbol{y}} \\ \vec{\boldsymbol{a}} \\ \vec{\boldsymbol{z}} \end{Bmatrix} = \begin{Bmatrix} \frac{dU_{R,G}}{dt}(T_0) \\ \vdots \\ \frac{dU_{R,G}}{dt}(t_n) \\ \vdots \\ \frac{dU_{R,G}}{dt}(T_F) \end{Bmatrix} =: \overrightarrow{\partial_t U_{R,G}} \quad (A.2)$$

Each inversion is assembled by flattening the indexed coefficients using $(A.1)$ and concatenating them into a single vector of information $\hat{\boldsymbol{x}} = \{\vec{y}, \vec{a}, \vec{z}\}$.

Book-keeping exercise in combinatorial counting

We write down the three equations used to organize $(A.2)$ based on $(A.1)$ in a $\#G = 3$ size model $g \in \{5,9,11\}$ with $|Layers| = 26$ risk information inputs with an arbitrary number of resources $\#R$. Such a model was also used in testing. Sharing/cooperative demand impact coefficients for the same resource across other FMZs from $(3a)$ are flattened by lag $s \in Lag(R,G)$, then FMZ g:

$$\overrightarrow{y_{R,G}} \coloneqq \left\{ \hat{y}_{g=5}^{s=1}, \hat{y}_{9}^{1}, \hat{y}_{11}^{1}, \dots, \hat{y}_{5}^{|Lag(R,G)|}, \hat{y}_{9}^{|Lag(R,G)|}, \hat{y}_{11}^{|Lag(R,G)|} \right\} \in \mathbb{R}^{3|\aleph|}.$$

Risk coefficients are flattened lag s, then risk factor i, and finally FMZ g:

$$\overrightarrow{a_{R,G}} \coloneqq \left\{ \hat{a}_{i=1,g=5}^{s=1}, \hat{a}_{1,9}^{1}, \hat{a}_{1,11}^{1}, \dots, \hat{a}_{26,5}^{1}, \hat{a}_{26,9}^{1}, \hat{a}_{26,11}^{1}, \dots, \hat{a}_{26,5}^{|Lag(R,G)|}, \hat{a}_{26,9}^{|Lag(R,G)|}, \hat{a}_{26,11}^{|Lag(R,G)|} \right\} \in \mathbb{R}^{3(26)|Lag(R,G)|}.$$

Reinforce/release demand impact coefficients for other resources with the FMZ from $(3b)$ flattens by lag s, then resource r

$$\overrightarrow{z_{R,G}} \coloneqq \left\{ \hat{z}_{r=1}^{s=1}, \dots, \hat{z}_{R}^{1}, \dots, \hat{z}_{1}^{|Lag(R,G)|}, \dots, \hat{z}_{R}^{|Lag(R,G)|} \right\} \in \mathbb{R}^{(\#R-1)|Lag(R,G)|}.$$

These can be checked against the inverse problem sizes and seen in the various visualizations throughout the paper.

APPENDIX 4.4 – LATEX CODEX FOR ALL RISK LAYERS

Number of GIS Layers = 11
D01 = $\texttt{constant}$
D02 = $\texttt{noise}$
D03 = $\texttt{MODIS}$
D04 = $\texttt{ERC}$
D05 = $\texttt{FOD}$
D06 = $\texttt{BI}$
D07 = $\texttt{regionPL}$
D08 = $\texttt{WindVel}$
D09 = $\texttt{geDIST}$ (static)
D10 = $\log \texttt{LSNITE}$ (static)
D11 = $\texttt{COST}$
Number of first differenced layers (from above) = 6
D12 = ∂_t $\texttt{MODIS}$
D13 = ∂_t $\texttt{ERC}$
D14 = ∂_t $\texttt{FOD}$
D15 = ∂_t $\texttt{BI}$
D16 = ∂_t $\texttt{regionPL}$
D17 = ∂_t $\texttt{WindVel}$
Number of mixed layers (from above) = 28
D18 = $\texttt{geDIST}$ (static) * $\texttt{MODIS}$
D19 = $\texttt{geDIST}$ (static) * $\texttt{ERC}$
D20 = $\texttt{geDIST}$ (static) * $\texttt{FOD}$
D21 = $\texttt{geDIST}$ (static) * $\texttt{BI}$
D22 = $\texttt{geDIST}$ (static) * $\texttt{regionPL}$
D23 = $\texttt{geDIST}$ (static) * $\texttt{WindVel}$
D24 = $\texttt{geDIST}$ (static) * ∂_t $\texttt{MODIS}$
D25 = $\texttt{geDIST}$ (static) * ∂_t $\texttt{ERC}$
D26 = $\texttt{geDIST}$ (static) * ∂_t $\texttt{FOD}$
D27 = $\texttt{geDIST}$ (static) * ∂_t $\texttt{BI}$
D28 = $\texttt{geDIST}$ (static) * ∂_t $\texttt{regionPL}$
D29 = $\texttt{geDIST}$ (static) * ∂_t $\texttt{WindVel}$
D30 = $\log \texttt{LSNITE}$ (static) * $\texttt{MODIS}$
D31 = $\log \texttt{LSNITE}$ (static) * $\texttt{ERC}$
D32 = $\log \texttt{LSNITE}$ (static) * $\texttt{FOD}$
D33 = $\log \texttt{LSNITE}$ (static) * $\texttt{BI}$
D34 = $\log \texttt{LSNITE}$ (static) * $\texttt{regionPL}$
D35 = $\log \texttt{LSNITE}$ (static) * $\texttt{WindVel}$
D36 = $\log \texttt{LSNITE}$ (static) * ∂_t $\texttt{MODIS}$
D37 = $\log \texttt{LSNITE}$ (static) * ∂_t $\texttt{ERC}$
D38 = $\log \texttt{LSNITE}$ (static) * ∂_t $\texttt{FOD}$
D39 = $\log \texttt{LSNITE}$ (static) * ∂_t $\texttt{BI}$
D40 = $\log \texttt{LSNITE}$ (static) * ∂_t $\texttt{regionPL}$
D41 = $\log \texttt{LSNITE}$ (static) * ∂_t $\texttt{WindVel}$
D42 = ∂_t $\texttt{MODIS}$ * ∂_t $\texttt{ERC}$
D43 = ∂_t $\texttt{MODIS}$ * ∂_t $\texttt{BI}$
D44 = ∂_t $\texttt{FOD}$ * ∂_t $\texttt{ERC}$
D45 = ∂_t $\texttt{FOD}$ * ∂_t $\texttt{BI}$
Number of extra layers = 0
Total number of GIS layers = 45

APPENDIX 4.5 – RESULTS TEST CASE (A), AN ALL-GACC INVERSION PROBLEM

Raw GIS Data Significance Tables
by PL Category

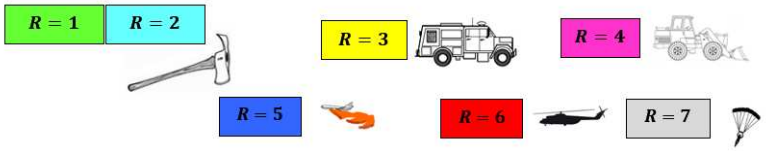

PL45	EACC	RMCC	SWCC	EGBCC	WGBCC	SACC	AKCC	NWCC	NRCC	NOCC	SOCC
constant	--34	--3-	1-3-	----	1---	12-4	1---	1---	--3-	123-	----
	---	---	56-	---	5-7	56-	---	-67	-67	567	-6-
MODIS	1---4	----	--3-	---4	--34	-2-4	1-3-	123-	12--	1---	----
	5-7	--7	5-7	-67	-6-	---	5--	---	-67	56-	---
ERC	1---	----	1-3-	1234	---4	-2--	12--	1-3-	-234	--3-	1---
	---	--7	567	5--	--7	---	---	567	56-	-67	---
FOD	12--	1---	1---	-234	12-4	12-4	1---	--34	1-34	1--4	12--
	--7	---	56-	-67	-67	---	---	567	-6-	-67	-6-
BI	1234	1-3-	---4	1234	--34	12-4	1---	---4	123-	123-	1---
	5-7	5-7	567	-67	-6-	---	---	---	-67	-67	---
regionPL	1-3-	-234	--3-	-2--	----	-2--	1---	12-4	----	----	--3-
	5--	---	56-	---	5--	---	---	---	5-7	-6-	--7
WindVel	123-	--34	123-	1---	1---4	12--	1---	123-	--3-	1234	1---
	---	5--	567	567	-6-	---	---	---	--7	---	-67
geDIST	--34	--3-	--3-	----	1---4	-2--	1---	1---	----	---4	1---
	5--	---	5--	---	--7	56-	---	---	--7	5--	---
log LSNITE	----	----	--3-	----	---4	-2--	1---	1---	---4	1---	----
	---	56-	56-	--7	---	---	---	---	--7	---	---
COST	12-4	123-	-2--	----	---4	-2-4	1---	1---	--3-	----	----
	---	---	-67	5-7	-67	-6-	---	---	5-7	5--	-6-

PL23	EACC	RMCC	SWCC	EGBCC	WGBCC	SACC	NWCC	NRCC	NOCC	SOCC
constant	---4	-2--	----	1---	---4	12-4	1---	----	12-4	----
	---	---	--7	-6-	56-	---	5--	5--	567	---
MODIS	---4	123-	----	----	1234	--3-	123-	12--	1234	-2--
	---	---	---	-67	56-	-6-	-6-	---	-6-	---
ERC	---4	-234	---4	12-4	-2--	-2--	12--	-2--	12-4	----
	5--	-6-	-67	-6-	56-	---	56-	---	567	--7
FOD	1--4	----	----	1-34	1234	--3-	12--	---4	123-	--34
	5--	-6-	--7	-6-	5-7	5--	567	---	567	-67
BI	---4	123-	----	-2--	-234	1-34	----	---4	---4	-23-
	---	-6-	5--	-67	---	5--	-6-	---	---	-6-
regionPL	---4	-23-	----	-23-	--34	-2-4	-2--	---4	12-4	----
	---	---	---	-67	567	-6-	56-	---	-67	---
WindVel	---4	-2-4	1---	1-34	1-34	----	-2-4	----	1---	----
	5--	-6-	---	-67	56-	---	-67	---	-6-	5--
geDIST	-2-4	12--	----	1-34	--34	12-4	---4	1---	12--	---4
	---	---	---	-67	56-	-6-	---	---	-6-	5--
log LSNITE	---4	123-	--3-	----	-2--	----	----	----	12--	----
	---	---	---	56-	56-	---	---	---	-6-	---
COST	---4	1-3-	1---	1-34	--34	---4	-2-4	----	-2-4	----
	5--	-6-	---	-6-	567	---	-6-	--7	-6-	---

APPENDIX 4.5 - *(continued)* *PL*23 DERIVED AND COMBINED LAYERS

	EACC	RMCC	SWCC	WGBCC	EGBCC	SACC	NWCC	NRCC	NOCC	SOCC
12	---4	1---	1---	1234	--34	1234	---4	---4	-234	---4
	---	---	--7	-67	-6-	---	--7	-6-	-67	567
13	---4	-2--	----	-234	---4	1---	----	----	1-3-	----
	---	---	---	-6-	567	-6-	---	---	56-	-6-
14	---4	-2-4	12--	1---	1234	-2--	12-4	----	12-4	-23-
	---	---	---	-6-	56-	---	---	---	-6-	---
15	---4	-2--	----	1---	----	--3-	----	----	1---	----
	---	---	-6-	-67	567	---	-6-	---	-67	-6-
16	---4	-2-4	----	----	123-	----	----	----	12--	----
	5--	---	---	-67	567	---	---	---	-67	---
17	---4	-2--	12--	1---	12--	---4	12-4	----	1234	-23-
	---	---	---	-6-	5--	-6-	---	---	-6-	---
18	---4	12--	1-34	-2--	--3-	----	-2--	----	1---	----
	---	---	---	567	5--	-6-	-6-	---	--7	---
19	---4	----	----	--34	12--	----	----	-23-	1---	----
	5--	---	---	-67	-6-	-6-	--7	---	--7	---
20	---4	-2--	12--	---4	----	----	-23-	----	1---	1---
	---	---	5--	567	567	---	5--	---	-6-	---
2	--34	-2-4	---4	----	----	----	12--	----	1---	---4
	---	---	--7	-67	56-	-6-	56-	---	-6-	56-
2	---4	-2--	----	--3-	-23-	----	----	----	1---	----
	---	---	--7	-6-	56-	---	--7	-67	-6-	56-
23	---4	-2--	12--	1---	----	----	---4	----	1---	1---
	---	-6-	--7	-6-	56-	---	-6-	56-	-6-	56-
24	---4	---4	---4	----	-234	----	---4	----	----	---4
	---	-6-	--7	---	-6-	-6-	-67	---	--7	567
25	---4	---4	---4	----	--3-	-2--	----	---4	----	----
	---	---	---	-6-	--7	---	---	-6-	-6-	56-
26	---4	-2--	-23-	----	----	----	----	--3-	12--	----
	-6-	---	-6-	-6-	56-	-6-	---	-6-	-67	---
27	---4	-2--	----	----	----	----	----	----	12--	----
	---	---	5--	-67	56-	---	-6-	---	-6-	--7
28	--34	-2--	---4	----	----	-2--	1---	1--4	1---	----
	---	-6-	---	-6-	56-	---	-6-	-6-	-6-	--7
29	---4	-2--	----	----	12--	----	----	----	1---	----
	---	---	---	-67	56-	-6-	---	---	-6-	-6-
30	---4	-2--	-2--	--34	-2--	--3-	----	-2--	1---	---4
	5--	---	5--	---	5--	---	-6-	--7	-6-	--7
31	--3-	----	---4	----	----	-23-	1---	----	--3-	---4
	---	-6-	---	---	---	---	-6-	---	---	--7
32	---4	----	12-4	----	---4	----	----	----	----	----
	---	-6-	---	-6-	---	---	---	---	-6-	---
33	--34	-2-4	----	----	----	----	----	----	1---	----
	---	---	---	-6-	567	---	---	---	567	---
34	---4	-234	--3-	----	---4	----	----	----	1---	----
	---	---	--7	-6-	56-	-6-	---	---	-6-	---
35	-2-4	-2--	1---	----	-2-4	----	----	----	1---	----
	---	---	-6-	-6-	56-	-6-	5--	---	56-	5--
36	-2-4	-234	1-3-	----	----	----	----	1---	1---	----
	---	---	---	-6-	56-	---	---	---	-67	---
37	12-4	--3-	----	-2--	---4	1---	----	----	12--	----
	---	---	---	---	5--	---	---	---	-6-	---
38	-2-4	-2--	1-34	-2--	----	12--	----	--3-	1234	----
	---	---	56-	-6-	56-	---	-6-	---	---	---
39	---4	-2--	--3-	----	---4	----	----	----	1---	-2--
	---	---	---	-6-	56-	-6-	---	---	-6-	---
40	---4	12--	----	----	----	----	1---	----	1234	-23-
	---	---	---	-6-	56-	---	---	---	56-	---
41	---4	12--	-2--	--3-	----	----	--3-	--3-	1---	----
	---	---	--7	-67	56-	---	--7	-6-	-6-	---
42	---4	-2--	----	----	----	----	----	----	1---	1---
	---	---	---	-6-	56-	---	---	---	-6-	---
43	1--4	12-4	----	12--	1--4	----	1---	----	----	1-3-
	---	---	---	5--	-6-	---	---	---	56-	---
44	----	123-	----	--34	----	----	--34	-234	1---	----
	---	56-	--7	---	---	-6-	--7	5--	-67	---
45	---4	12--	----	123-	--3-	----	----	----	----	----
	---	---	---	-6-	---	---	---	---	---	---

APPENDIX 4.5 - *PL*45 DERIVED AND COMBINED LAYERS

	EACC	RMCC	SWCC	WGBCC	EGBCC	SACC	NWCC	NRCC	NOCC	SOCC
12	--34	--34	12--	---4	1234	12--	1---	1234	---4	--3-
	5--	--7	-6-	-67	--7	5--	--7	---	5-7	-6-
13	----	----	--3-	12--	----	-2-4	1-34	1---	-234	--3-
	---	---	5--	---	56-	---	---	-67	567	---
14	---4	1---	--3-	-2--	--3-	-2--	12-4	----	--3-	1--4
	-6-	-67	5--	5--	---	---	---	--7	---	---
15	--34	----	--3-	1---	----	-234	1---	--34	1---	-23-
	---	56-	5--	5--	-67	---	-6-	-67	-6-	---
16	--3-	----	--34	12--	---4	-2--	1---	--3-	--34	----
	---	---	5--	---	5--	---	---	-67	---	---
17	---4	1---	--3-	-23-	----	-2--	12-4	-234	-2--	1---
	56-	-67	567	--7	---	5--	---	567	---	---
18	-234	12--	----	-2--	----	---4	----	----	1-34	1---
	---	--7	5--	---	-6-	---	---	--7	-6-	---
19	--3-	----	---4	1---	-234	-2--	1--4	--3-	-23-	----
	---	---	---	---	---	---	---	-6-	-6-	---
20	-2-4	----	123-	1---	--3-	-23-	1---	--3-	----	----
	---	---	567	---	---	5--	---	--7	---	-67
21	1-3-	12--	--3-	-2--	--3-	-2--	12--	----	----	1---
	-6-	---	5--	---	---	---	---	-67	---	---
22	---4	12--	--3-	----	----	-2--	1--4	--3-	----	---4
	---	5--	5--	---	---	5--	---	--7	---	---
23	--3-	12--	-23-	----	---4	-2--	12--	----	----	----
	---	---	567	---	---	---	---	--7	---	---
24	1--4	12-4	----	----	--3-	-2--	----	----	----	--34
	---	---	--7	-6-	---	5--	-6-	-6-	---	---
25	1-3-	12--	1---	----	--34	-2--	--3-	--34	--34	----
	--7	5--	---	---	---	56-	---	---	5--	---
26	12--	--3-	--3-	---4	----	-2--	12--	1--4	----	--3-
	5--	---	5--	---	---	---	-6-	567	---	---
27	----	----	1-3-	-23-	----	-2--	1--4	----	1234	----
	---	--7	5-7	-6-	--7	---	---	--7	---	56-
28	1-3-	----	-23-	--34	----	-2--	1--4	----	1---	----
	---	---	5--	5--	5--	---	---	5-7	---	--7
29	----	----	1-3-	----	----	-2--	1---	----	-234	----
	---	---	5-7	---	---	---	---	--7	---	---
30	----	----	--3-	-23-	----	-234	---4	----	--3-	----
	---	---	5--	-6-	5--	5--	---	--7	---	-6-
31	----	1---	-2--	1--4	--3-	----	----	----	1---	----
	5-7	5--	56-	---	---	---	--7	---	---	---
32	----	1-3-	----	----	---4	-2--	1---	1---	1---	-23-
	---	---	---	---	---	5--	---	5--	-67	5--
33	1-34	--3-	1-3-	----	----	-2--	1---	----	----	----
	---	5--	5-7	---	--7	---	---	--7	5--	---
34	----	----	--34	----	--3-	-2--	12-4	----	1---	----
	---	---	5--	---	---	---	---	--7	---	---
35	----	----	--3-	----	----	12--	1---	----	---4	----
	---	---	5--	-6-	---	---	---	--7	---	---
36	----	--3-	--3-	----	----	-2--	1---	----	---4	----
	---	5--	5--	---	---	---	---	--7	---	---
37	----	1---	---4	---4	-2--	-2--	----	1---	1---	1---
	56-	---	---	---	---	---	56-	---	---	---
38	-2--	----	--3-	-2--	----	12--	1--4	---4	---4	1---
	-6-	---	5--	-6-	5--	---	---	---	---	---
39	1---	--3-	123-	----	----	12--	1---	----	----	----
	--7	---	5--	---	---	---	---	--7	---	---
40	----	---4	--3-	----	----	-2--	1-34	--3-	----	----
	---	---	5--	---	-6-	---	--7	--7	5--	---
41	--3-	-2-4	--34	----	----	-2--	1---	----	-2--	-234
	---	5--	5-7	---	---	---	---	--7	5--	--7
42	---4	----	--3-	----	----	-2--	1-34	----	----	--3-
	--7	---	5--	--7	-6-	---	---	--7	5--	--7
43	-2--	--34	--3-	1---	----	-2--	-23-	--3-	--3-	----
	---	---	5--	---	---	---	--7	---	-6-	---
44	--3-	---4	1--4	-2--	----	----	---4	---4	-2--	12--
	--7	---	--7	---	---	---	---	---	---	--7
45	----	----	---4	----	----	-2--	1---	----	-2--	1234
	---	---	5--	---	---	---	---	--7	5--	---

APPENDIX 4.6 – RUN TIME AND DATA SIZE ANALYIS

The research code batches three distinct phases: **prepODE.m**, **setupODE.m**, and **evalODE.m,** runs them in parallel across $\max(\#R, \#G)$. Parallel loops were a speedy way to distribute the computer processing workloads as code was debugged. Each phase works with less data than before. Development involved saving intermediate files; the size of these data dumps for an $18km$ resolution quadrature with our full suite of risk factors $i_{max} = 45$ was recorded in columns 2 and 4 below

Storage and run-time requirements, test cases **(B1)** and **(B2)**

Phase	Input data size	Run time $(CPU\ days)$	Output data size	Extra features
prepODE.m	23.3 Gb	14	10.4 Gb	*GIS data visualization risk/demand console*
setupODE.m	10.4 Gb	0.375	494.3 Mb	*Assemble lag structure*
evalODE.m	494.3 Mb	0.006944	4.0 Mb	*Redundant inversion methodologies*

Test case **(A)** revealed a memory limit for the model with $\langle \#R = \#G = 12, N = 16, E = 17 \rangle$. This problem was on the CONUS, Alaska, and Hawaii, ground-aerial-command models. On a Intel(R) Core(TM) i7-4770 CPU @ 3.40 GHz with 32 Gb memory, version R2017b of MATLAB was unable to sufficiently compress and save a workable test case **(A)**. The data cache of **prepODE.m** was 71.2 Gb in this case. Working with post-processing of results was time consuming, but many open avenues of research are ongoing. Sub-model approaches, as in test cases **(B1)** and **(B2)** run and store more quickly.

Here is further evidence of the Np-hardness of this problem. Even in a relatively small test case the combinatorial indexes spaces involve a lot of data pre-processing. Part of the excitement of this project was to work away from big data into tangible visuals, statistics, and ultimately a PDE.

APPENDIX 4.7 – RISK STENCILS

Risk assessment for national fire managers must take place in a two-dimensional plane, i.e., the cardinal directions. We assumed fire risk update comes in kernels of information $R_i(t, lx, ly)$. Map components to the demand potential highlight a thought experiment from (Farlow 1993). Therein the author explains the crux of a $\dim = 2$ finite difference method using a drunkard. We stick with the mountaineer and the assumption that fire managers would have a set of risk information maps at hand. Moreover, their set of maps would be subject to constant spatiotemporal update. The thought experiment is thus. Consider two North-South-East-West two risk scenarios:

	Scenario A	**Scenario B**
Risk at (t, x) is…	…spatially uniform.	…greater to the Northwest.

Scenario B sketch

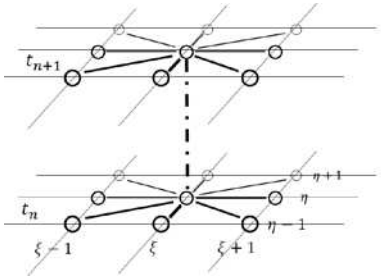

Implicit computational stencil
in transformed coordinates (ξ, η)

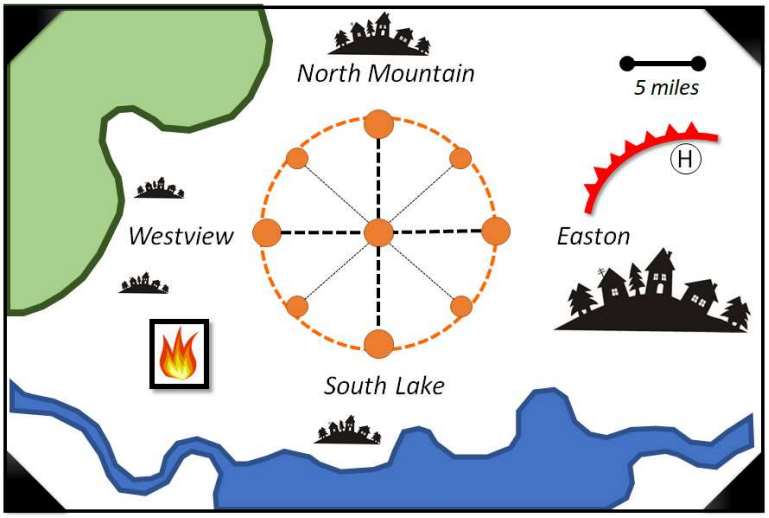

When discussing local response to spatially heterogeneous risk like Scenario B we need a two-dimensional map to explain our numerical experiments. So henceforth we assume two spatial variates $(t_n, \xi, \eta) \in \mathbb{R} \cup \mathbb{R}^2$ (i.e., latitude longitude from some GIS time series data).

The continuous model is for time-space triplets (t, lx, ly). When risk is uniform, the direction of the allocation is arbitrary. When we start forcing and changing the motion in this field, call it $\overrightarrow{\Phi_S}$ for supply potential. Any directional preference strategy or data pattern would mean the supply $\overrightarrow{\Phi_S}(t, lx, ly)$ might follow a similarly structured risk model $\vec{\mathcal{R}}(t, lx, ly)$. In contrast, when risk is greater to the Northwest, allocation options have an important directionality. A fire manager might address the risk directly showing a spatial preference allocating the supply along the gradient risk kernel $\vec{\nabla} R_i$. Or, if the risk was too extreme for a direct allocation, the manager might allocate along some contouring direction, perhaps to the North or West.

Risk anticipation drive the PDE model equilibrium. Supply and demand response are characterized with our notations so far. In Scenario A diffuse allocation in a random direction is optimal. Scenario B is advection-dominated and Northwest is clearly the best call, or at least not Southeast so as to be ready. The PDE equation for $\mathcal{G}$ must permit diffusion-dominated allocation like Scenario A, advection-dominated allocation like Scenario B, and combinations where random directions, gradient-following, and gradient-contouring allocations might be present in strategic directional basis.

APPENDIX 4.8 – LINEAR PROGRAM RELAXATION

The nonlinearity can be approached directly or indirectly. Directly, using nonlinear optimization in MATLAB's fmincon.m function. For an indirect approach, we relaxed the problem to a mixed binary linear program by restricting continuous coefficients α_i to binaries $y_i = 0$ to pass over for fit layer D_i and $y_i = 1$ to go ahead and fit it. All mixed products nonlinearities in the calibration problem have the form $y_i \cdot u$. This relaxation is a well-known trick (Bisschop 2006, *Integer Linear Programming Tricks*, Table 7.1) that adds a single dummy variable z_i wherever $y_i \cdot u$ appears in the equations, which are numerous times given all the mxed products from the covariant derivatives. The expense is adding four extra constraints to control z_i's behavior:

$$\begin{cases} z_i \le y_i & (A) \\ z_i \le u & (B) \\ z_i \ge y_i + u - 1 & (C) \\ z_i \ge 0 & (D) \end{cases}$$

The model is essentially a pie-chart of risk using weights α_i. Our linear relaxation ultimately relies on proving the following lemma:

Lemma… Suppose y_i is binary and u is continuous, nonegative, and bounded above by unity i.e. $0 \le u \le 1$. If (A), (B), (C), and (D) hold, then $z_i = y_i \cdot u$.

Proof… We complete the proof in two cases.

($y_i = 0$ case) Inequality (A) means $z_i \le 0$ and inequality (D) implies $z_i \ge 0$. Neither (B) nor (C) is violated. In (B) $z_i = 0 \le u$ is okay because $u \ge 0$. In (C) $z_i \ge y_i + u - 1 = 0 + u - 1 = u - 1$, which is satisfied since $u \le 1$ means $u - 1 \le 0$. So we find $z_i = 0 = 0 \cdot u = y_i \cdot u$ in this case.

($y_i = 1$ case) Compute (C) $z_i \geq y_i + u - 1 = 1 + u - 1 = u$ to see $z_i \geq u$. Since (B) enforces $z_i \leq u$, it must be that $z_i = u$. So we again find $z_i = u = 1 \cdot u = y_i \cdot u$ in this case.

Having proven both possible cases for y_i for any $0 \leq u \leq 1$, the lemma is valid ■

APPENDIX 4.9 – LONG RANGE ALLOCATION IN ALASKA

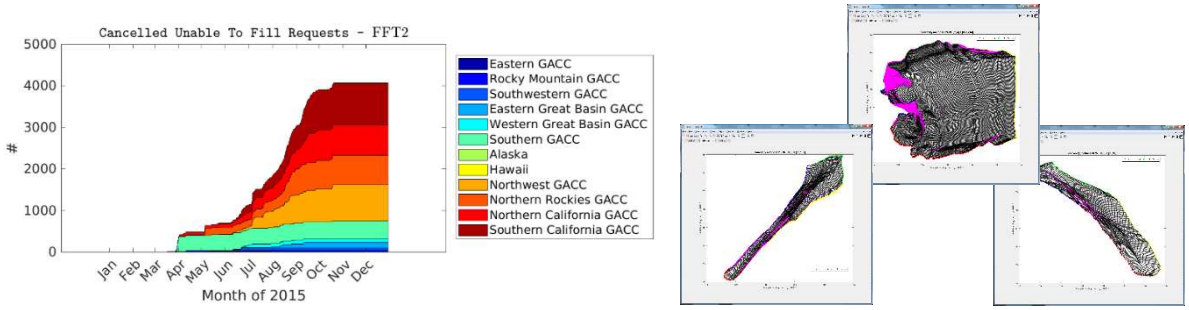

Caption:

Long range allocation to Alaska is interesting to our theory:

(left) Here is a count-based time series showing Alaska in the green bar at bottom. Over the Month of 2015 with Cancelled Unable To Fill data. In the red hues are late California season fires; oranges hues are fires in the Northwest and Northern Rockies.

(right) Alaska again in meshing, Highlight (Barrera-Sánchez et al. 2009) and transfinite interpolations. Other regions are easier to mesh with quality structured convex grids. Convexity (folding) corrections per (Ivanenko 1999) are shown in pink.

APPENDIX 4.10 – MODIS EDGE FEATURES

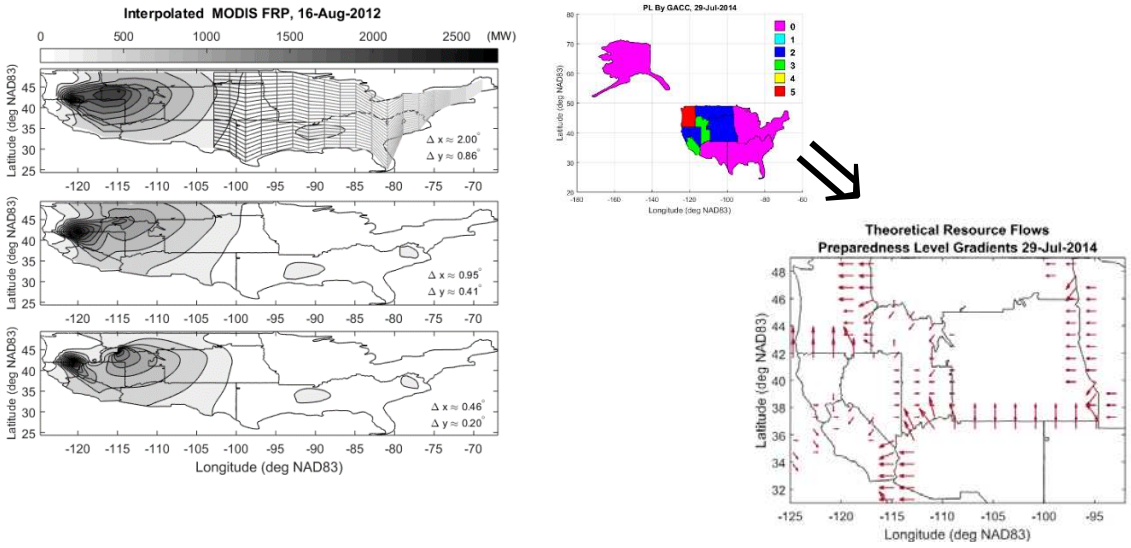

Caption

Grid resolution impact on MODIS large fire interpolation. $\kappa > 0$ interacted with the scatteredInterpolant and clustering procedure. (Left, top) Low resolution works well for quadrature averaging. (Left, middle) Nice balance between some long-range signals and a focus on the super complexes. (Left, bottom) Lower resolution modeling goal for PDE dynamics: anisotropic grid 0.46 by 0.20 degrees. (Right, pair) Showing our idea for a PL-based boundary condition. Resources near GACC boundaries will cross them when a PL gradient exists.

APPENDIX 4.11– POTENTIAL MODELS IN MOUNTAINEERING

A common math-physics model for expressed risk is a potential Φ. Conceptually, potential is ubiquitous in both wildland firefighting system data and mountaineering. Risk perception on wildfires can be subjective, i.e. subject to one's own opinion, experience, ability, mood, etc. Much of the fire suppression model can be compared to a hiker's mental model of risk as they scale a mountain. The hiker will likely consider elevation gradients $\vec{\nabla}\,\Phi(x)$ through the mountainous terrain (x, y) . In addition, an ensemble of spatiotemporal risk update information matters as well. The weather, equipment, experience, trail level, exposure ratings, fatigue, and food supply all effect how the hiker chooses to climb a mountain. Even in the case that the climber is only concerned with elevation case, spatiotemporal risk update is subject to expert opinion. Similarly, in wildland fire resource allocation, many factors influence the allocation decisions (i.e., the fatigue levels, team coordination and tactics) across many fires at once. We can expect the number of relevant factors to be substantially greater than just elevation Φ and management does not always think alike. Some might follow gradients $\vec{\nabla}\Phi$ and others might contour them.

Fire management allocation differs from this mountaineering example in several obvious ways. First, instead of a fixed peak to set the directional goal, fire starts are pseudorandom points (Preisler and Westerling 2007). Second, climbing teams on the toughest mountains, find only a limited few route alternatives. Terrain constrains a single party to a few limited routes. Fire management involves the supply of a pool of resources based in many locations. Allocations might have degenerate optimal solutions. In other words, this problem is alternative rich and there may be multiple ways to allocate resources. Third, in addition to the tradeoffs in the supply

pool, there are tradeoffs and opportunity costs to manage multiple fires as if multiple peaks were being summited over the next week or two.

Additional mountaineering models were prepared as part of $\frac{1}{4}$-time GTA for F 422: Quantitative Methods in Forest Management, *Fall,* 2016 and 2017. A modeling project was assigned in lieu of a written examination.